

POLITECNICO DI TORINO

Master's Degree in MECHATRONIC ENGINEERING



Master's Degree Thesis

Linear Elastic Fracture Mechanics Assessment of a Gas Turbine Vane

Supervisors

Prof. Daniele BOTTO

Eng. Simone SOLAZZI

Eng. Andrea BESSONE

Candidate

Blanca ORENES MORENO

March 2022

Summary

The continuous evolution of heavy duty gas turbines, with the aim of improving the machine performance, has resulted in a significant increase of its working conditions, in particular in terms of temperatures and stresses. Especially regarding the expansion section of the engine, gas turbines blades and vanes of the front stages, due to its closed position to the combustion chamber, have to withstand extremely harsh operating conditions that lead to damage mechanisms. These damage mechanisms, as creep, fatigue and oxidation ones, play an important role in the crack initiation and propagation.

Under the present work, at *Ansaldo Energia Group*, it has been studied, by means of Linear Elastic Fracture Mechanics (LEFM) approach, the evaluation of a crack propagation behaviour, localised at the most critical locations of a second-stage vane of a gas turbine for power generation (F-class).

Furthermore, it has been developed a Mechanical Integrity (MI) assessment to the FE model, observing that in the Outer Platform Trailing Edge the required creep limits of the material were overcome according to FE calculations.

For this reason the application of Fracture Mechanics (FM) approach is mandatory in order to estimate the component lifing before to achieve the critical crack size. Namely, the evaluation of the number of firing hours or cycles that the vane can accomplish with a stable crack propagation can be calculated, avoiding the unstable crack behaviour that could lead to catastrophic failure.

In this way, via FEM using the *Fracture Tool* within *ANSYS Workbench* environment, the whole procedure of crack modelling and evaluation of fracture parameters have been developed, in particular the Stress Intensity Factors (SIFs). Moreover, thanks to the sub-modelling technique, a more accurate mesh and hence more precise results of the interested area have been obtained. Nevertheless, before this assessment, the correct functioning of the Fracture Tool has validated by means of a simple model: a plate with a crack inside. A comparison of this model and results with direct calculation by formula has been performed to appreciate the increase of the stress intensity factor K_I (Mode I) with the rise of the crack length a .

Additionally, through an in-house AEN program, called *Propagangui*, the crack

growth due to the effects of creep, fatigue and oxidation phenomena has been studied considering the working conditions of the component.

The results obtained from the first analysis show an unexpected behaviour of the KI, which is in contrast with the theoretical approach: a KI reduction has been obtained with the a increase. Moreover, in the SIF assessment it has been observed that KII and KIII are of the same order of magnitude than KI, but lower. As a consequence, it has been chosen KI as the dominant SIF, which will represent in a better way the dynamics of the crack propagation. However, it is important to mention that the KII and KIII have not been neglected in the crack growth study.

The obtained results can be explained not only due to the complex geometry of the component, but also to the extreme operating conditions. Furthermore, due to the stress status, it seems to be performed a redistribution of the stresses along the critical location with the increase of the crack length. This fact does not create an unstable increase of the stress around the crack. Additionally, it should be outlined that the obtained SIFs values are considerably smaller than the fracture toughness of the material. As a consequence, no unstable propagation is expected from this first analysis phase.

On the other hand, the stable propagation of the crack due to creep, fatigue and oxidation has been validated from the second performed analysis (crack growth assessment), where it has not achieved neither plastic collapse nor unstable propagation. In fact, it has been obtained the slow down of the crack growth rate as the crack length increases due to the reduction of KI. So, the observed redistribution of stresses helps the achieved propagation of the crack to become slower. To evaluate the final life of the component, different end-of-life lines at different "critical" crack sizes have been drawn. These latter will give the number of cycles or firing hours needed to achieve the critical crack size.

From this evaluation, a final comment can be done about crack propagation: while the propagation length between 2 mm and 5 mm happens within low number of cycles (or firing hours), the propagation to achieve 10 mm crack size needs more time. This behaviour confirms that the crack slows down as it evolves.

Summarizing, it can be concluded that the behaviour of the crack follows a stable propagation. The evolution of the crack tends to slow down its growth rate and therefore no unstable fracture is expected.

Acknowledgements

I would like to express my gratitude to all the MI group for their entire support and guidance during the whole path of this thesis. Especially, I would like to thank Eng. Simone Solazzi, for making this final work more pleasant with his help and kindness. I would also like to thank Eng. Andrea Bessone, Professor Eng. Daniele Botto and again Eng. Simone Solazzi for all their mentoring during the elaboration of this work.

Finally, I would like to dedicate this last space to all the members of the company that make my stay more comfortable and enjoyable, to all my friends and especially to my family who have always been by my side supporting me in every step I take.

Table of Contents

List of Tables	VIII
List of Figures	IX
Acronyms	XIV
1 Introduction	1
1.1 Thesis Goals	3
2 Mechanical Integrity of Gas Turbine	5
2.1 Gas Turbine Overview	5
2.2 Gas Turbine Materials	14
2.3 Production process	18
2.4 Workflow of GT Blade and Vane	24
2.5 Mechanical Integrity Assessment	25
2.6 General static stress description on components	26
2.6.1 Thermal Stress	27
2.7 General dynamic stresses description on components	27
2.7.1 Vibrations	28
2.7.2 Flutter	32
2.8 GT Damage Mechanisms	32
2.8.1 Fatigue Fracture	33
2.8.2 Creep	36
2.8.3 Oxidation	36
3 Fracture Mechanics	37
3.1 Fundamentals of Fracture Mechanics	37
3.2 Linear Elastic Fracture Mechanics	39
3.2.1 Griffith energy balance	40
3.2.2 Stress Intensity Factor (SIF)	41
3.3 Crack growth in gas turbine components	46

3.3.1	Fatigue Crack Growth	48
3.3.2	Creep Crack Growth	51
3.3.3	Oxidation Crack Growth	53
4	Application to a Gas Turbine Vane	55
4.1	System description	55
4.2	Critical locations detection	58
4.3	Submodel	64
4.4	Crack modeling	72
4.5	Stress Intensity Factors evaluation	77
4.6	Crack growth assessment	87
5	Conclusions	98
	Bibliography	101

List of Tables

4.1	Values of $\bar{K}I$ as a function of the crack length (a) of the plate . . .	81
4.2	Values of $\bar{K}I$ as a function of the crack length (a) at the PETE of the vane	84
4.3	FAD Options with the requested inputs	89

List of Figures

1.1	Evolution of Gas Turbines [1]	1
2.1	Gas Turbine Engine [7]	6
2.2	Bryton cycle [9]	7
2.3	P - v and T - s Diagrams of the Bryton Cycle [9]	7
2.4	Combined Cycle Power Plant Layout [10]	8
2.5	Example of temperature evolution at the different stages of a GT [13]	9
2.6	Turbine Vane [15]	10
2.7	Turbine Blade [16]	10
2.8	U-Ring	11
2.9	Parts of the expansion turbine section [17]	11
2.10	Example of the cooling system of a vane [13]	12
2.11	Example of the cooling system of a blade with PS = Pressure Side and SS = Suction Side [17]	13
2.12	Cooling Evolution in the years Vs TIT [1]	13
2.13	Temperature capability Vs oxidation resistance of some superalloys and steels [1]	14
2.14	Role of alloying elements for superalloys [1]	15
2.15	Role of alloying elements with corrosion and oxidation resistance [1]	16
2.16	Microstructures of Superalloys [1]	17
2.17	Microstructure Evolution of Superalloys [1]	17
2.18	Production Process of GT vanes and blades [13]	19
2.19	Solidification Process of GT vanes and blades [1]	20
2.20	Different grain microstructure of a GT blade [13]	20
2.21	Creep rupture life of CC, DS, and SC Alloys [1]	21
2.22	Thermal Fatigue Life of CC, DS and SC Alloys [1]	21
2.23	Creep Behaviors of CC/DS/SC Alloys [1]	22
2.24	Creep strength with temperature for different groups of materials [1]	22
2.25	Evolution of the production processes with the temperature capability [1]	23
2.26	Evolution of TIT thank to the introduced cooling technologies [1]	24

2.27	Example of a spring with a mass	28
2.28	Oscillating up and down mode of the spring with a mass [23]	29
2.29	Modes of vibrations for a single blade from the FEA [24]	30
2.30	Campbell diagram [17]	31
2.31	S-N Curve [26]	34
2.32	Left - An alternating stress with no mean stress. Right - An alternating stress with a mean stress offset [27]	35
2.33	Goodman line [17]	35
3.1	Fracture mechanics important parameters [31]	38
3.2	Fracture mechanics approaches [31]	39
3.3	The Griffith crack[31]	40
3.4	Evolution of the stress on a crack[35]	42
3.5	Stress evolution on the crack tip by LEFM with a small scale yielding [36]	43
3.6	Modes of crack displacement. Mode I or opening; Mode II or sliding; Mode III or tearing [38]	43
3.7	Stress components at a crack tip [31]	44
3.8	Evolution of K_C with the thickness of the specimen[38]	45
3.9	a. Crack Growth during time; b. Residual strength curve [41]	47
3.10	Fatigue Crack Growth curve [41]	49
3.11	Fatigue Crack Growth [38]	50
3.12	Fatigue Crack Growth curve	51
3.13	Creep crack growth by diffusion mechanism [40]	52
3.14	Creep curve. Strain Vs Time	53
3.15	Creep Fatigue Interaction diagram [50]	54
4.1	TV2	56
4.2	Anti-oxidation and corrosion processes.	56
4.3	Cooling system scheme	57
4.4	U-Ring	57
4.5	FEM model of the whole component; Turbine Vane Carrier, Turbine Vane and U-ring	58
4.6	FEM model of each single component. On the left the TV2; at the top right the turbine vane carrier sector; at the bottom right the U-ring sector	59
4.7	Pressure distribution on the TV2	60
4.8	Thermal analysis on the TV2	60
4.9	Displacements analysis on the TV2. From left to right; Radial displacement, axial displacement, circumferential displacement and total displacement	61

4.10	Von Mises Stress distribution, normalized to the maximum value . .	61
4.11	Creep strain vs Firing hours	62
4.12	Creep Analysis at 66kFH where it is remarked the overcome of the strain limit at the PETE and PITE	63
4.13	LCF Analysis with no stress relaxation	64
4.14	Submodel of the TV2 focused around the PETE area	65
4.15	Submodel attached to the engineering data and solution of the full model in ANSYS Workbench	66
4.16	Displacement field of the whole model applied to the submodel as boundary condition	67
4.17	Temperature gradient of the whole model applied to the submodel as boundary condition	68
4.18	Imported pressure load on the pressure side of the airfoil	69
4.19	Imported pressure load on the suction side of the airfoil	69
4.20	Imported pressure load on the pressure side of the exterior platform of the vane	70
4.21	Imported pressure load on the suction side of the exterior platform of the vane	70
4.22	Imported pressure load on the internal cooling channels of the vane	71
4.23	Comparison between whole model stress status and submodel stress status	71
4.24	SOLID 187 Geometry [55]	72
4.25	Mesh around the PETE with a sphere of influence of radius 8 mm and 0.5 mm of element size	73
4.26	Final mesh on the whole submodel	73
4.27	Mesh result around the PETE due to the sphere of influence	74
4.28	Crack modelisation with a circular surface body at the PETE	75
4.29	New Coordinate System at the crack apex	75
4.30	ANSYS Details of Arbitrary Crack method	76
4.31	Named Selection on the top face of the arbitrary crack (NS ArbCrack TopFace)	77
4.32	(a) Test plate with a rectangular crack shape in the middle of the specimen. (b) Test plate with the normal force applied on the top surface (A) and a fixed support at the opposite surface (B)	79
4.33	Mesh of the test plate	79
4.34	KI along the crack front with $a = 10\text{mm}$ calculated in the 5 paths at the plate	80
4.35	Evolution of $\bar{K}I$ with the length of the crack (a) of the plate	81
4.36	Stress status at the crack front of the test plate	82
4.37	KI of each crack length along the crack front	82
4.38	KI along the crack front with $a = 10\text{ mm}$ calculated in the 5 paths	83

4.39	Crack front. The label 1 represents the start of it while the label 2 represent the end of the crack front	83
4.40	Evolution of $\bar{K}I$ with the length of the crack (a) at the PETE of the vane	84
4.41	Distribution of the stress around the PETE on the pressure side at the different crack lengths	85
4.42	Distribution of the stress around the PETE on the suction side at the different crack lengths	86
4.43	Evolution of the SIFs with the length of the crack (a) at the PETE of the vane compared with the Fracture Toughness of the material .	87
4.44	Comparison of the different Failure Assessment Diagram options . .	89
4.45	Stress status comparison between all loads, mechanical loads and thermal loads, normalized to the maximum value	91
4.46	Operating cycle. Start-up, base load and shut down	92
4.47	Crack Evolution at an operation cycle of 10 firing hours	93
4.48	Crack Evolution Growth in terms of SIFs at an operation cycle of 10 firing hours	93
4.49	FAD of the crack	94
4.50	Hypothetical End-of-life line	95
4.51	Crack Evolution with the different operating cycles	96
4.52	End of life lines of the different crack sizes	97

Acronyms

APDL

ANSYS Parametric Design Language

ASME

American Society of Mechanical Engineers

ASTM

American Society for Testing and Materials

BEM

Boundary Element Method

CAD

Computer Aided Design

DS

Directionally solidified

EPFM

Elastic Plastic Fracture Mechanics

FAD

Failure Assessment Diagram

FEA

Finite Element Analysis

FEM

Finite Element Method

FH

Firing Hours

FM

Fracture Mechanics

GT

Gas Turbine

HCF

High Cycle Fatigue

HGP

Hot Gas Path

HRSG

Heat Recovery Steam Generator

HT

Heat Transfer

ID

Inner Diameter

LCF

Low Cycle Fatigue

LEFM

Linear Elastic Fracture Mechanics

MD

Mechanical Design

MI

Mechanical Integrity

OD

Outer Diameter

PETE

Platform External Trailing Edge

PITE

Platform Internal Trailing Edge

SIF

Stress Intensity Factor

ST

Steam Turbine

SX-SC

Single-Crystal

TBC

Thermal Barrier Coating

TIT

Turbine Inlet Temperature

TVC

Turbine Vane Carrier

TV2

Second stage Turbine Vane

XFEM

Extended Finite Element Method

Chapter 1

Introduction

The constant Gas Turbine (GT) technology evolution, with the aim of improving its efficiency, has resulted in a considerable temperature and stress increment of the GT parts, as it can be appreciated in Fig. 1.1, where the evolution of General Electric GT, from frame E to frame H, is shown. Especially, first stages GT vanes and blades are the ones that have to bear the worst working conditions. For this reason, it is not unexpected that a crack may nucleate on these parts and propagate, resulting in a catastrophic failure.

As a consequence, Fracture Mechanics (FM) is each time getting more and more importance on heavy duty GT development and analysis, not only for studying the possible crack behavior, but also for assessing the preliminary activities.

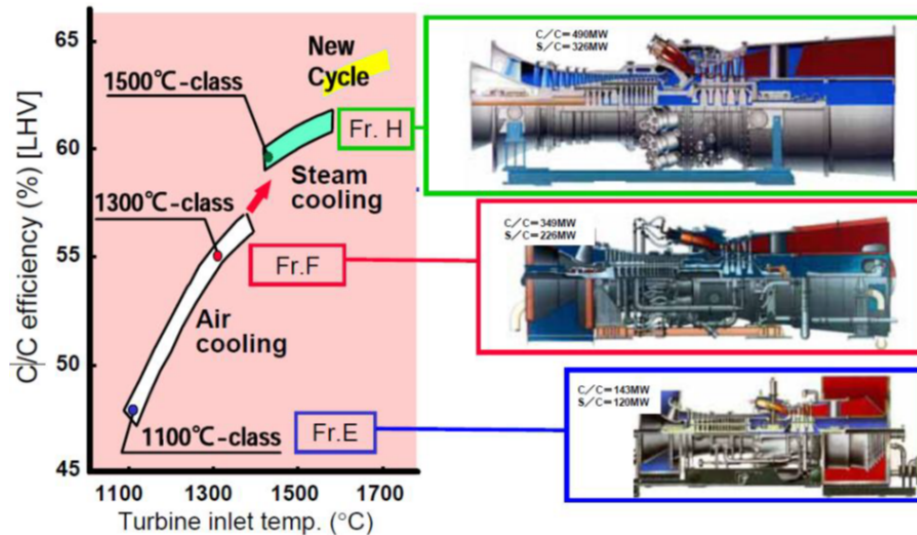


Figure 1.1: Evolution of Gas Turbines [1]

For instance, FM calculations are important in order to select the required materials during the vanes and blades design, choosing the material that best fit with the crack propagation behaviour and fracture toughness. Additionally, the component safe-life design is also used in FM, providing the crack propagation calculation at a given location, avoiding the component catastrophic failure. Furthermore, FM together with technological issues and structural integrity, are considered to define the repair criteria, such as the definition of the minimum flaw size that cannot be repaired.

Looking back over the years, many structures have suddenly failed, but it was not until the Second World War, with the catastrophic failure of the Liberty Ships, that materials instantaneous failures and its prevention, were started to investigate. In that sense, with the Griffith's investigations, carried out in 1921, as basis, when explained that the differences between the theoretical and the real fracture strength of a glass were due to the presence of defects on the material, a new science was born, *Fracture Mechanics*. [2]

The development of this discipline was of great importance since cracks and flaws happen much more frequently that what can be expected. There can either pre-exist in a component due to a bad surface finish, or can be created later as a result of the harsh working conditions. Moreover, the stress intensification that these defects create around the crack apex, leads to an adverse situation that can result in unstable crack propagation, also called as *fast fracture*.

For this reason, the evolution of this science supposed a turning point on the component design criteria, which started to being conceived in terms of damage tolerance. Tanks to Irwin's studies in 1957, within the LEFM approach, the rise in stress could be quantified via the stress intensity factor. From here on, the failure criteria was no more considering only the strength of the material (either yield strength or ultimate strength) but considering the material's fracture toughness, which describes how easily a crack grows under externally applied stress. [3]

The linear elastic mechanics approach stated before is built upon the analysis of cracks in linear elastic materials. It is mainly used to solve most of the engineering mechanical problems, like safety and life estimation of cracked components. Its principal parameters can be determined by either analytical methods or numerical ones. Meanwhile the analytical solutions can be applied only to very idealized scenarios of geometry and stress distribution, the numerical tools, are more accurate when dealing with more complex geometry and boundary conditions. [4]

Despite the abundance of numerical methods recently developed to simulate crack propagation mechanisms, such as Boundary Element Method (BEM), Extended Finite Element Method (XFEM), meshless methods, under this work, it will be focused on the Finite Element Method (FEM). This one is the most used as a result of its simplicity to model complex systems. [5]

1.1 Thesis Goals

In general terms, the main objective of this work is, by means of FM, in particular within the Linear Elastic Fracture Mechanics (LEFM) approach, the assessment of a possible crack propagation, originated at the most critical location, of a second-stage GT vane for power generation plants. The study of the way that the crack will propagate, obtaining the number of cycles, or number of firing hours (working hours), that the component can bear without failing.

Entering into the details, in order to achieve the required task, the main aim can be divided at the same time into the following different sub-objectives:

- Mechanical Integrity (MI) analysis of the whole vane to evaluate its performance and its design-life via *ANSYS Workbench* and *ANSYS APDL*.
- Critical location acquisition where the crack may nucleate, obtained from the previous analysis.
- Preparation of the model to be analysed. In this sense, it has opted to do a submodel of the interested area, obtaining more accurate results and avoiding to increase too much the computational time. Additionally, a sensitive analysis of the mesh is needed to be done in order to obtain the one that best fit with the case to study.
- Crack modelisation and FM parameters evaluation through *ANSYS Workbench*.
- Crack growth evaluation in terms of fatigue, creep and oxidation via an in-home software called *Propagangui*.
- Different end-of-life lines formulation depending on the critical crack size.

To achieve all these targets, the present work has been subdivided in five chapters. After this introductory one, in Chapter 2, an overview of GT fundamentals is detailed, where the main theoretical aspects of its working principle, the parts that compose it, the materials, coatings and casting techniques that conform the GT and additionally, the principal stresses and phenomena that the machine is subjected to, can be found.

On the other hand, in Chapter 3, FM basis will be established, where in first place, the different approaches to study cracks propagation within the LEFM theory, will be explained. Then, the way the crack evolves in GT, the phenomena present that result in its propagation (fatigue, creep and oxidation), and how these effects are considered in FM will be discussed.

In Chapter 4, the main objective will be developed; its the chapter related to the case study, where all the applied procedure and the obtained results will be described step by step.

Finally, in Chapter 5, the obtained results will be detailed.

Chapter 2

Mechanical Integrity of Gas Turbine

The information presented under this chapter, provides an overview of Gas Turbines (GT) fundamentals. To begin with, a fast introduction of the GT engine will be done, giving some details of its working principle. Secondly, it will be described the main parts of the expansion turbine section, where more emphasis will be put on the stationary vane: studied component of this work. Additionally, the main materials, casting techniques and coatings that compose the turbine parts will be defined. And finally, closing this chapter, a fast Mechanical Integrity (MI) Assessment will be done, where the main causes that can lead to premature failure of the gas turbine components will be explained.

2.1 Gas Turbine Overview

Gas turbine, also known as combustion turbine, is a type of continuous and internal combustion engine, which produces power generation by spinning a turbine thanks to the hot-pressured gas expansion. The main three parts that comprise gas turbines, mounted on the same shaft, as illustrated in Fig. 2.1, are: [6]

1. Compressor
2. Combustor chamber
3. Expansion turbine

The gas turbine operates based on Brayton's cycle principle, with air as working fluid. The atmospheric air is incrementally compressed as it passes through the different stages of the compressor, normally axial, producing an increase of the

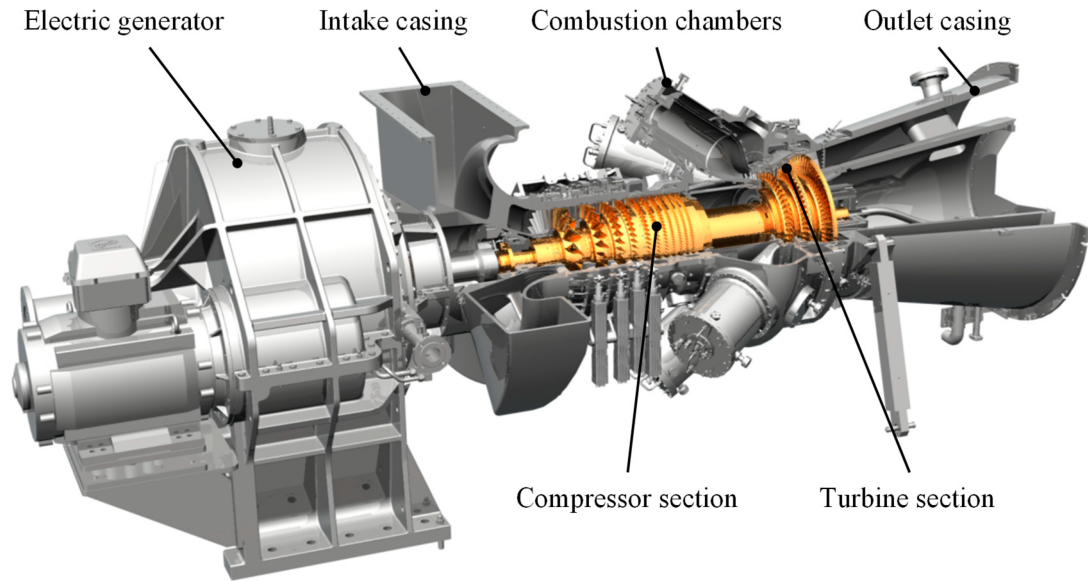


Figure 2.1: Gas Turbine Engine [7]

pressure, a slightly increase of the temperature (although no heat is added on this stage) and a reduction of the air volume, accelerating therefore the air. Then, due to the necessity of a certain speed on the compressor before the combustion process, an initial momentum is imparted to the shaft of the turbine through an external motor, or the generator itself. Once the compressor has reached the firing speed, the compressed air is mixed with fuel injected through nozzles, and the ignition can happen under constant pressure conditions. In addition, the produced hot combustion gases are then directed through the expansion turbine, where it expands rapidly, transforming the hot gas energy into mechanical energy to the shaft.[8] The following figures, Fig. 2.2 and 2.3, illustrate this cycle and its correspondent $P-v$ and $T-s$ diagrams.

According to [8], approximately 55 to 65 percent of this mechanical energy will be used to drive the compressor, keeping it working continuously, and the remaining shaft power will be used to drive the generator that will produce the electricity. It is also important to mention that, in order to optimize the transfer of kinetic energy from the combustion gases to shaft rotation, gas turbines can have multiple compressor and turbine stages.

It also should be highlighted, that these engines commonly work together with Steam Turbines (ST) in power plants, to produce up to 50 percent more energy than a traditional simple-cycle plant. This cycle is called *combined cycle*, and it is composed by the GT, the ST and a Heat Recovery Steam Generator (HRSG). Mainly, its principal objective is the transformation of gas natural thermal energy

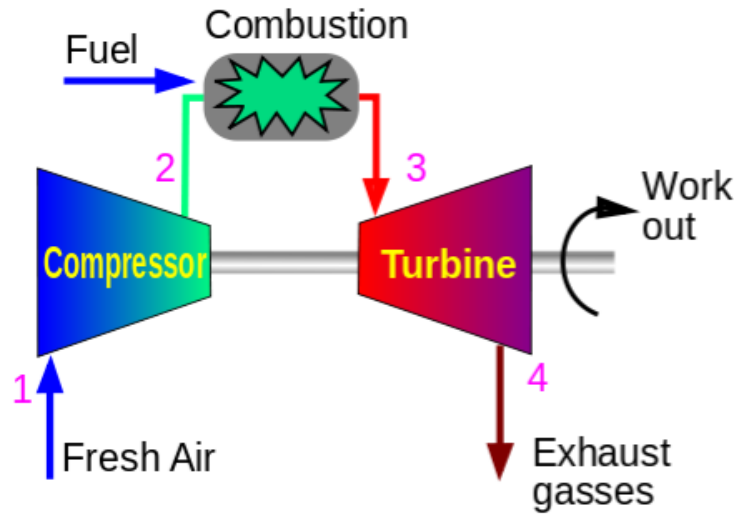


Figure 2.2: Bryton cycle [9]

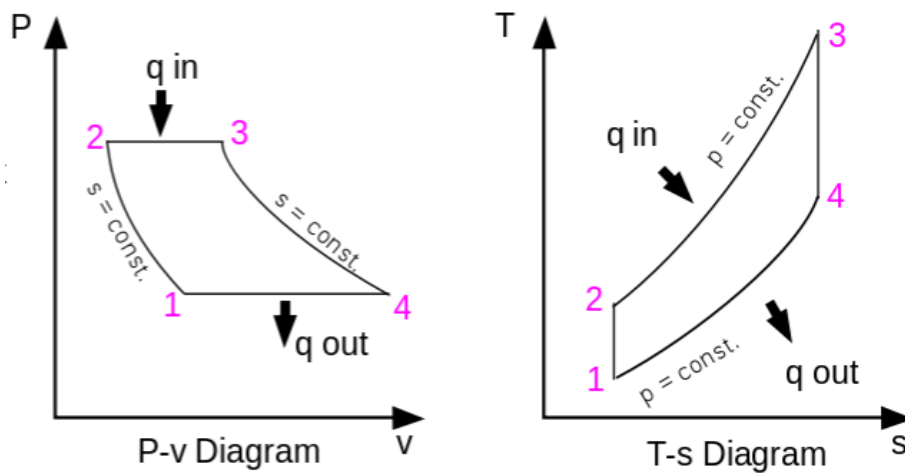


Figure 2.3: P - v and T - s Diagrams of the Bryton Cycle [9]

into electricity, under the joint work of the two turbines. Therefore, the process implies the implementation of the Bryton cycle, corresponding to the GT, and the

Rankine cycle, relevant to the ST. [10]

This combined cycle is characterised by the use of the GT hot combustion gases, that otherwise would escape through the exhaust stack, to produce steam. The steam is then supplied to the ST, generating electric power. So, the GT hot combustion gases, are forwarded to the heat recovery boiler (HRSG), that is basically a heat exchanger, producing steam by passing the gases through banks of heat exchanger tubes, in which hot water circulates. As the gases flow past the tubes, it is produced a heat transfer that will convert the water into steam. From this moment, it starts the Rankine cycle, where the steam turns the turbine generating electricity. Furthermore, at the outlet of the ST, the steam is condensed (turning back into water) returning to the boiler, starting a new cycle of steam production. [11]

In general the GT and the ST are coupled to the same shaft, driving the same electric generator. In the Fig. 2.4, it can be appreciated a scheme of a combined cycle power plant.

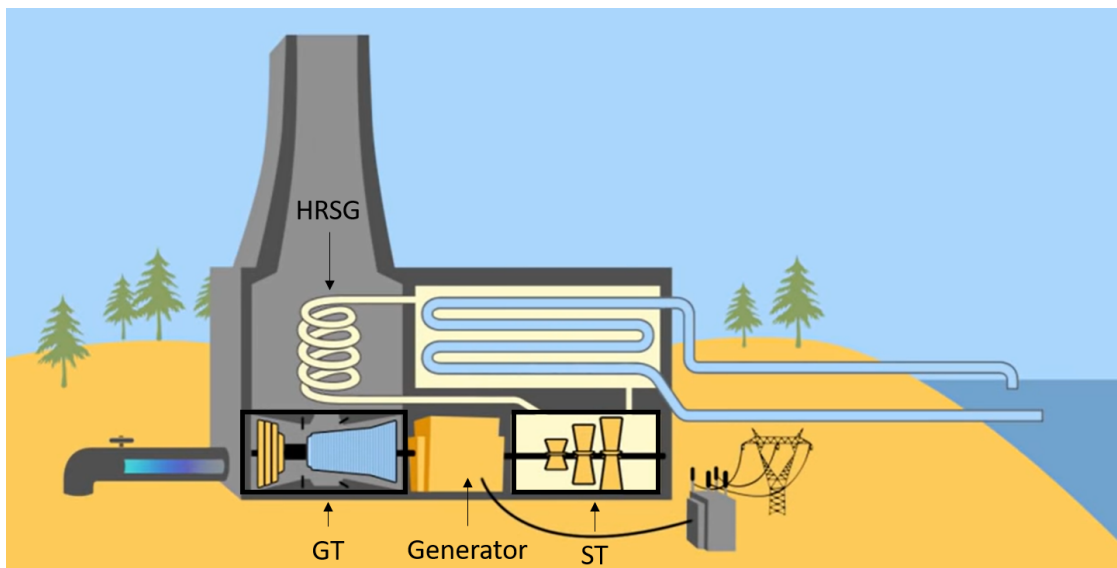


Figure 2.4: Combined Cycle Power Plant Layout [10]

As it has been told before, under this thesis, special emphasis will be put on the expansion turbine, whose aim is the transformation of the hot gas enthalpy into mechanical energy. To achieve this task, different stages (normally four) working in favourable pressure gradient conditions are comprised. It should be highlighted, as illustrated in Fig. 2.5, that first stages (closer to the combustion chamber) are the ones that bear highest temperatures and stresses. [12]

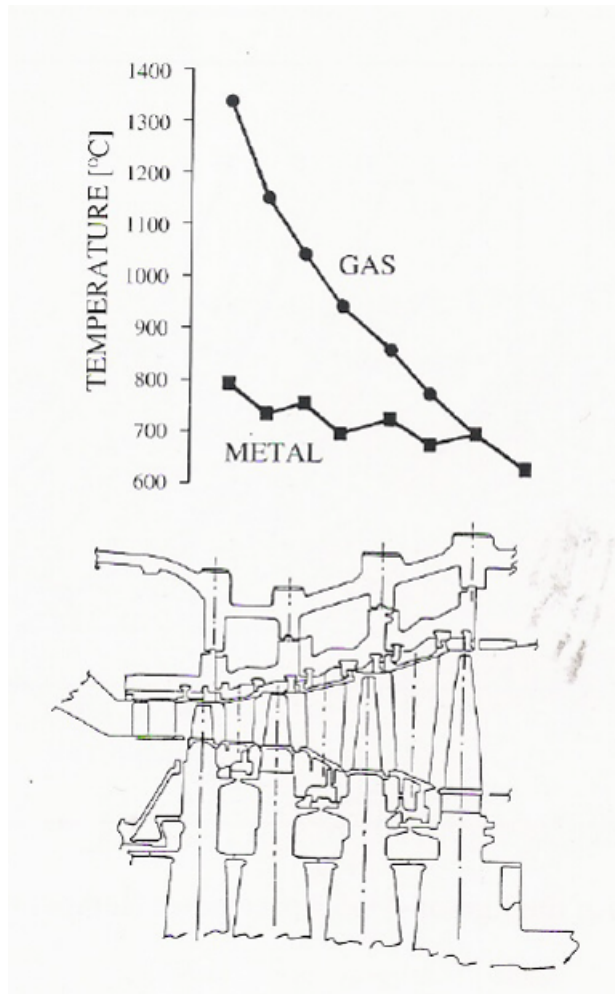


Figure 2.5: Example of temperature evolution at the different stages of a GT [13]

The main parts of the expansion turbine are the following [14]:

- *Vanes*: these are the stationary components of the turbine. Their main tasks are the transformation of hot gas enthalpy into kinetic energy and to direct the flow, guaranteeing optimal transformation on the turbine blades. These components are assembled in the Turbine Vane Carrier (TVC) that will be mounted into the turbine casing. As it can be observed from the Fig. 2.6, the vane is composed of an outer diameter (OD) platform, an inner diameter (ID) platform and the airfoil.

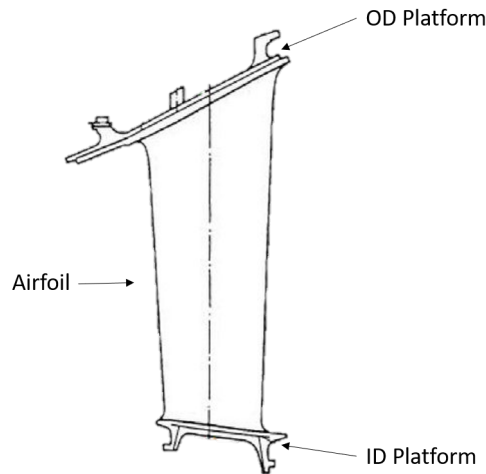


Figure 2.6: Turbine Vane [15]

- *Blades*: these are the rotating parts of the turbine, responsible of the transformation of enthalpy and hot gas kinetic energy into rotational mechanical energy, transferring it to the rotor. As it has been said previously, not all this energy will be available to turn the generator but a percentage will be directed to drive the compressor. Blades are attached to the turbine disc and are composed by the airfoil, which is tapered toward its tip and twisted an angle in order to increase its velocity and to guarantee an optimal incident angle with the hot gas, a platform at the inner diameter and the root. This last component, normally with a fir-tree geometry, must be designed properly in order to withstand the high centrifugal and thermal loads.

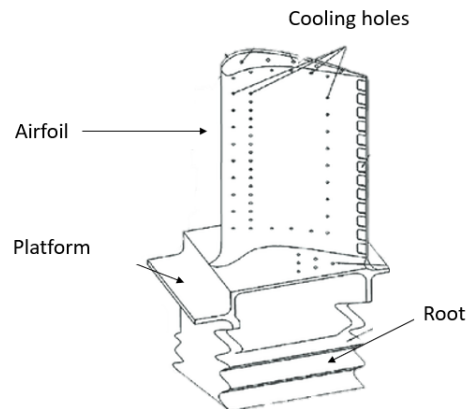


Figure 2.7: Turbine Blade [16]

- *Guide ring or Stator Heat Shield*: its main function is to keep the vane carrier from being in contact with the hot gas and the creation of the hot gas path profile contiguous to the rotating blades. These components share with the vanes, material, fixation and coatings solutions.
- *Rotor Heat Shield*: this component serves as a protection to the rotor from the hot gas underneath the turbine vanes. It is composed of a platform, leg and root. Its structure with its fins, gives the proper sealing condition to ensure the require protection.
- *U-Ring*: this last component is an alternative to the rotor heat shield. It acts as a leakage flow controller, preventing the ingestion of the hot gas path into the rotor. It is comprised of two halves U-rings.

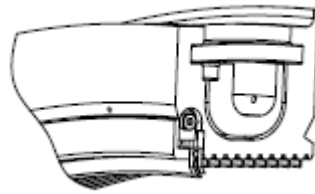


Figure 2.8: U-Ring

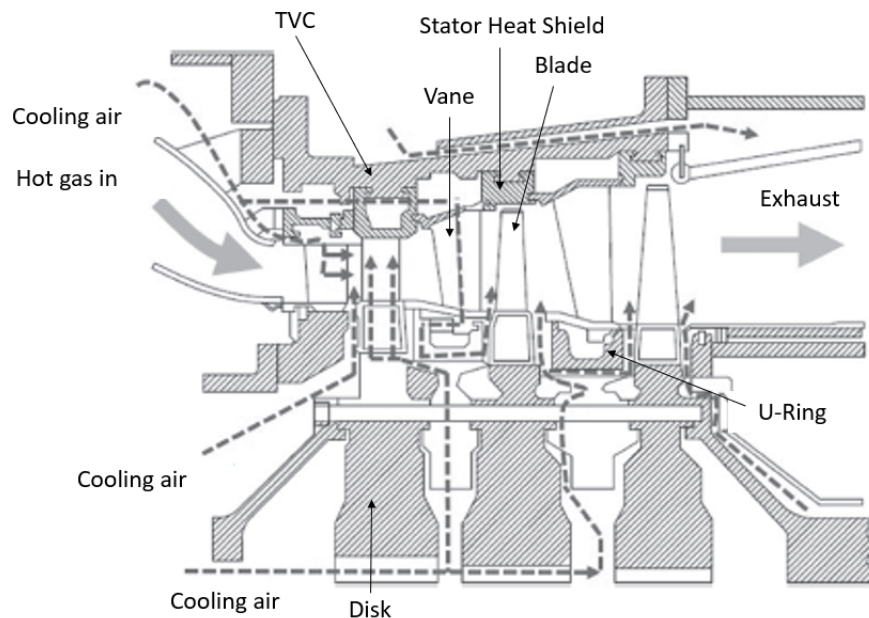


Figure 2.9: Parts of the expansion turbine section [17]

From the Fig. 2.9, it can be appreciated the parts of the expansion turbine already defined. Furthermore, it can also be observed the Hot Gas Path (HGP) and the cooling air path. From the HGP, it should be highlighted the importance of confining it, since a gas leak could produce a fast degradation and damage of the rest turbine components. Basically, this fact is due to the different materials that compose the parts that suffer the hot gas (vanes and blades) from the rest ones (disc and TVC). The different materials components will be explained more in depth in the following subsection (Section 2.2).

On the other hand, with respect to the air cooling system, it should be outlined that in modern gas turbine engines, up to 20 percent of the compressor flow is taken to perform cooling and sealing of the hot section components. [18] There can be remarked several methods such convection cooling, film cooling and impingement cooling that improve the performance of the GT by reducing up to 200 °C or more, the temperature of its blades and vanes. In the Figs. 2.10 and 2.11, it can be appreciated an example of the cooling system of a vane and a blade. Additionally, in the Fig. 2.12, it can be appreciated how the development of these methods allowed each time higher Turbine Inlet Temperatures (TIT), increasing therefore the GT efficiency.

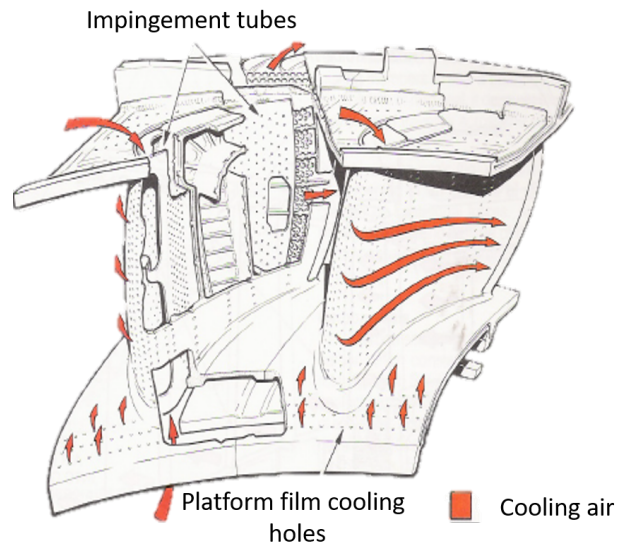


Figure 2.10: Example of the cooling system of a vane [13]

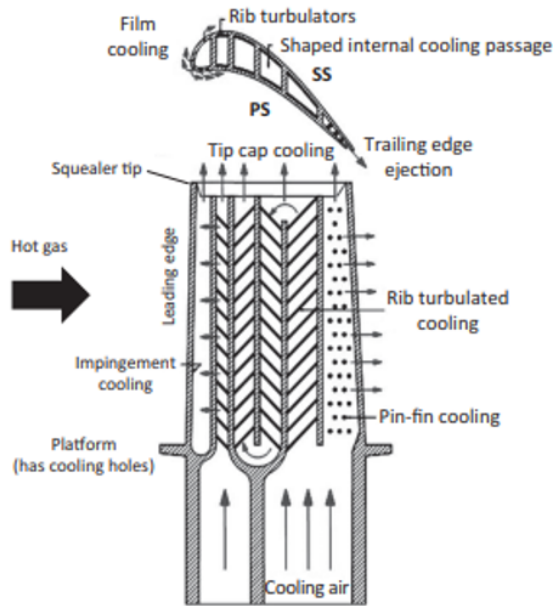


Figure 2.11: Example of the cooling system of a blade with PS = Pressure Side and SS = Suction Side [17]

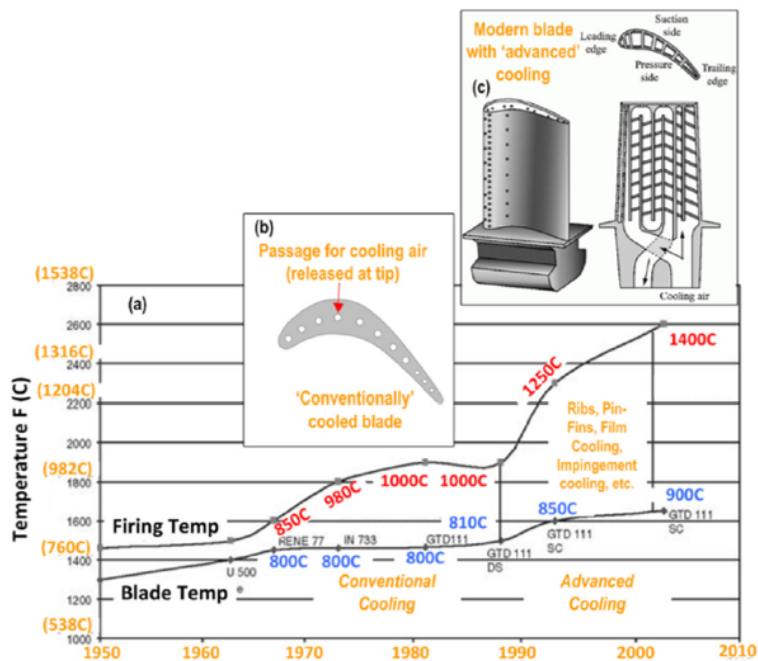


Figure 2.12: Cooling Evolution in the years Vs TIT [1]

2.2 Gas Turbine Materials

One of the most important requirements of GT components is the strength and mechanical integrity preservation, when subjected to the harsh working conditions, high pressures and temperatures in addition with corrosive environments. [14]

Important materials progresses were done within the end of the Second World War, when more knowledge about metallurgy was gained. It is clear that the perfect material, that it is able to bear all these adverse conditions has not been found, but each time, thanks to the advancement in technology, the applied coatings and the different casting techniques, the parts more stressed can tolerate higher temperatures.

The main materials used on the construction of GT are metals, mostly steels and super-alloys. While steels are especially for the disk, the TVC and the compressor stages, where the temperatures are not the highest, the alloys, in particular superalloys, compose the parts where the HGP flows, mainly the vanes and blades of the expansion turbine.[13]

Superalloys are a group of metal alloy, characterized by its good creep and oxidation resistance. Therefore, these materials are perfectly suited for working under high mechanical stresses and temperatures. The Fig 2.13 illustrates the better characteristics, in terms of temperature capability and oxidation resistance of the superalloys, with respect to the steels.

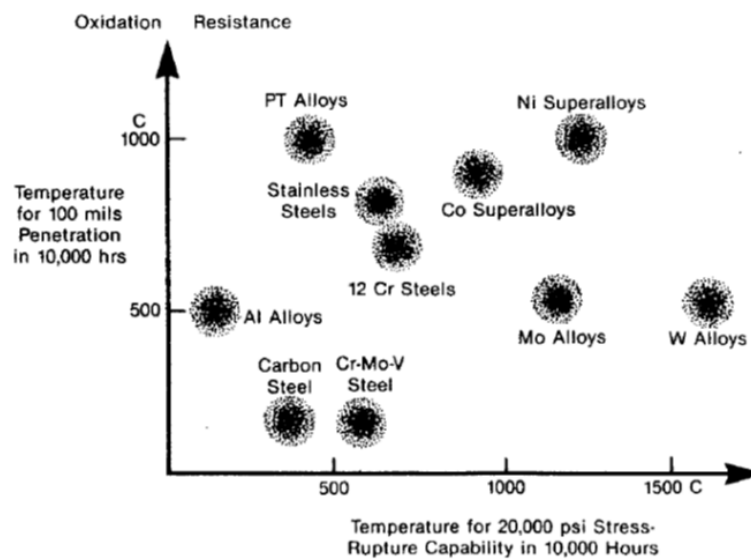


Figure 2.13: Temperature capability Vs oxidation resistance of some superalloys and steels [1]

Indeed, to quote from [17], superalloys can be used at temperatures as high as

85 percent of their melting point (around 1,260-1,270°C). Moreover, they can be divided in three groups:

- Cobalt-based superalloys
- Nickel-based superalloys
- Iron-based superalloys

It is important to remark that superalloys contain multiple alloying elements to improve its mechanical properties. For instance, some important elements for solid solution strengthening are Co, Mo and W. Also, in reduced quantities, elements such C, B, Zr and Hf can be present for a grain boundary strengthening. Moreover, in the Fig. 2.14, it can be appreciated the different elements introduced to Co and Ni-base superalloys with the correspondent achieved effects. Furthermore, in the Fig. 2.15, it can be appreciated the effects of the alloying elements but in this case in terms of corrosion and oxidation resistance.

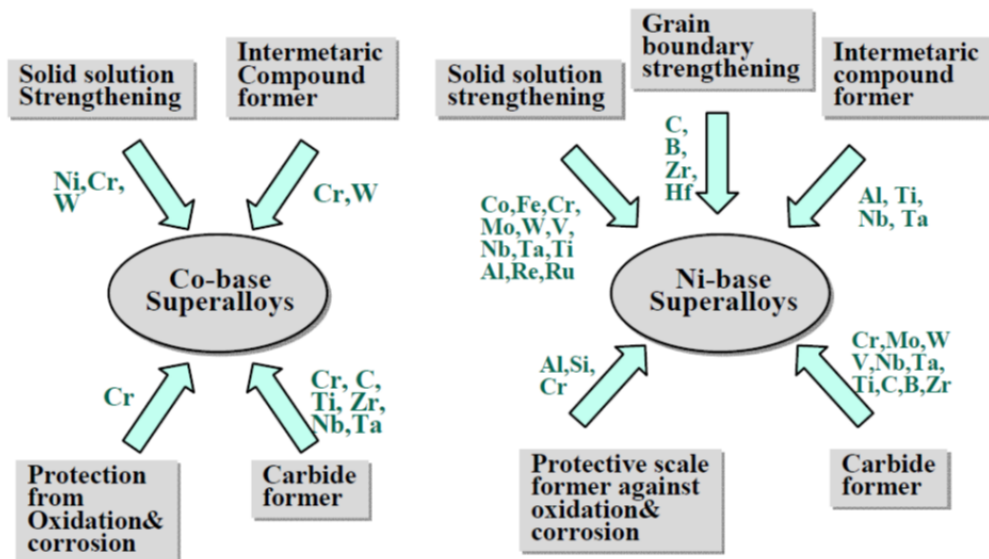


Figure 2.14: Role of alloying elements for superalloys [1]

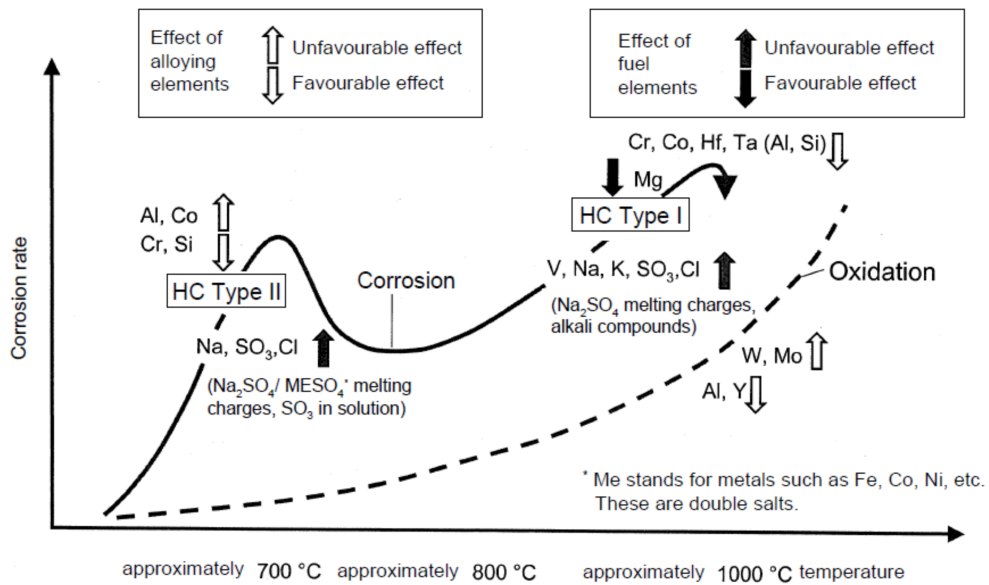


Figure 2.15: Role of alloying elements with corrosion and oxidation resistance [1]

In particular, nickel-based superalloys are the most important and used ones, due to two main reasons: the absence of an allotropic transformation of its base element and the possibility of strengthening by precipitation of a second phase called γ' . This phase is an intermetallic composite (Ni_3Al), that has its maximum strengthening effect at high temperature.[13] It is also important to outline another important phase within Ni-based superalloys, carbides. They are usually formed at grain boundaries during solidification process, giving important creep characteristics by inhibiting grain boundary deformation. The main carbides present in Ni superalloys are MC , M_6C and $M_{23}C_6$ with M representing Ti , Cr , Nb , Mo , Hf and Ta . [19] In Fig. 2.16, it can be observed the microstructure of some superalloys, whereas in Fig. 2.17, it can be seen its evolution.

As a result, nickel-based superalloys are the materials of choice to manufacture turbine HGP components, such as vanes, rotor blades, stationary and rotating airfoils, etc. However, another aspect of big importance when finding the proper material, is the consideration of the following statements:

- Type of component (stator vane or rotor blade)
- Hot gas path location (stage 1,2,3 or 4)
- Output and efficiency
- Rotational speed
- Cooling scheme

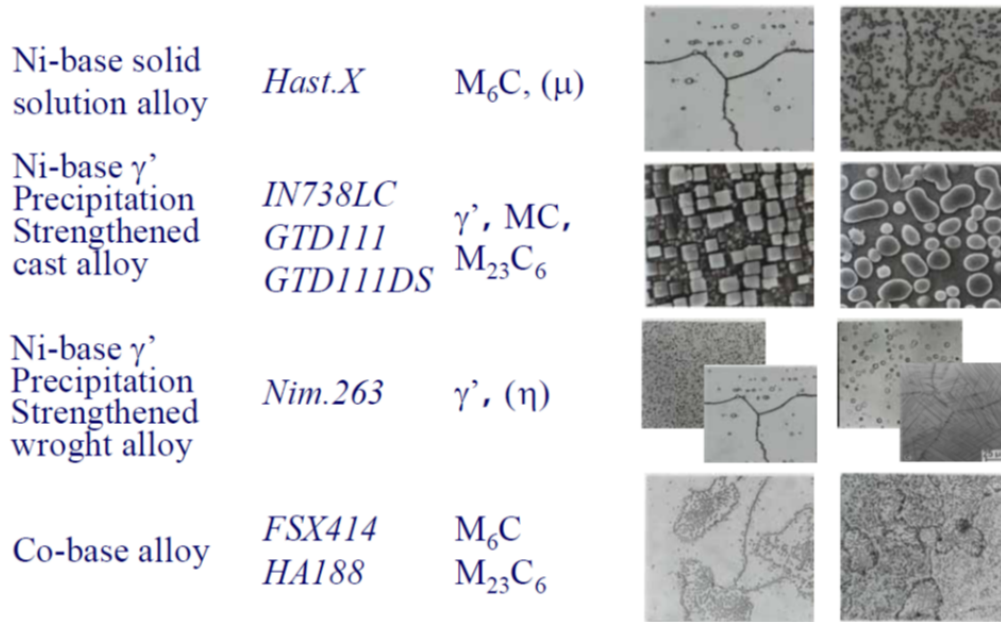


Figure 2.16: Microstructures of Superalloys [1]

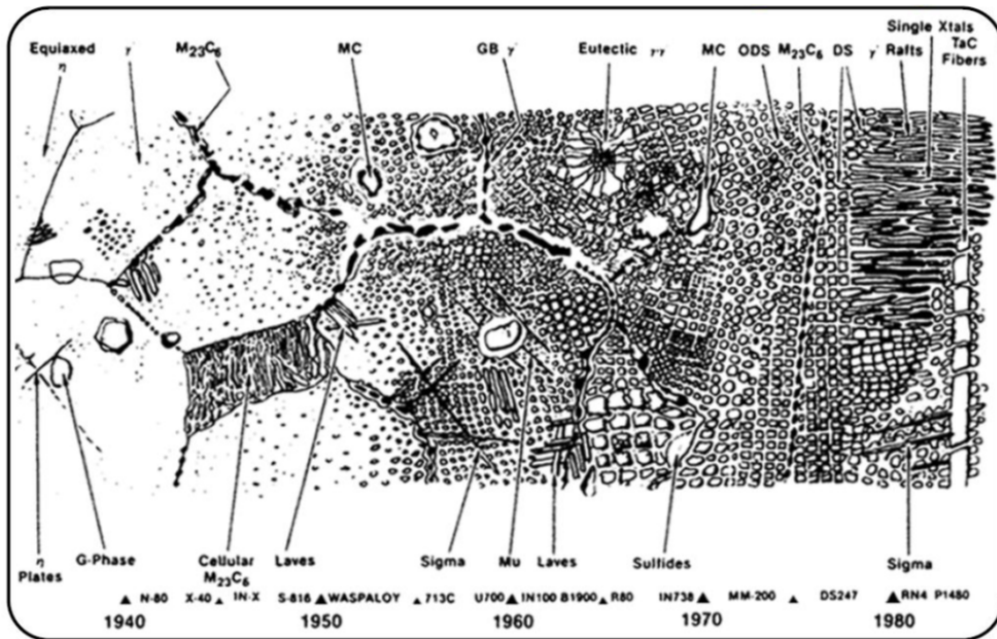


Figure 2.17: Microstructure Evolution of Superalloys [1]

- Fuel type

- Maintenance inspection intervals.

Finally, it is remarkable to say that several trademarks in advanced industrial GT appear frequently when it is talked about nickel-based superalloys such as Inconel, Udimet, René, etc.

2.3 Production process

The great difficulty of the cooling configuration of GT vanes and blades, in addition with its complex geometry, has resulted in the need of casting technology to produce them. The precision casting process, also called "lost wax process" is based on mould patterns. Copies of the blades are first formed by pouring wax into these metal molds. Once the wax shape has formed, it is removed from the mold and it is immersed in a ceramic slurry bath, creating a ceramic coating. Then, each group of ceramic coatings is heated to harden the ceramic and melting the wax. In this stage production, it is also formed the internal air cooling passages within each blade. Molten metal is now introduced into the hollow left by the melted wax.[20]

The following process, the solidification, will determine the grain structure within the turbine-blade superalloy material ("equi-axed", "directionally solidified" or "single crystal"). This step takes place in computer-controlled ovens, in which the blades are carefully heated according to precise specifications. The metal grains will assume the correct configuration as they cool, following their removal from the ovens. [20] Therefore, depending on the required mechanical characteristics of the component, it will be opted for realizing one of the following casting process [21]:

- **Conventional or equiaxed grain investment casting:** characterised by small grains of similar size without preferential orientation. Most used for the cooler parts of the engine.
- **Vacuum casting with directional solidification (DS):** significant advantages are found in terms of mechanical characteristics with respect to the previous one, due to the preferred crystallographic orientation of the grains and the avoidance of transverse grain boundaries.
- **Single-crystal (SC or SX):** the final component comprises only a single grain. The absence of grain boundaries provides much better creep and thermal fatigue resistance compared to polycrystalline alloys, giving therefore the best performance. However, due to the expensive costs that implies its production, the DS ones are the most used in the hottest parts of the engine.

Lastly, the final shape will be given via machining processes, where also holes will be formed via laser beam or by spark erosion, finishing the interior cooling passageways.

In Fig. 2.18, it can be observed the whole production process of these components. Instead, in Fig. 2.19, it can be appreciated the solidification process to get each grain microstructure stated, where in Fig. 2.20 the final result in a blade is illustrated.

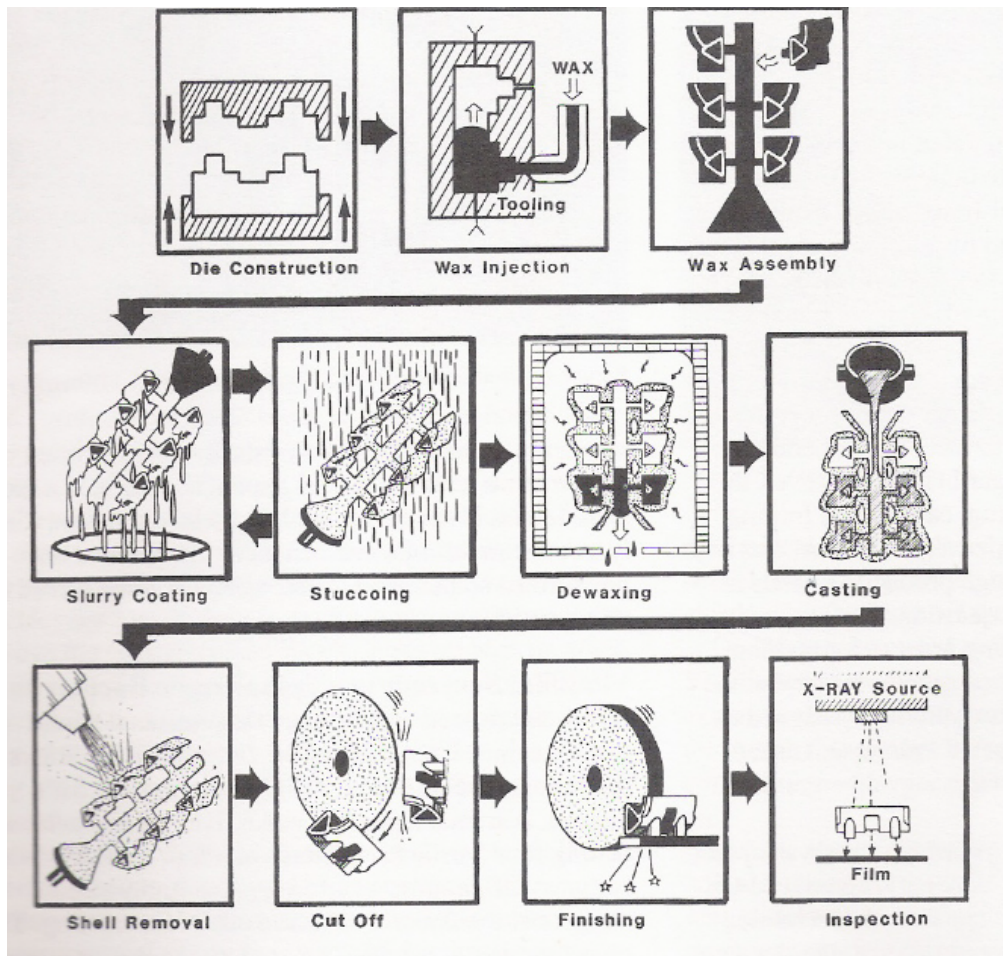


Figure 2.18: Production Process of GT vanes and blades [13]

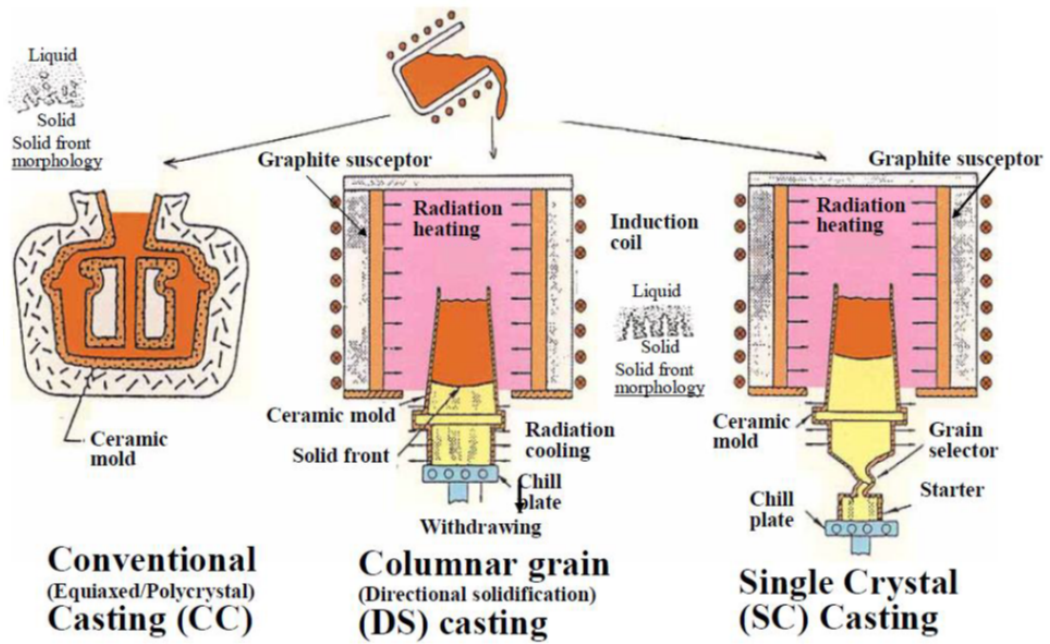


Figure 2.19: Solidification Process of GT vanes and blades [1]

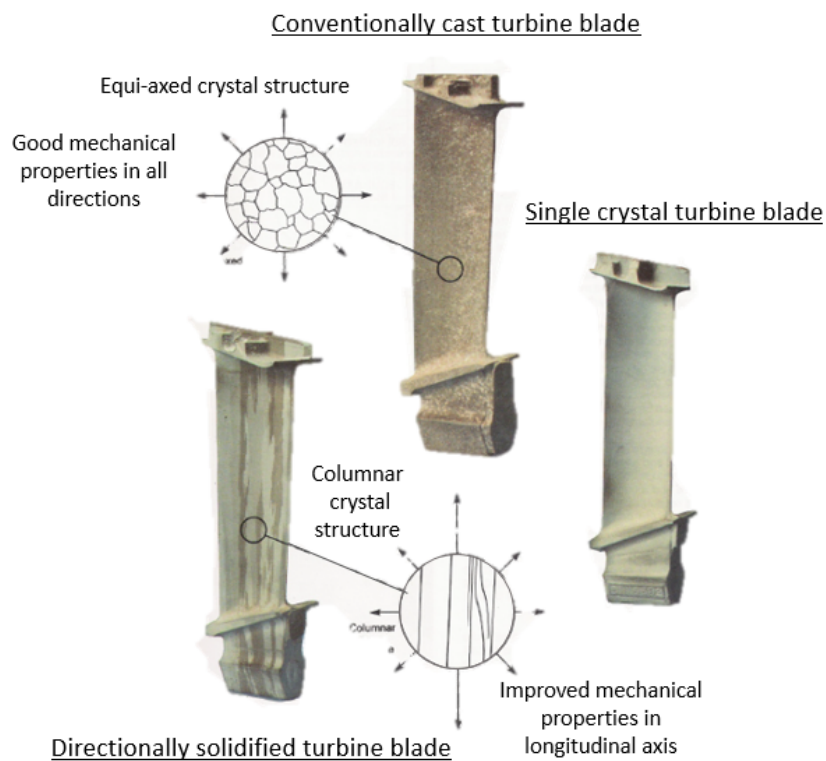


Figure 2.20: Different grain microstructure of a GT blade [13]

In the figure above (Fig. 2.20), it is noticeable the improvement in terms of creep strength and ductility of the columnar grains aligned parallel to the primary stress axis of the DS and SC casting, resulting also in higher resistance to thermal fatigue at elevated temperatures.

From the figures below (2.21 , 2.22 and 2.23), these statements are illustrated graphically, where it can be appreciated the best creep and fatigue characteristics on SC casting alloys. Furthermore, in the Fig. 2.24, it can be observed the creep strength with the temperature for different group of materials, obtaining once more, the best creep characteristics for SC *Ni*-based superalloys. Therefore, blades and vanes of the first two stages of the turbine (which suffer from highest temperatures as illustrated in Fig. 2.5) are manufactured following SC casting techniques. [17]

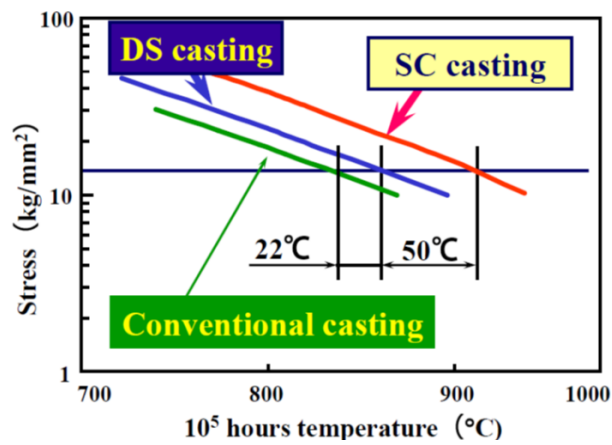


Figure 2.21: Creep rupture life of CC, DS, and SC Alloys [1]

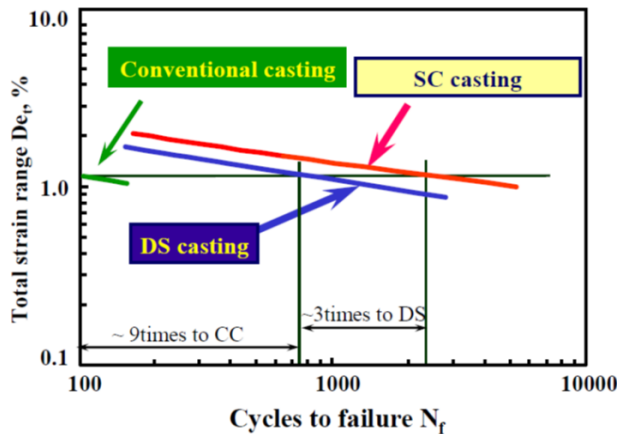


Figure 2.22: Thermal Fatigue Life of CC, DS and SC Alloys [1]

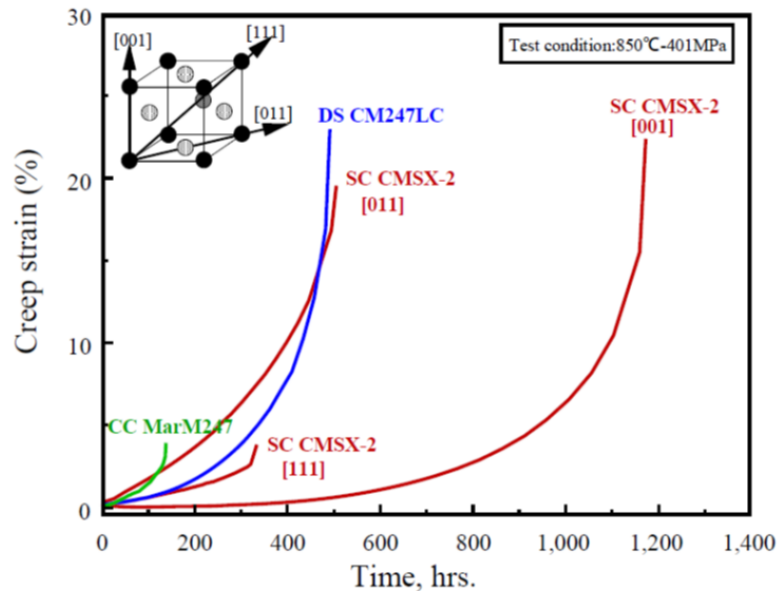


Figure 2.23: Creep Behaviors of CC/DS/SC Alloys [1]

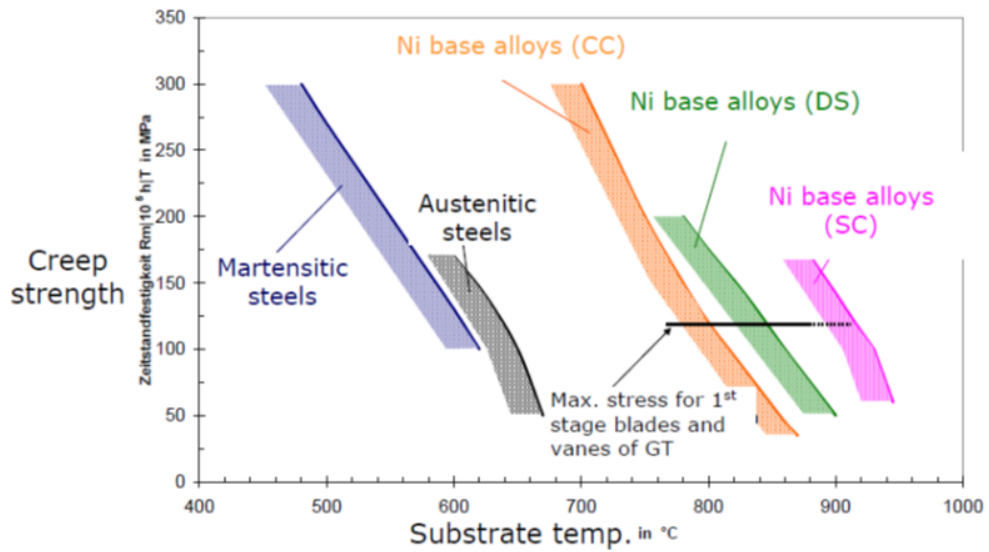


Figure 2.24: Creep strength with temperature for different groups of materials [1]

Furthermore, it is interesting to observe in the following figure (2.25), the production process evolution, from the wrought techniques, which did not allow elevated inlet temperatures, up to the nowadays single crystal techniques.

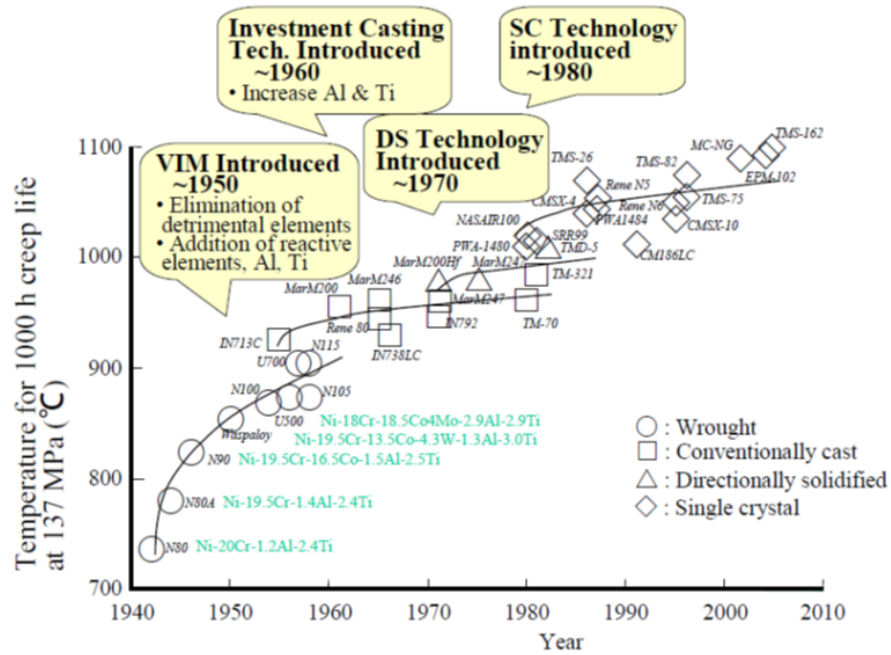


Figure 2.25: Evolution of the production processes with the temperature capability [1]

Finally, it is also important to mention the necessity of special coatings. These ones will supply the required corrosion and oxidation resistance, since the low amount of Cr on the superalloy (to make space for refractory metals) does not guarantee the proper protection against these phenomena. The protective coatings are mainly of two types: *diffusion* ones such as platinum-aluminide or *overlay* coatings such as $MCrAlY$ where M is Co , Ni or Co/Ni .

Furthermore, a second ceramic layer called TBC (Thermal Barrier Coating) is applied on top of this first protection, reducing thermal loadings. So, the combination of the coatings in addition with the different casting techniques already stated, make possible the increase of the turbine inlet temperatures (TITs) up to $1,600^{\circ}C$ with long maintenance intervals. For instance, in Fig.2.26, it is represented the evolution in temperature's capability, where it can be observed that thanks to the TBCs development and film cooling techniques, the components can withstand each time higher temperatures.

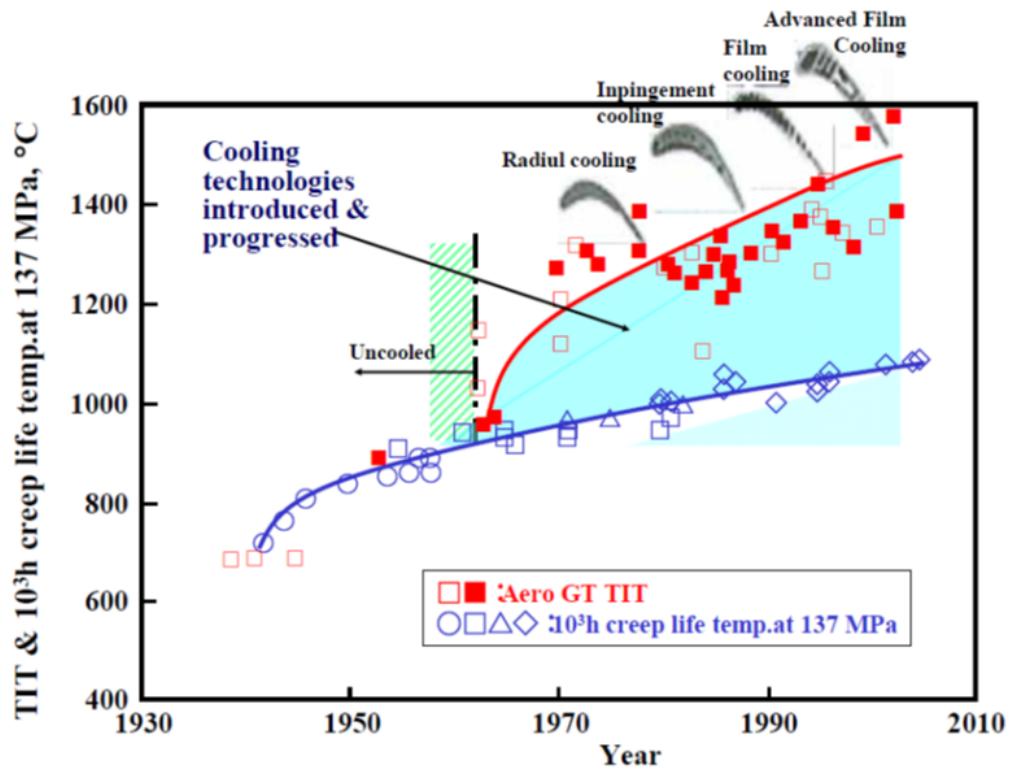


Figure 2.26: Evolution of TIT thank to the introduced cooling technologies [1]

2.4 Workflow of GT Blade and Vane

Regarding the expansion turbine development, several disciplines work together, bringing the whole component out. A new GT blade vane project starts from aerodynamic evaluation (AERO). This discipline defines the external profile of the new airfoils, then heat transfer team (HT) works on the internal details, for example cooling system scheme, film cooling holes and internal turbulence promoters.

After that a preliminary 3D CAD model is prepared by mechanical design team (MD), considering external profiles from AERO and internal features from HT. This 3D preliminary model is transferred to mechanical integrity group (MI) for preliminary evaluation of stresses, lifing and dynamic behaviour.

All this design loop must be repeated up to arrive to compromise solution able to achieve the aero performance and component lifing foreseen from the product specification.

At the end of this process a final 3D CAD model is released to start the production qualification process with the casting and special process suppliers.

2.5 Mechanical Integrity Assessment

In this work, it has been worked under the MI discipline, therefore, once the main parts of the downstream turbine and its proper materials have been discussed, it is important to know the required evaluation that these components must pass through. As a result, in this section, it will be provided a fast overview of the major phenomena that make the components fail prematurely.

As it has been said previously the *perfect material* does not exist. As a consequence, they are subjected to a mechanical properties degradation (strength and resistance to corrosion) while working under harsh conditions, leading to shortening of the component design life.[17]

These reasons, the ones that affect directly the integrity of the base material, are called *direct* ones and can be divided into two categories: *thermo-mechanical* and *corrosion*. However, electric power generation GT burns mostly natural gas, which reduces considerably the last term. Nevertheless, it is important to maintain an inlet air filtration system as well as an appropriate water treatment in order to reduce the presence of contaminants that coexist in ambient air, minimizing possible corrosion. [17] On the other hand, the *thermo-mechanical* ones are a consequence of the working conditions that the turbine components are subjected to. In particular, they have to withstand high surface temperatures (up to 1000°C locally and up to 800°C average on a section), which produce important temperatures gradients in the wall thickness, pressure loads between the coolant flow and the hot gas, centrifugal loads for rotating parts, forces coming from other components through contact faces, vibrations and start-up/shut down cycles and full load cycles. All these conditions generate stress situations, producing thermo-mechanical effects. The main three are *creep, fatigue and brittle failure*. [14]

Alternatively, it must also be outlined the *indirect* causes. These ones are related to the degradation of the coatings, the lowering of air-cooling efficiency and dimensional changes that do not alter the materials but still produce a degradation of the integrity of the whole component. [14]

As a result, it can be said that one of the most important objectives of a designer is to guarantee the mechanical integrity of the gas turbine components. Therefore a MI assessment (studying the direct and indirect causes) must be done during the whole operation of the gas turbine in order to control and monitor them continuously.

2.6 General static stress description on components

The already stated GT operation conditions lead into stress situations within the GT components. The stress on the GT components can be divided into [14]:

- **Primary stress:** normal or shear stress produced by mechanical loads (the imposed loading) that satisfies the laws of equilibrium (internal and external forces and moments). Its main property is that is not self-limiting and therefore, a considerably overcome of the yield strength will result in failure or at least, great distortion. Simultaneously, primary stress can be categorized into:
 - **Membrane stress:** primary stress component that is distributed in a uniform way, being equal to the average value of the stress across the thickness of the section of consideration. Here, no redistribution of stress occurs as a result of yielding. Discontinuities and concentrations are excluded.
 - **Local stress:** primary stress component that produces great distortion in the transfer of load to other parts of the component. Here, it is again the average of the primary stress across the solid section, but taking into account the discontinuities. However it does not take into account the concentrations.
 - **Bending stress:** primary stress component that is proportional to the distance from the solid section centroid. It does not consider either discontinuities or concentrations.
- **Secondary stress:** normal or shear stress created by adjacent parts constraints or by self-constraints of a structure. It is self-limiting and failure can happen due to local yielding or minor distortions that satisfy failure conditions. Secondary stress is created mainly by **thermal stress**, which is characterized for being a self-balancing stress, created by a non-uniform distribution of temperature or by different thermal expansion coefficients, to satisfy structure continuity. This stress will be explained in detail in the following subsection, since it is the principal stress that vanes are subjected to.
- **Peak stress:** represents the increment added to the primary or secondary stress by a concentration. It does not cause any noticeable distortion and it is objectionable only as a fatigue crack or brittle fracture possible source.

It also should be outlined, that residual stresses are not consider in the design criteria: the component is supposed to be relieved from them before new operation.

2.6.1 Thermal Stress

Thermal stresses are the principal ones for GT vanes, for this reason, a more detailed explanation will be done under this subsection. In Applied Mechanics, thermal stress is defined as a mechanical stress created due to changes in temperature of the base material. Those changes can produce plastic deformation or even fracture of the component. The two main causes that generate this phenomenon are *constrained thermal expansion or contraction* and *temperature gradients*.

In the first case, when a body with free movement is heated or cooled, since there are no constraints that prohibit its movement, it can expand or contract freely. Whereas, if the same body is heated or cooled, but in this instance, it is constrained, this is to say it can no longer expand or contract freely, thermal stresses, *compressive* and *tensile*, will appear respectively. Furthermore, this thermal stress can be represented as:

$$\sigma = E \frac{\alpha}{1 - \nu} (T_i - T_f) \quad (2.1)$$

Where T_i refers to the initial temperature and T_f to the final one, E is the elastic or Young's modulus, α is the linear coefficient of thermal expansion and ν is Poisson's ratio, where all are function of the temperature.[17] From the Eq. 2.1, it is remarkable that the thermal stress depends highly on the thermal expansion coefficient that changes from material to material. Mostly, the greater is the temperature change, the higher the level of stress will be.

On the other hand, the second cause are the temperature gradients across a body that is heated or cooled. In this concept, it is important to remark the word *rapid*, since *gradual* changes in temperature over a long period do not produce thermal stress, (there is thermal equilibrium between the solid and the ambient). However, with fast changes, when a body is heated, the external wall of the body becomes hotter than the interior one, and therefore, it expands more. This movement produce compressive stresses on the external face of the body, whereas in the internal one will appear tensile stresses, balancing each other, obtaining the required mechanical equilibrium.

This last cause is one of the major problems of turbine vanes; the aerodynamic shape of the airfoil, makes difficult to have the same degree of cooling in all the areas. This fact leads to an uneven cooling of the vane, translating into temperature gradients in the wall thickness and along the airfoil.

2.7 General dynamic stresses description on components

The description of GT dynamic is reported for sake of completeness. The GT components dynamic analysis is a very demanding task for the structural designer,

who must avoid resonance conditions within the machine operation range or, alternatively, control the amplitude of vibration by introducing additional damping into the system.

Under this subsection a fast overview of the two main dynamics phenomena will be explained. The dynamics analysis necessarily starts from the modal analysis of the system in order to identify its natural frequencies and its own modes. Then, having identified the typical frequencies of the force, it will be necessary to check for the presence of resonances within the machine operating range and calculate the response amplitude.

2.7.1 Vibrations

The study of vibrations in rotoric components is of fundamental importance, since it is one of the major causes of blades failure. Such investigation requires the analysis of the two key parameters *mode* and *natural frequency*. However, due to their complexity in a turbine blade, they will be illustrated in a much easier example: a spring with a mass, as illustrated in Fig. 2.27.

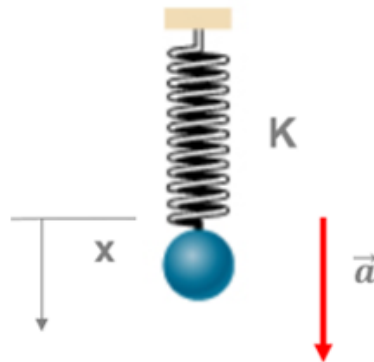


Figure 2.27: Example of a spring with a mass

The term *mode* is defined as the motion pattern of a system oscillating at its natural frequency.[22] Therefore, the mode of this system (spring and mass) is the up and down oscillation around the equilibrium point as the Fig. 2.28 shows.

Whereas, the *natural frequency* is defined as the frequency at which a system tends to oscillate in the absence of any driving or damping force.[22] In this case, the natural frequency is equal to:

$$f_n = \sqrt{\frac{k}{m}} \quad (2.2)$$

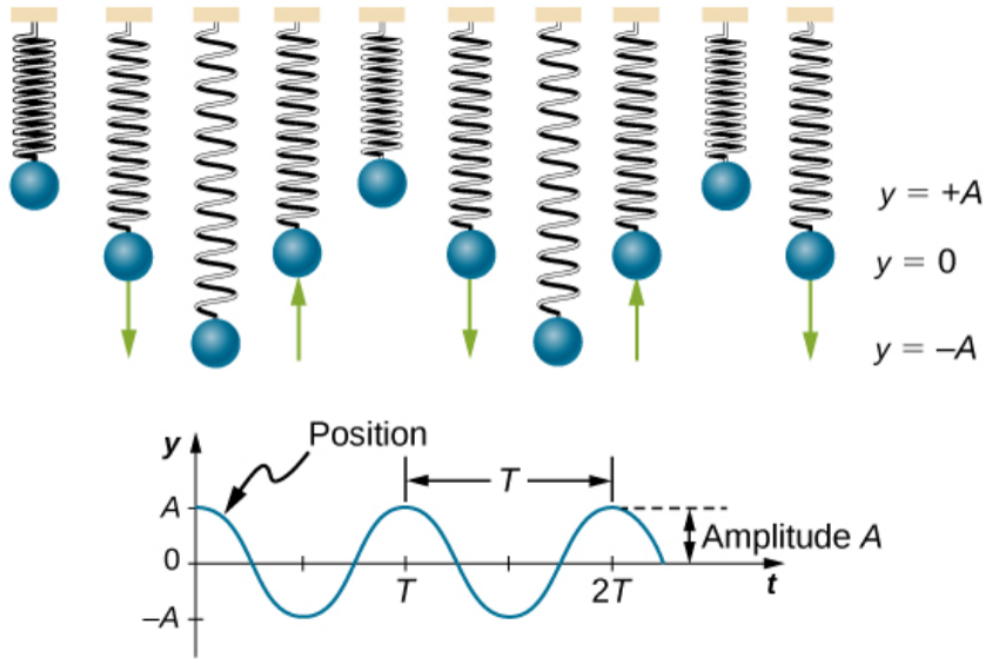


Figure 2.28: Oscillating up and down mode of the spring with a mass [23]

where k is the spring constant and m is the mass. The unit of the frequency is Hz or s^{-1} [17]. If the oscillating system is driven now by an external force, $F = F_0 \sin \omega t$, with $\omega = 2\pi f$ (angular frequency, rad/s), the oscillations of this system will be represented mathematically in the following equation:

$$A = \frac{F_0}{\sqrt{k^2 \left(1 - \frac{\omega^2}{\omega_n^2}\right)^2 + c^2 \omega^2}} \quad (2.3)$$

where c represents the "viscous damper" of the system, A , the amplitude of the system, ω_n , the natural angular frequency in rad/s and the rest parameters that have been already defined. From the Eq. 2.3, it is noticeable that when there is no damping ($c=0$) and, when the natural frequency coincides with the frequency of the exciting force ($\omega = \omega_n$), the amplitude becomes infinite ($A \rightarrow \infty$). Although, it will not be the case when the system has damping ($c \neq 0$), the amplitude can achieve extremely high values. This effect is called *resonance* and avoiding it, is of extreme importance.

Coming back to the blades, it is important to highlight that they have several modes of oscillation, (Fig. 2.29 represents three of them), and each mode, i , has its natural frequency, f_i . As it has been said, due to its difficulty, the help of external

and powerful tools, as finite element analysis (FEA), are needed to obtain them. In addition, it is important to remark that larger blades, since they have higher mass ($f \propto \frac{1}{\sqrt{m}}$), have lower natural frequencies than the shorter ones. Therefore, they can be excited by lower harmonics¹(below the eighth harmonic) [17].

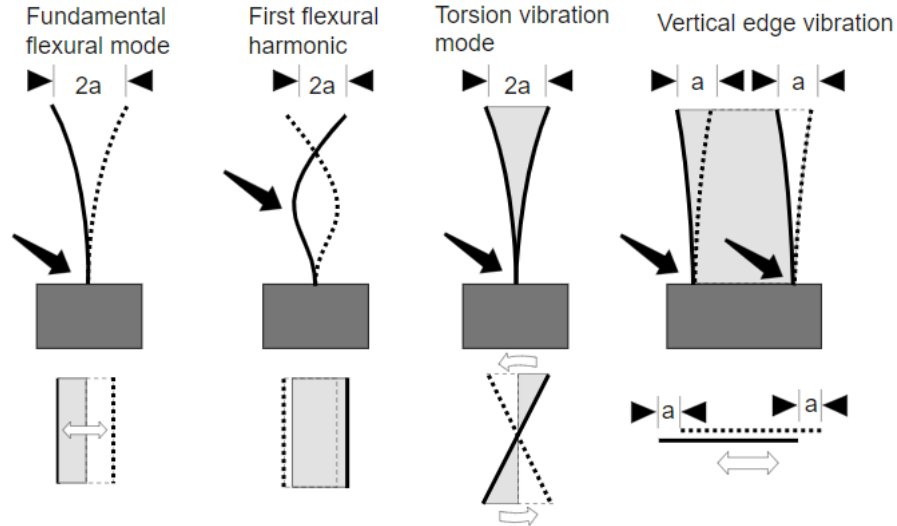


Figure 2.29: Modes of vibrations for a single blade from the FEA [24]

It is evident that, this effect should be avoided by engineers, since it can bring the component to failure via HCF (High Cycle Fatigue). *Campbell Diagram*, which represents on the abscissa, the turbine speed and on the ordinate, the frequency, as it is illustrated in Fig 2.30, will be of special help to attain this task. From this figure, it is also noticeable, on one hand, the different natural frequencies for different vibration modes on the ordinate. And, on the other hand, it can be appreciated the different excitation frequencies (Engine Orders), such as the running speed and its six harmonics. As it has been said, the coincidence of the exciting frequencies with the natural frequencies leads to resonance, although it is important to remark that this intersection does not necessary imply dangerous conditions, since it will be also required appropriate phase and modal couplings. [25]

The main vibration excitation sources in a gas turbine are the following [17]:

- Non-uniform flow or complex axial to radial flow behaviour or even flow

¹The harmonic of a wave is a component frequency of the signal that is an integer multiple of the fundamental frequency (i.e., if the fundamental frequency is f , the harmonics will be $2f$, $3f$, $4f$, etc.). In turbomachinery, this term is called *engine order* [17]

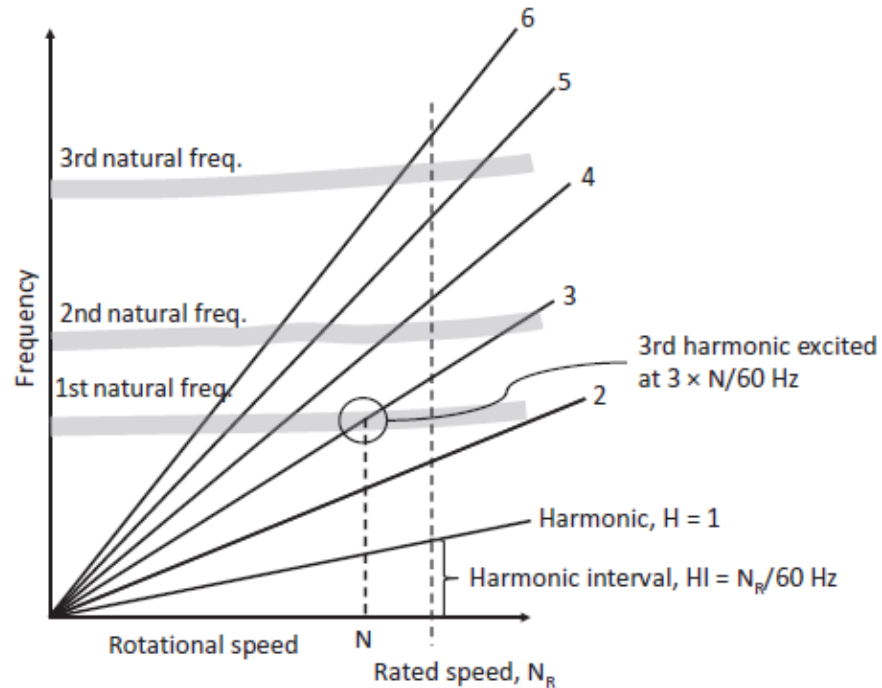


Figure 2.30: Campbell diagram [17]

distortion.

- Periodic effects due to manufacturing constraints.
- Nozzle excitation when the blade passes a stationary vane.

The first two sources, produce excitation at lower harmonics of the rotational speed, whereas the last one creates excitation at much higher frequency. Generally, the higher the harmonic, the lower the amplitude of vibration will be. [17]

All these problems can be "detuned" by adding or removing mass to or from the shrouding, or by adjusting the blade mass near the tip. In large blades, the damping can be accomplished by adding tip shrouds or snubbers.

Concluding, it can be said that the main goal for blades designers is to prevent resonance in the band around the design rotational speed (50 or 60 Hz), and in the low-cycle operational range. However, the passage through resonance zones during start-up and shutdown is unavoidable.[17]

2.7.2 Flutter

There is a second kind of vibration called *flutter*. It is described as an aeroelastic instability that can lead to *self-excitation*, due to the exchange of energy between the structure and the fluid. Thus, this type of vibration is not related with the engine orders, but with phenomena related to acoustic resonances, unsteady flow separation or even surface pressure fluctuations. So, in other words, flutter is a special case of non-synchronous vibration at low to moderate "reduced frequencies".[17] This phenomenon can be divided into two categories:

- *Stalled flutter*. In gas turbines, when the airfoil is subjected to a negative angle of attack at low loads or high back pressures, stalled flutter occurs. It creates a stalled region at the trailing edge, that degenerates into an unstable vibration. It is normally limited in the upper part of the blade due to the centrifugal forces effect. In addition, this phenomenon can lead into blade failure via HCF due to an accumulation of a high number of cycles in a short period of time. [17]
- *Unstalled flutter*. It is created when there is no flow separation and, the flow is attached to the airfoil during the whole time, without stall conditions and at high rates. Principally, it comes with the creation of a vortex that sheds downstream of the blade's trailing edge. If the frequency of the vortex equals the natural frequency of the blade, this phenomenon occurs and can lead to HCF.[17]

2.8 GT Damage Mechanisms

The extremely high temperatures and stresses attained at the GT expansion turbine section, result in the creation of damage mechanisms that can lead to the component premature failure.

Fracture mechanics is the discipline that studies the mechanical performance of cracked components subjected to applied loads. In other words, it studies the crack evolution due to these damage mechanisms, mainly fatigue, creep and oxidation or a combination of them. Therefore, the overall lifing of the component is estimated, $N_{cyclic} = N_{LCF} + N_{FM}$, where the first term refers the predicted LCF (Low Cycle Fatigue) cycles to crack initiation and, the second term, the number of cycles with stable crack propagation.[14]

Hereafter, it will be explained briefly these phenomena that lead to crack initiation, where in the following chapter (Chapter 3), a more thorough analysis will be done trough all these subjects.

2.8.1 Fatigue Fracture

The term fatigue references the phenomenon that under the action of repeated or fluctuated stresses, with maximum values lower than the tensile strength of the material, results in fracture. It is characterized for being progressive, starting as micro cracks that evolve under the fluctuating stresses. [17] It can be divided into:

- *HCF (High Cycle Fatigue)*, which takes place at high numbers of cycles as indicates its name (\propto 1,000-1,000,000 cycles) or large stress applications.
- *LCF (Low Cycle Fatigue)*, which takes place with a number of cycles between 10 to a few hundred per year. A typical case is the thermo-mechanical stresses created in the start-stop cycle of a power plant.

It is important to remark that, there is not a clear distinction between LCF and HCF, but generally, it is said that HCF does not lead to plastic deformation, categorised as *brittle fracture*. Meanwhile LCF can form some permanent plastic deformation, remaining after the elimination of the load or force that originated it in first place. [17]

Several methods are employed by engineers in order to estimate the number of cycles to failure. One of the most used, is the *S-N curve* or also called *the Wöhler curve*, illustrated in Fig. 2.31. This method plots on the *x*-axis the number of cycles before a reduction of stress is observed (supposing that failure may take place) and on the *y*-axis the alternating stress amplitude in MPa or psi. It can be observed that a reduction of the stress leads to an increase of the component life.

The following terms shall be defined for a S-N curve [26]:

- *Fatigue limit*, also called *endurance limit*. It is the stress level below which fatigue failure does not happen.
- *Fatigue strength*, S_{Nf} , as the ASTM stated (American Society for Testing and Materials), is the value of stress at which failure occurs after some specified number of cycles.
- *Fatigue life*, is defined as the number of cycles to failure at a specified stress level, taken from the S-N plot.

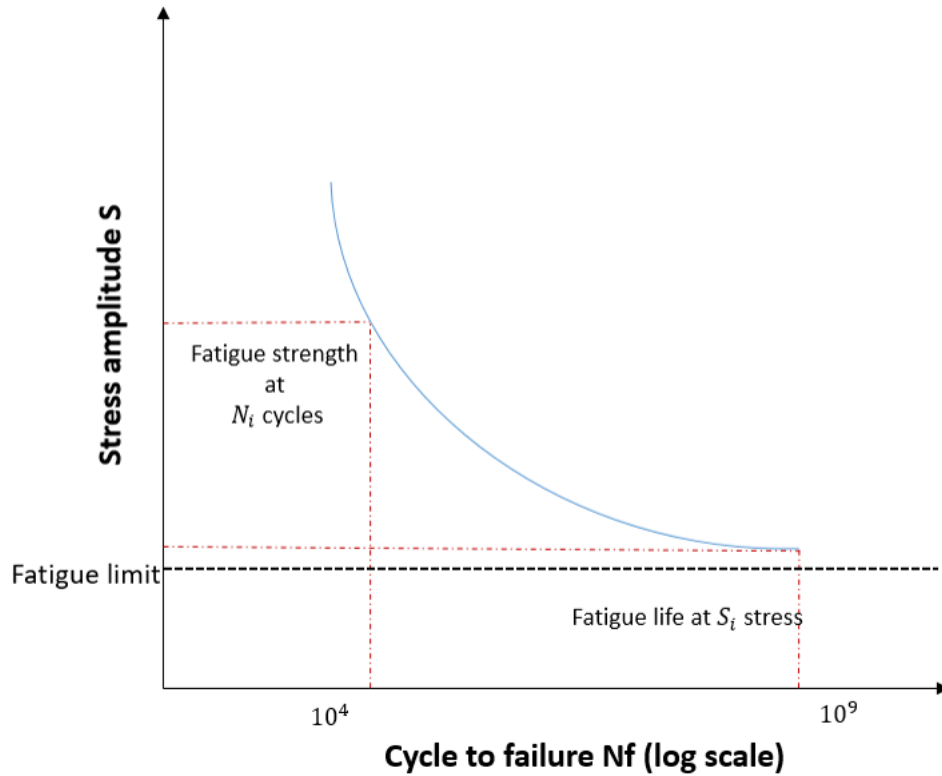


Figure 2.31: S-N Curve [26]

It is important to remark, that when a element is subjected to repeated cycles loads, these ones can have an *alternating* component and a *mean (offset)* component as illustrated in Fig. 2.32. Since S-N Curve is created with an alternating stress with no mean factor, it will be needed a mean stress correction for the parts that are subjected to loads with this last term. [27]

One possible choice to achieve this task is by the *Goodman* line (illustrated in Fig. 2.33), where the alternating stress is represented in the y -axis, being σ_e' , the purely alternating stress that will cause failure at N_f cycles. Whereas the mean stress is plotted on the x -axis, being σ_u , the ultimate tensile strength of the material. If the combination of the alternating and mean stresses remains under the Goodman line, the part will survive. If it lies above it, the component will fail. [17]

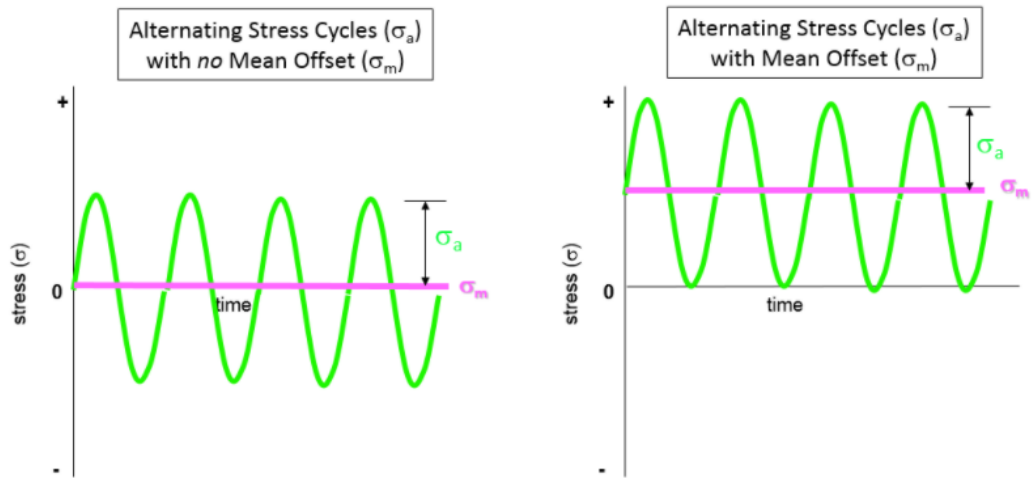


Figure 2.32: Left - An alternating stress with no mean stress. Right - An alternating stress with a mean stress offset [27]

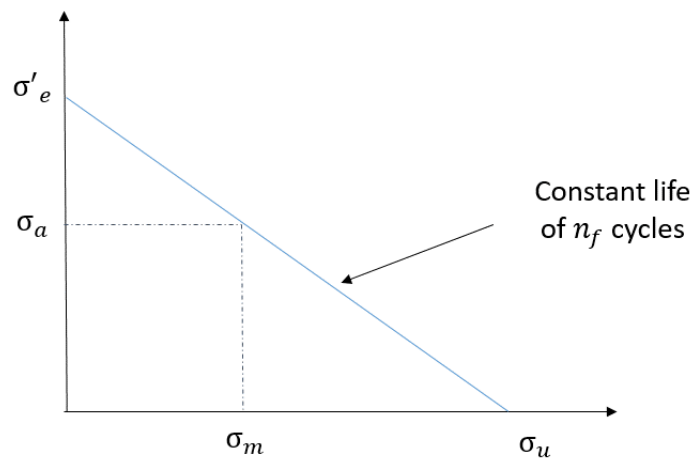


Figure 2.33: Goodman line [17]

In turbine blades analysis, the total stresses are a combination of static (centrifugal) and vibratory (gas bending) stresses, σ_m and σ_a respectively.

2.8.2 Creep

Creep is defined as a time-dependent phenomenon that leads to visco-plastic deformation on components that are subjected to high temperatures and applied loads. The important parameter is the one called *time to rupture*, which depends on the *yield strength* of the material (its inherent strength) and the environmental conditions (temperature and stress). A rise in either or both working conditions will diminish the time to rupture. [17]

From a gas turbine perspective, the major concern is the long-term, high-temperature creep. Therefore, a material with excellent creep properties and good coatings should be selected, guaranteeing a good margin of safety under the harsh conditions.

Additionally, it is important to remark that in turbine components, the creep effect happens under constantly applied loads (pressure, centrifugal), meanwhile there is another effect called *stress relaxation* that takes place under the effect of thermal stresses and displacement restraints. The combination of both phenomena leads to permanent deformation in the component. Moreover if the creep is in an advanced state, it can result in void formation, what is called as *creep cracking*, in the base material. It is mandatory to avoid those effects to ensure safe operation on the parts.[14]

2.8.3 Oxidation

Oxidation process is defined as an electrochemical reaction between Oxygen molecules and other substances, such as metals or living tissues. Technically, it is described as the loss of at least one electron when two or more substances interact.

In turbine parts, this phenomenon happens when they are subjected to high temperatures, which results in wall thickness reduction and loss of material strength. For this reason, it is very important its protection by metallic coatings.[28]

Chapter 3

Fracture Mechanics

In the following chapter, a more in depth analysis of fracture mechanics will be done. In first place, it will be presented the main concepts of fracture, analyzing the two approaches that study crack propagation within the Linear Elastic Fracture Mechanics (LEFM) limits. Then, crack propagation concepts will be discussed, presenting the main effects that produce crack growth in GT and the tools used for estimating the final component life.

3.1 Fundamentals of Fracture Mechanics

The study and development of fracture mechanics is each time of greater importance, mostly in industrial fields, due to the necessity of avoiding suddenly failures. Fracture mechanics theory is based on the hypothesis that real components have inherent cracks and flaws. These ones may be originated during the manufacturing stage or later as a result of the working conditions.[29] Its presence makes of vital importance the progress of this science, since they degrade the mechanical integrity of the components under the action of applied loads and environmental status.[30]

Fracture mechanics employs applied mechanics concepts to study crack growth, understanding the stress and deformation fields around its apex.[30] As its name indicates, it deals with fracture phenomena. At microscopic level, a material will fracture when the stress is sufficient to break the bonds that hold together the atoms, where the bond strength is supplied by the attractive forces between them. [31] Fracture can also be defined as the separation of a material into two or more pieces under the action of an applied stress. It is the final culmination of the plastic deformation process.

The two main modes of fracture in metals are *brittle* and *ductile*. Brittle fracture is characterized for negligible plastic deformation at the crack apex, breaking without warning in an unstable way, whereas ductile fracture experiences plastic

deformation propagating slowly. In other words, the components will undergo continuous deformation only propagating when more stress is applied. However, independently of the type of fracture, during failure, the material will experience crack formation and its propagation in response to the applied stress. [32] For this reason, the three main parameters that fracture mechanics analyzes are [31]:

1. The global *stress* applied on the component (σ).
2. The resistance to fracture called *fracture toughness*, that is a material characteristic.
3. The flaw *size* present on the component.

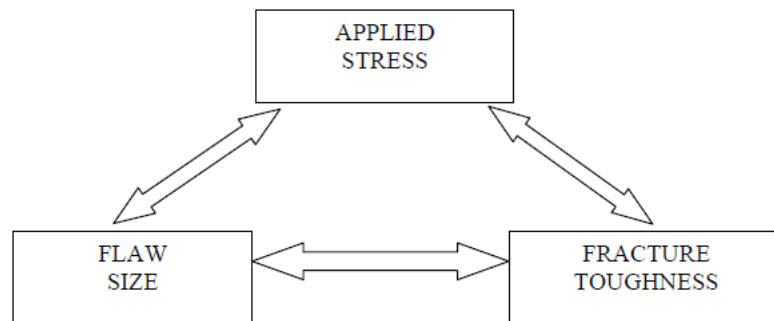


Figure 3.1: Fracture mechanics important parameters [31]

This science first took place thanks to the investigations of Griffith in 1921, about the crack growth based on energies transformation. In simple terms, the energetic formulation of fracture mechanics, consists on the comparison between the available energy for crack propagation in a structure and the energy needed to produce its cracking. Later, in 1957, Irwin introduced a big advance on fracture mechanics when formulated the analysis in terms of stresses. This concept was not proposed before since theoretically, in the crack apex, the stresses tended to infinite. To formulate it, Irwin posed that the fracture process could not concentrate in a single point, as it is deduced in a analysis purely elastic, but it presents a small and finite region, called *process zone* where the stresses are no longer infinite due to the conversion of elastic energy into plastic deformation at the crack apex. The main concept introduced with this formulation was the *intensity factor* (K), of great importance in fracture mechanics.[33]

Furthermore, there are many approaches used to study fracture mechanics, but the main two are: *Linear Elastic Fracture Mechanics (LEFM)* and *Elastic Plastic Fracture Mechanics (EPFM)*. While the first approach is mainly used for the analysis of brittle-elastic materials, like high-strength steel, the second one will

be employed for the study of ductile materials, like low-carbon steel or stainless steel, etc. [29] Under this work, the kind of fracture analyzed is mainly brittle, for this reason, it has been focused mainly on the first approach (LEFM).

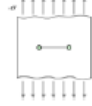
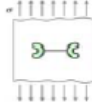
Category	Material Property	Parameter	Effective Regime
Linear Elastic Fracture Mechanics (LEFM)	Linear, time-independent	Stress intensity factor(K), Energy release rate(G)	
Elastic Plastic Fracture Mechanics	Non-linear, time-independent	J- Integral, Crack tip opening displacement (CTOD)	

Figure 3.2: Fracture mechanics approaches [31]

3.2 Linear Elastic Fracture Mechanics

Linear Elastic Fracture Mechanics is the basic theory of fracture, initially developed by Griffith in 1921 and completed by Irwin in 1957. It analyzes the cracks making two main hypothesis; considering the material **isotropic** and **linear elastic**. Under these assumptions, the stress status around the crack apex will be calculated with the **elasticity theory**. The advantage of this method is, precisely, the linearity that makes easily the combination of the theoretical, numerical and experimental analyses of fracture.

This approach can be applied to any material considered elastic except, in a very small region at the crack apex, called *process zone*, where a kind of inelasticity takes place due to the stress exceeding the yielding limit. However, if the size of this inelastic zone is small relative to the linear dimensions of the body, then, the disturbance introduced by this small region is also small, and therefore, LEFM is valid. [34]

The main goal of fracture mechanics is to predict whether a crack on a component will have a stable behaviour, or on the contrary, it will propagate. To proceed, under LEFM, they are two principal methods; the first one in terms of energetic balance, and the second one in terms of stresses. In both of them, the failure criteria will be related with the material fracture toughness. [31]

3.2.1 Griffith energy balance

The formulation done by Griffith in 1921, established the basis of fracture mechanics. His work was motivated in order to explain the discrepancy between the theoretical strength of a glass $\sigma_{th} \cong \frac{E}{10}$, and the real fracture strength found experimentally, that was 10 to 1000 times below the theoretical value. He introduced that, this inequality, was due to the presence of cracks on the materials, that degraded its mechanical integrity.

Griffith developed his study with a plane plate of a linear elastic material, with a crack of length $2a$, illustrated in Fig. 3.3. The plate was assumed to be infinite, its in-plane dimensions were much bigger than the length of the crack. It was subjected to a constant and uni-axial load, σ , which was normal to the crack plane. [31]

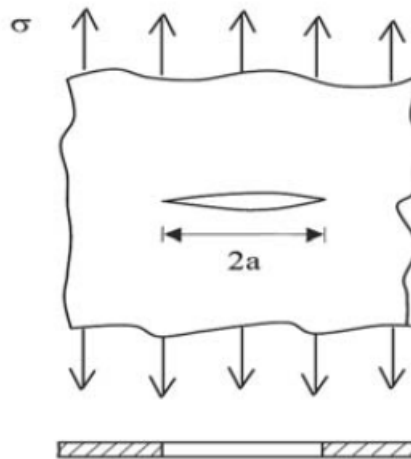


Figure 3.3: The Griffith crack[31]

His theory, was based on a thermodynamic approach in order to avoid the problem of infinite stresses at the crack tip. More precisely, it was based on the First Law of Thermodynamics, which states that, when a system goes from a non equilibrium state, to equilibrium, there will be a net decrease in energy. [31] Applying this idea to crack creation, Griffith realised that, the strain energy of the body was partly released by the crack propagation. Additionally, he observed that new surfaces in the body, were created at the same time, which were related with a certain surface energy (characteristic of a material). According to him, the condition for failure was achieved when, the released strain energy that corresponds to a certain crack growth, was greater than the consumed surface energy.

Griffith determined, thanks to the stress status in the plate with a elliptic hole,

the elastic strain energy U , depending on the crack length as:

$$U(a) = U_0 - \frac{\pi\sigma^2 a^2}{E} \quad (3.1)$$

Where U_0 , is the strain energy in the plate without considering the crack, σ , is the nominal stress in the crack plane and E , is Young's modulus.

As the crack evolves, it is produced the unload (elastic energy released) of the material that is close to the new crack surfaces. This energy, released per unit length of crack growth at the crack tip, also called *crack extension force* G , is mathematically represented as:

$$G = -\frac{dU(a)}{da} = \frac{\pi\sigma^2 a^2}{E} \quad (3.2)$$

The condition for crack propagation is, therefore, a certain energy level required to create new crack surfaces. This energy per unit crack length, is called *critical crack extension force*, G_c . Hence:

- If $G < G_c$, there is no crack propagation and it is under stable conditions.
- If $G = G_c$, there is a possible quasi-static crack growth extension.
- If $G > G_c$, there is unstable crack propagation, producing the material fracture.

It can be concluded that failure happens when stress, crack length and critical crack extension force are ligated as:

$$G_c = \frac{\pi\sigma_c^2 a_c^2}{E} \quad (3.3)$$

With, σ_c , the critical stress at fracture and, a_c , the critical crack length.

3.2.2 Stress Intensity Factor (SIF)

Thanks to Irwin's theory, a second approach based on stress analysis, was realized in order to study crack growth, when considering that a small zone of the crack tip experiences plastic deformation. Similarly to the notches, the presence of cracks, produce an intensification of the stress status around its apex, leading to premature failure (see Fig. 3.4). This stress raise, is proportional to $1/\sqrt{r}$, where, r , is the distance ahead of the crack tip. However, when r goes to zero, the stress around the apex, will not tend to infinite because the material will experience plastic strain when the yield stress is reached, as it can be observed in Fig. 3.5. Nevertheless, as long as this plastic deformation, is small enough compared to the sample size, the LEFM theory will still apply.

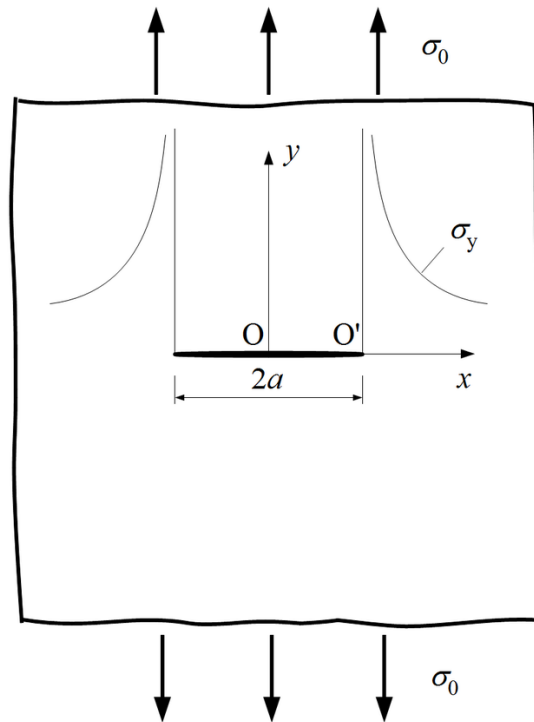


Figure 3.4: Evolution of the stress on a crack[35]

This amplification depends on the way the crack is being extended. For this reason, in fracture mechanics, it is essential the study of the crack apex movements, in order to calculate the stress status on it. A crack displacement can be characterized by three modes (Fig. 3.6) [37]:

- *Mode I*, also called *opening* or *tensile* mode, is the one where the crack surfaces move directly apart. The crack opens due to the application of the tensile stress normal to the fracture plane.
- *Mode II*, known as well as *shearing* or *sliding* mode, is the one where the crack surfaces slide over one another perpendicularly to the leading edge of the crack. This motion is due to the shearing stress.
- *Mode III*, also known as *tearing* or *out of plane* mode, is the one where surfaces move relative to one another and parallel to the leading edge of the crack. Again, this motion is due to the shearing stress, but in this case, it propagates in a perpendicular direction to the shear one.

Generally, a crack will propagate due to a combination of these modes. However, since the Mode I is the most dangerous, it will be the one used to do all the

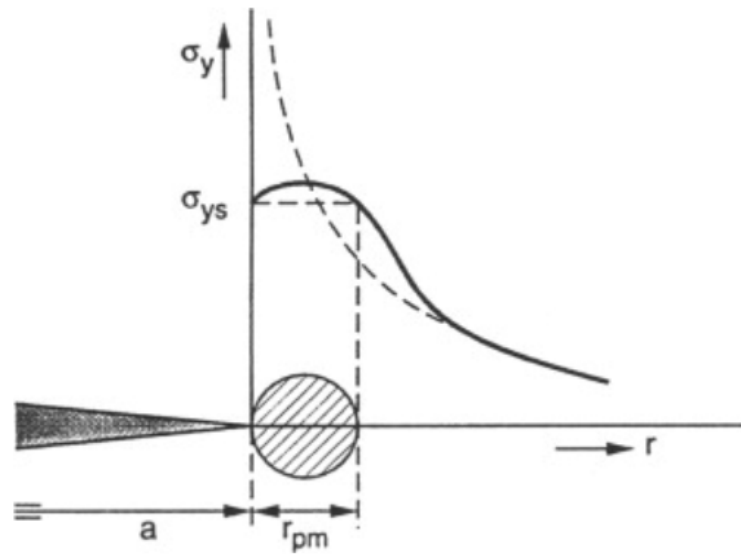


Figure 3.5: Stress evolution on the crack tip by LEFM with a small scale yielding [36]

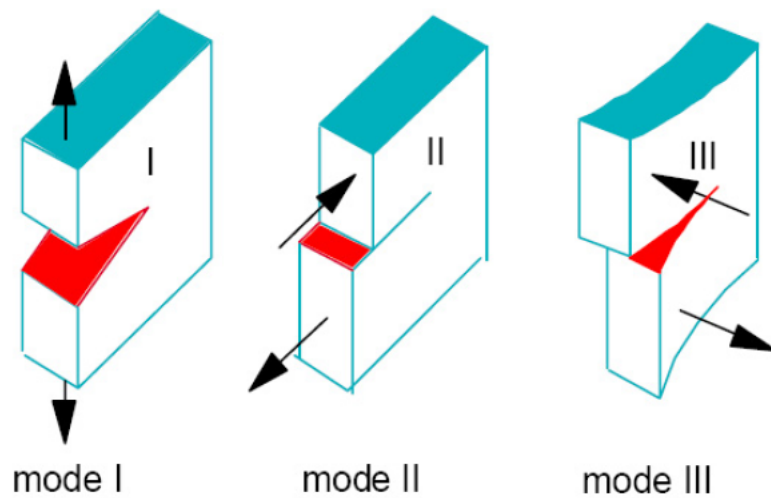


Figure 3.6: Modes of crack displacement. Mode I or opening; Mode II or sliding; Mode III or tearing [38]

analysis. In Fig. 3.7, is illustrated the different stress components of the crack and its orientation, where the crack is situated in the xz -plane and its front is along the z -axis. The stress field around the crack tip for the first mode of a linear elastic

material is given by the following equations [31]:

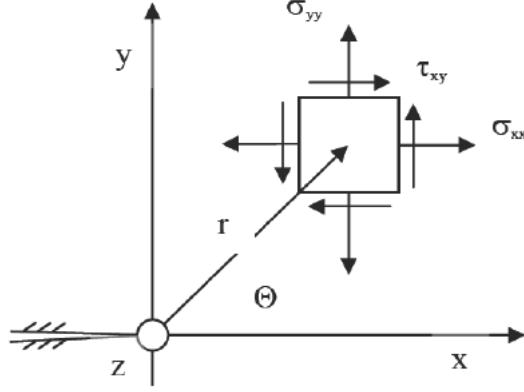


Figure 3.7: Stress components at a crack tip [31]

$$\sigma_{xx} = \frac{K_I}{\sqrt{2\pi r}} \cos \frac{\theta}{2} \left(1 - \sin \frac{\theta}{2} \sin \frac{3\theta}{2} \right) \quad (3.4)$$

$$\sigma_{yy} = \frac{K_I}{\sqrt{2\pi r}} \cos \frac{\theta}{2} \left(1 + \sin \frac{\theta}{2} \sin \frac{3\theta}{2} \right) \quad (3.5)$$

$$\tau_{xy} = \frac{K_I}{\sqrt{2\pi r}} \cos \frac{\theta}{2} \sin \frac{\theta}{2} \cos \frac{3\theta}{2} \quad (3.6)$$

In the plane of the crack, $y = 0$, and with $r = x$ and $\theta = 0$ ahead of the crack, the Eqs. 3.4, 3.5 and 3.6, reduce to an easier form:

$$\sigma_{xx} = \sigma_{yy} = \frac{K_I}{\sqrt{2\pi x}} \quad (3.7)$$

$$\tau_{xy} = 0 \quad (3.8)$$

As it can be observed, the stress status is proportional to the factor K_I , commonly known as the *stress intensification factor*. Thanks to the Irwin model, it can be demonstrated that the energy released per unit crack length is:

$$-\frac{dU}{da} = \frac{K_I^2}{E} \quad (3.9)$$

Making a comparison between Eq. 3.3 and Eq. 3.9, the stress intensity factor for the Griffith plate can be further acquired as:

$$K_I = \sigma \sqrt{\pi a} \quad (3.10)$$

In practice, the used form of the SIF (Stress Intensity Factor) is:

$$K_I = Y\sigma\sqrt{\pi a} \quad (3.11)$$

Where Y , is a dimensionless function which depends on the geometry of the considered cracked body. [31]

The stress intensity factors already obtained, are widely used in engineering applications in order to find out if the material can withstand the new stress status around the crack tip. To do so, it is important to define the *fracture toughness* (K_C). This parameter, varies with the thickness of the specimen until reaching a constant value. This value is called *plane-strain fracture toughness* (K_{IC}), which is an inherent material characteristic and, as its name indicates, it is obtained under plane strain conditions ($\epsilon_z = 0$ and $\sigma_z = \nu(\sigma_x + \sigma_y)$). It will be the critical stress intensity factor upon which the failure will occur, propagating the crack rapidly. [39]

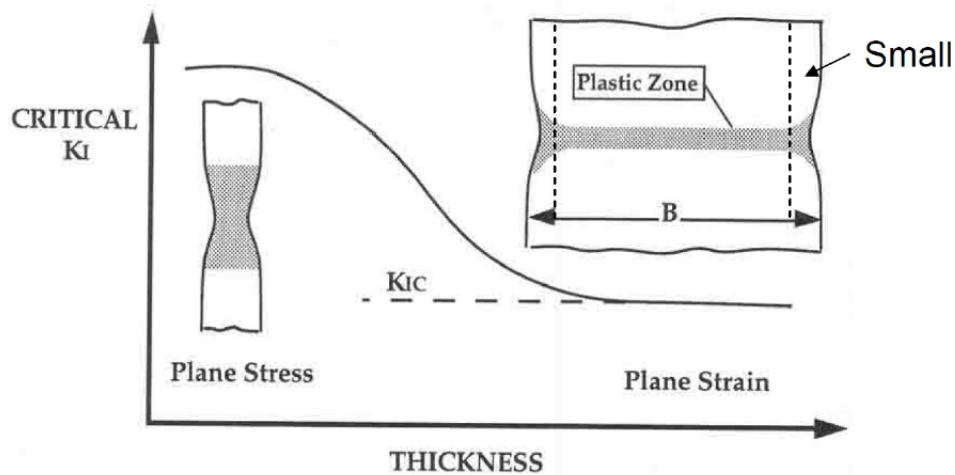


Figure 3.8: Evolution of K_C with the thickness of the specimen[38]

Therefore, similarly to the energetic approach, it is obtained the following statements:

- If $K_I < K_{IC}$, there is no crack propagation and it is under stable conditions.
- If $K_I = K_{IC}$, there is a possible quasi-static crack growth extension.
- If $K_I > K_{IC}$, there is unstable crack propagation and hence the material will fracture.

Where, K_I , represents the level of stress at the crack tip, while K_{IC} , represents the highest value of stress intensity that a material, under plane-strain conditions, can withstand without fracture.

Finally, it is also interesting to remark that design based on fracture mechanics considers the three main variables: K_{IC} , σ and a . If for instance, the first two (K_{IC} and σ) are specified by the design situation, the maximum crack length permitted will be:

$$a_c \leq \frac{1}{\pi} \left(\frac{K_{IC}}{Y\sigma} \right)^2 \quad (3.12)$$

Whereas if the specified parameters are K_{IC} and a by design criteria, the maximum stress that the material will be able to bear will be:

$$\sigma_c \leq \left(\frac{K_{IC}}{Y\sqrt{\pi a}} \right) \quad (3.13)$$

3.3 Crack growth in gas turbine components

Gas turbine components, as blades and vanes, are subjected to several damage mechanisms, such fast fracture, due to their operating conditions, high temperatures and stresses. Mainly, stress concentration is the principal crack nucleation cause. This stress status can belong, either to a surface defect, such as a machining mark (pre-existing micro crack), which provides a highly localised stress concentration, or to defect-free surfaces, where dislocations and diffusion processes at the microscopical level play an important role in crack initiation. [40]

On the basis that no defects exist on the surfaces (the second case), these microscopical movements are driven by fatigue and creep phenomenon. Then, once the crack has been initiated, oxidation plays as well a crucial role in crack propagation. For this reason, in the following subsections, a more in depth explanation will be done to these thermo-mechanical causes that create unstable crack propagation.

Fast fracture, thus, is a failure mechanism which entails *unstable* propagation of cracked component. This is to say, once the crack begins to open, the applied loads are such that cause accelerating growth. Mostly, this kind of failure is produced by lower applied stress than the design one, calculated with appropriate methods. This failure can be explained due to the structure's strength reduction as a result of the crack presence. The residual strength of the structure diminishes with the augmentation of the crack size, as represented in Fig. 3.9. After a certain time, the residual strength is so low that the structure can no longer bear with the normal service conditions, and fracture occurs. [41]

Commonly, this kind of fracture is called as brittle, although the microscopic mechanisms that make crack propagation, may be anything from low strain cleavage or intergranular fracture to fully ductile shear separation. However, in practical

terms, it must be referred the term brittle, to the instability effect that occurs when the applied stress is less than the general yield stress. Moreover, it is important to add that a brittle fracture must include stress concentrator because of the necessity to limit the cracking mechanism to a small and localised region. For this reason, it is interested to study in fracture mechanics, the way in which fracture can be developed ahead of a crack, and the relation between it and the loading conditions. [42]

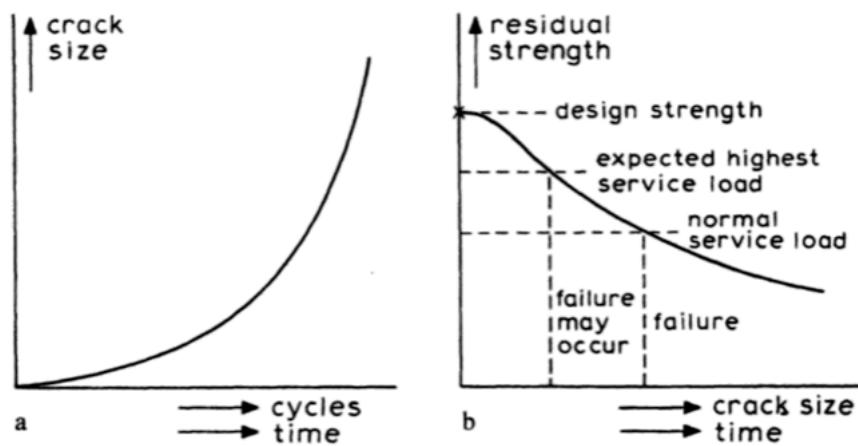


Figure 3.9: a. Crack Growth during time; b. Residual strength curve [41]

Accordingly, it can be said that one of the main scopes of fracture mechanics, is to find the answer of some of these questions [41]:

- What is the maximum crack size that can be tolerated at load service?
- How long does it take for a crack to grow from a initial crack size to the critical one?
- What size of pre-existing flaw can be tolerated at the initial service life?
- How often should the structure be inspected?
- What is the residual strength as a function of the crack size?

Although this science establishes the basis for answering some of them, it still needs a lot of investigation to give proper ones. Under the practical case of this work, it will be tried to respond some of them.

3.3.1 Fatigue Crack Growth

Fatigue phenomenon, it is without hesitation one of the most important causes that leads to crack propagation. Components under the action of cyclic loads, can bring into fracture failure at stress levels well below of the material yield stress. Crack growth related to fatigue effect, is mainly due to the plastic deformation attained at the crack apex. This plastic deformation, in the microscopical level, occurs via the motion of dislocations (line defects in crystalline lattice), promoted by the loading cycles, creating stress concentration. Therefore cracks originated by fatigue, are initiated within the grains and then propagate through them, causing the transgranular fracture phenomenon. [40]

For decades, fracture mechanics approaches have been used in order to estimate fatigue crack propagation, obtaining the number of cycles spent until the arrival to the critical size. Typically, the crack growth can be plotted as shown in Fig. 3.9, where the crack size, a , is a function of the number of cycles, N . Generally, most of the component life is spent with relatively small cracks. The instantaneous slope of this curve is called *crack growth rate* (da/dN) and, as it can be observed, the crack grows very slowly at the beginning, accelerating with the increase of the crack size. The reason of this acceleration is mainly, due to the stress intensity factor at the crack apex, which is dependent of the crack size.

$$K = Y\sigma\sqrt{\pi a} \quad (3.14)$$

As the crack grows, the stress intensity factor raises, generating a faster growth. This growth will go on until it reaches the critical size, where failure will occur. [43]

Generally, the crack propagation under constant amplitude stresses depends, mainly, on the range of the stresses in the fatigue cycle ($\sigma_{max}, \sigma_{min}$), and on the crack length, a . Additionally, it is also affected by the stress ratio $R = \sigma_{min}/\sigma_{max}$. Equation 3.16, can be written as a function of these parameters as:

$$\Delta K = Y\Delta\sigma\sqrt{\pi a} \quad (3.15)$$

$$\Delta K = K_{max}(1 - R) \quad (3.16)$$

To correlate them, experiments have been done, finding a relation between crack growth rate, da/dN , and the SIF range logarithm, $\log \Delta K$, as illustrated in Fig. 3.10. As it can be observed, the fatigue crack propagation can be divided in three main zones [44]:

- *Region I*, it is the most difficult one to estimate since it is microstructure and flow properties material dependent. It has a threshold value, ΔK_{th} , which approaches a vertical asymptote, below which fatigue cracks will not propagate,

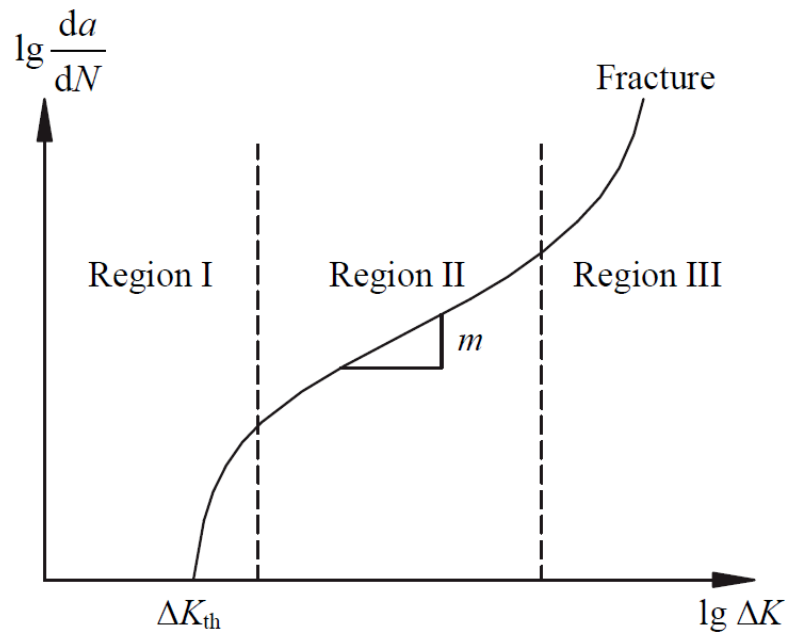


Figure 3.10: Fatigue Crack Growth curve [41]

because it does not reach the stress concentration needed. However, above this value, the crack will propagate along high shear stress planes (45 degrees) as represented in Fig. 3.11. These, are the preferred planes along which, dislocation motion occurs, also called *slip planes*. In this region, the crack can be decelerated, or even may come to an arrest, by microstructural barriers such inclusions, grains boundaries, pearlitic zones, that con not accommodate the crack growth direction. As a consequence, sometimes concentric marks, called *beach marks*, can be appreciated due to successive crack growth arrests or decreases. Hence, fatigue strength increased can by achieved with grain refinement, by the insertion of microstructural barriers.

- *Region II*, in this stage, as the stress intensifies, the shear stress effect is gradually suppressed by the plastic deformation mechanism, becoming this last one the driving force. Therefore, the propagation now is perpendicular to the load direction. The increase of the K is mainly a consequence of either crack growth, or higher applied stress. This zone is characterized by its linearity, being the dominating part of the fatigue life. As a result, the main applications of LEFM concepts that describe crack growth behaviour are associated within this region. Furthermore, it is important to remark that this phase is not sensitive to microstructure or flow properties. Many models have been proposed to fit with this region, being Paris equation (1960), the

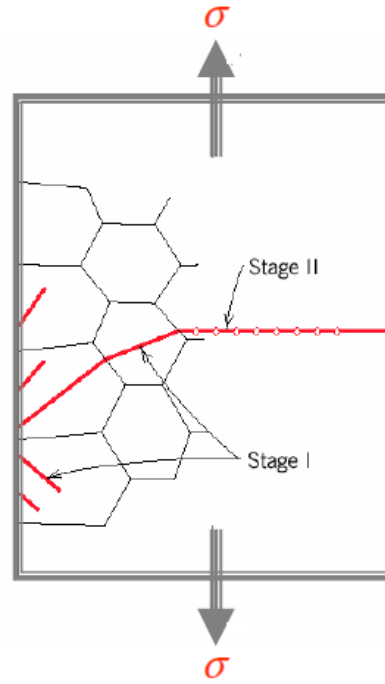


Figure 3.11: Fatigue Crack Growth [38]

most widely accepted.

$$\frac{da}{dN} = C(\Delta K)^m \quad (3.17)$$

Where C and m are material constants and ΔK is the stress intensity range. Note that the Paris equation does not count for the stress ratio R , for this reason, when analyzing non zero stress ratio, an appropriate value of C must be taken into account. Integrating Eq 3.18, crack growth life can be estimated in terms of cycles to failure.

$$N_f = \int_{a_i}^{a_f} \frac{da}{C(\Delta K)^m} \quad (3.18)$$

With a_i , the initial crack length, and a_f , the final crack length. [45] It is important to remark that fatigue life estimation, depends strongly on a_i , not being sensitive to a_f ; large changes of this last value leads to small changes of N_f as illustrated in Fig. 3.12.

- *Region III*, is the final one related with unstable crack propagation. Here, K_{max} will be the equivalent to the fracture toughness K_{IC} , upon which the

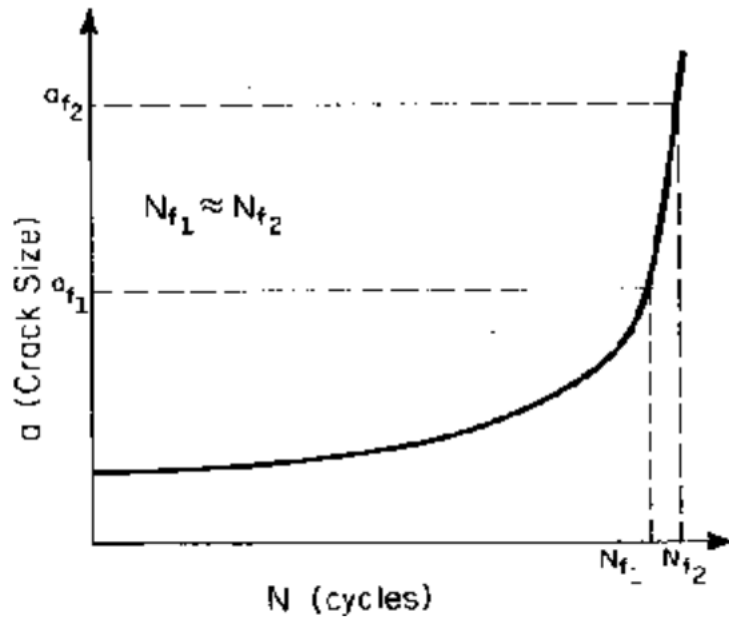


Figure 3.12: Fatigue Crack Growth curve

material will fail. This region is very sensitive to the microstructure, load ratio and stress state. Corresponds to the final fracture and mostly, presents a fibrous and irregular appearance. The failure can be either brittle or ductile, depending on the material's properties, dimensions and loading conditions.

The exact area of each region at the fracture will depend on the level of load applied. Meanwhile high applied loads leads to small stable crack propagation areas, lower loads results in smaller areas of fast fracture, because the crack will need more time to propagate.

3.3.2 Creep Crack Growth

The presence of cracked components operating at creep range temperatures (above $0.4 \cdot T_m$ with T_m the absolute melting temperature), has required crack growth techniques evolution. The principal problem of creep phenomenon is the plastic deformation that involves.[46] Once again, fracture mechanics concepts can be applied in order to estimate it. Nevertheless, LEFM application has a very limited extent; it can only be used to highly creep resistant materials, such as nickel-based superalloys and other creep-brittle materials. This is to say, if the plastic deformation attained, is embedded in the elastic field, the K parameter will no longer be a uniquely quantity to determine crack apex stresses, needing additional terms that quantify the plastic contribution. [47]

Under the creep mechanism, micro cracks and voids are developed, propagating along the grain boundaries, as it can be appreciated in Fig. 3.13. Generally, the growth is attributed to diffusion processes presented as vacancies movements. [40]

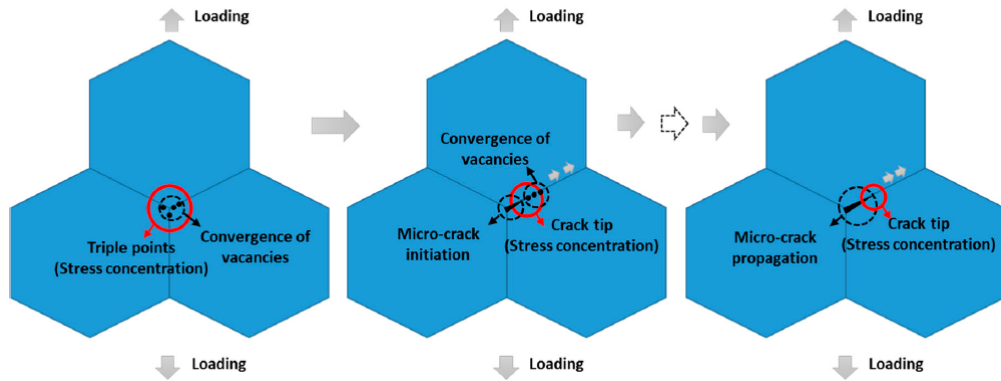


Figure 3.13: Creep crack growth by diffusion mechanism [40]

Crack propagation can be divided into three different stages, illustrated in the Fig. 3.14, where it should be outlined that the slope of the curve represents the *creep rate* ($\dot{\epsilon}$).

The first stage is characterized by a rapid deformation at the beginning, followed by a reduction of the creep rate with time, due to the hardening effect. In this stage, initial incubation of vacancies occurs.

Then, once the process of micro cracks has been initiated, the second stage arrives, where is characterized by an almost constant creep rate, being the period that conforms the majority of the component creep life. This stage entails highly localised stress around the crack apex, resulting into plastic deformation (crack opening), and favouring diffusion process of the vacancies along the grain boundary, leading to grain elongation and therefore further crack opening. [40] Additionally, since the atoms diffuse from high to low concentration regions, more vacancies are generated and converged at the crack apex, where highly localised stress is presented, providing a more favourable situation for creep damage (grain elongation). It is also remarkable that high temperatures give rise to favourable conditions for diffusion behaviour, advancing the creep crack along the grain boundaries. Thus creep failure is strongly temperature dependent.

Finally in the last stage, creep rate accelerates as the stress per unit area increases, ending in fast fracture due to the intense creep damage.

It is clear that each phenomenon (fatigue and creep), leads to a different way of crack propagation.[48] In order to evaluate the overall contribution of both effects, the ASME (American Society of Mechanical Engineers) Code provides the

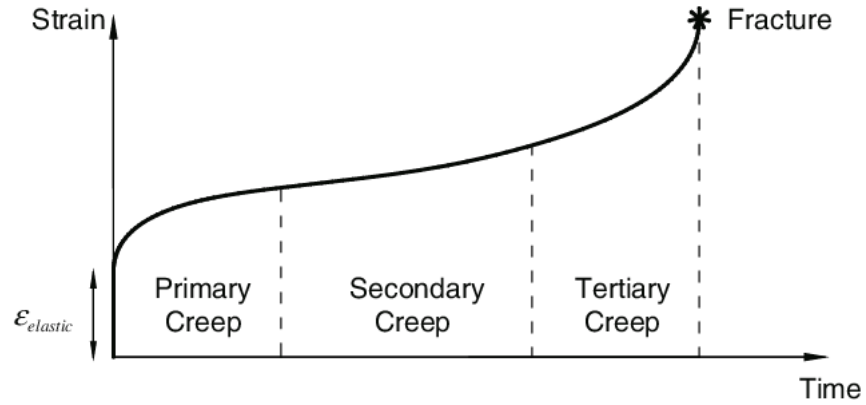


Figure 3.14: Creep curve. Strain Vs Time

following criterion in which *creep-fatigue life* is evaluated:

$$\sum_j \left(\frac{n}{N_d} \right)_j + \sum_k \left(\frac{\Delta t}{T_d} \right)_k \leq D \quad (3.19)$$

It is a *linear damage summation rule*. The first term is the cyclic damage, being n the number of cycles of type j , and N_d , the allowable number of cycles of the same cycle type. The second term refers to the creep damage, with Δt , the actual time at the stress level k , and T_d , the allowable time at that stress level. D , is the allowable combined damage fraction. It can be appreciated that both terms are analysed in an uncoupled way; the creep effect is considered in terms of time fraction, and the fatigue one in terms of number of cycles.[49]

This contribution can also be represented graphically in the Fig. 3.15, where failure will occur if the total damage overcomes the line. It can be observed the influence of both phenomena. When creep is dominant, the failure of the component will be intergranular due to grain boundary damage accumulation. Whereas, with fatigue dominant conditions, transgranular failure will be attained due to the crack growth through grains. For creep-fatigue interaction, it can be observed both effects.[50]

3.3.3 Oxidation Crack Growth

Once the crack has been initiated, the oxidation effect takes importance into crack propagation as a consequence of the loss of protection at the alloy's base, near the crack apex, provided by the surface coatings. This phenomenon results in the creation of oxidation layers, at the crack surfaces, as a result of long time exposures to hot combustion gases at high temperatures.

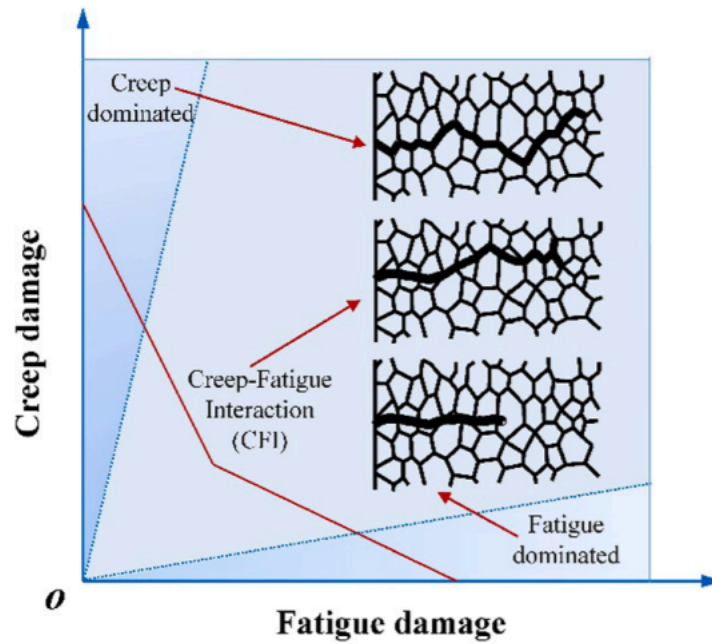


Figure 3.15: Creep Fatigue Interaction diagram [50]

The mechanism is based on the conversion of all the metallic elements within the alloy, into their correspondent oxides.[51] Mainly, in Ni-based superalloys, the main effect of the oxidation process is the loss of γ' precipitates at the crack apex. Its principal consequence is the decrease of the material's mechanical properties, since γ' is characterized by its excellent mechanical properties under high temperatures. As a result of this depletion, the component is prone to local rupture, accelerating therefore, the crack growth rate.

The γ' depletion represents a time and temperature dependent damage increment. Its growth per cycle can be described with the following exponential Arrhenius equation:

$$\Delta a_{0,t_i} = d_{\gamma'} = (A_{O,0} e^{\frac{-Q_0}{RT_i}} t_i)^{1/n} \quad (3.20)$$

Where $d_{\gamma'}$ is the thickness of the γ' -free zone, n is the power law exponent, Q is the activation energy needed for the depletion process, $A_{O,0}$ is a constant and R is the universal gas constant. [52]

Chapter 4

Application to a Gas Turbine Vane

Under this chapter, the main scope of this work is presented. In first place, the system description is explained, followed by the MI Assessment done to the turbine vane, where the critical location in which the crack nucleation may start, is obtained. Hereafter, the preparation of the model is performed, where the sub-modelling technique and the crack modeling are detailed. Finally, the two analyses, done to the studied component, are exposed; SIF evaluation and crack growth assessment in terms of fatigue, creep and oxidation, where the end-of-life lines are represented.

4.1 System description

Under this work, in the frame of crack assessment, an evaluation of a possible crack propagation at the most critical point of a GT second-stage vane (TV2) for power generation, has been developed.

The GT is a single-shaft turbomachinery used for power generation plants. It is connected to the generator on the compressor side, and counts with an annular combustion chamber. It is designed to operate at 50 Hz, in both open and combined cycle, being suitable for operating in base load mode. The expansion turbine is composed of four axial stages in which, every stator vane and rotor blade, except the rotor ones of the last stage, are cooled by air.

Going into details of the component to analyze, it is important to remark that it is a nickel-based superalloy (René 80), with an equiassic grain casting, comprised of an airfoil and two platforms (inner and outer), connected at the airfoil extremes as it can be observed in Fig. 4.1.

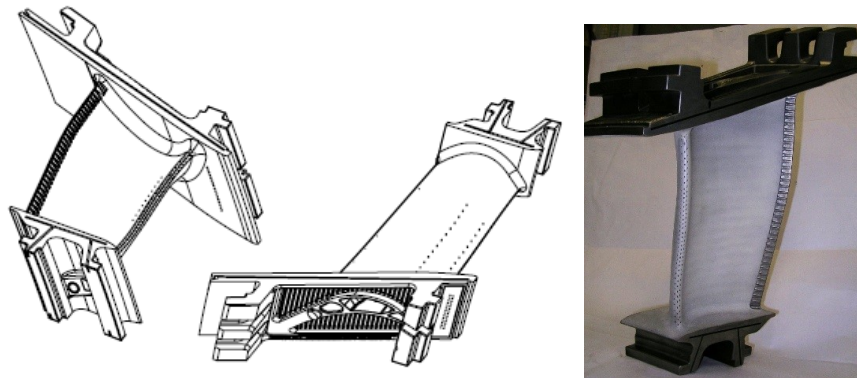


Figure 4.1: TV2

Moreover, in order to guarantee the required airfoil protection against corrosion and oxidation, the vane has been undergone to different processes and coatings, such as TBC and metallic coatings.

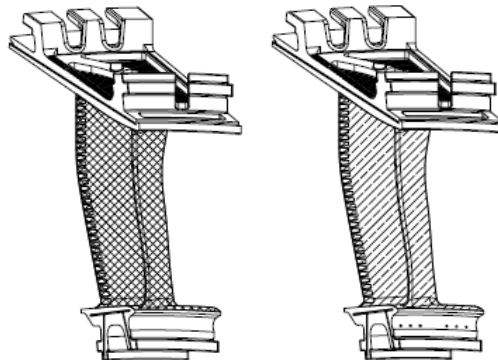


Figure 4.2: Anti-oxidation and corrosion processes.

Additionally, with the aim of ensuring the cooling of the vane, inside the profile, it can be found internal channels and a multi-pass coil, which allow the implementation of the principal air cooling solutions such shower head cooling, airfoil film cooling and shroud cooling system which counts with turbulence promoters for increasing the cool effect. Indeed, the multi-pass coil also counts with these angled promoters increasing the turbulence of the air flow and therefore the efficiency of the cooling. In the following picture, it can be appreciated a scheme of the cooling system (Fig. 4.3).

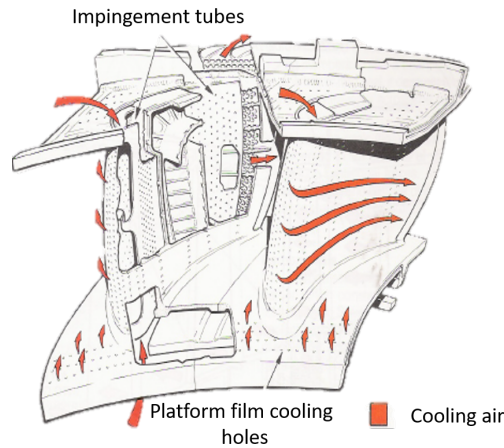


Figure 4.3: Cooling system scheme

Moreover, the excess of air flowing through the channels feeds the U-ring (shown in Fig. 4.4), which is placed at the base of the vane, ensuring the sealing between the platforms and therefore preventing the ingestion of hot gases between the blades. This U-ring is connected to the inner platform by two hooks, the front one allows the coupling in the radial direction and the rear one in the radial and axial direction. Meanwhile, the circumferential coupling will be achieved through a single anti-rotation pin for the ring sector with the relative slot of the rear hook, solution on five vanes for each upper and lower half-row.

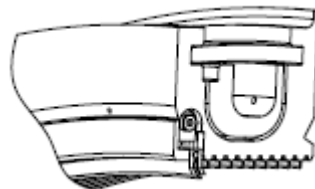


Figure 4.4: U-Ring

On the other hand, the outer platform will be attached to the Turbine Vane Carrier (TVC) via two hooks, where the front one will constraint the axial and radial direction while the rear one will be able to slide inside the TVC, compensating the displacements of the components in operating conditions. Furthermore, the front hook has a slot for the anti-rotation pin of the TVC, constraining the component in the circumferential direction, allowing at the same time its free thermal expansion.

4.2 Critical locations detection

Before starting with the analysis of possible cracks propagation, it is important to perform a FEM analysis of the component (TV2), in order to evaluate its behaviour at the working conditions and to obtain the critical points where the cracks may initiate.

In this way, thanks to the software *ANSYS Workbench* and *ANSYS Mechanical APDL* a static analysis within the elastic field has been developed to the given stationary component. In the following figure (Fig. 4.5), it can be observed the whole FEM model, composed by the vane, the turbine vane carrier sector (TVC) and the corresponded U-ring sector, where it can be appreciated a refined mesh for obtaining accurate results. This 3D model has been obtained from the software *NX*.

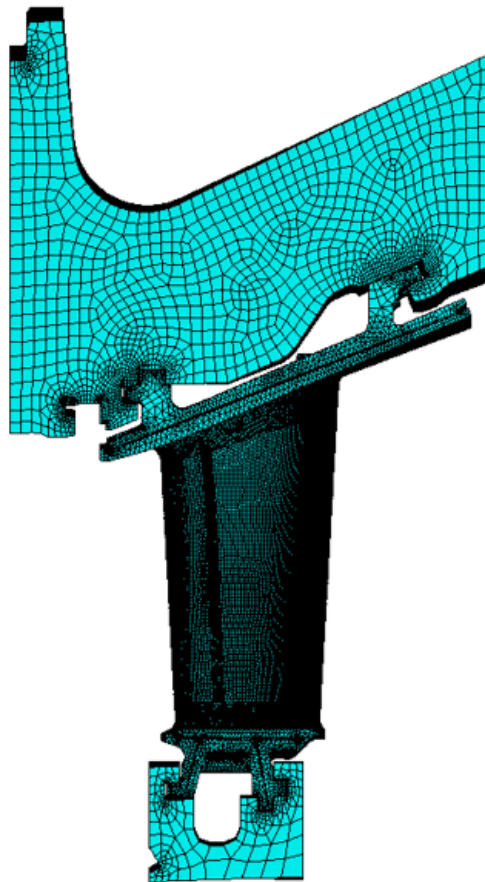


Figure 4.5: FEM model of the whole component; Turbine Vane Carrier, Turbine Vane and U-ring

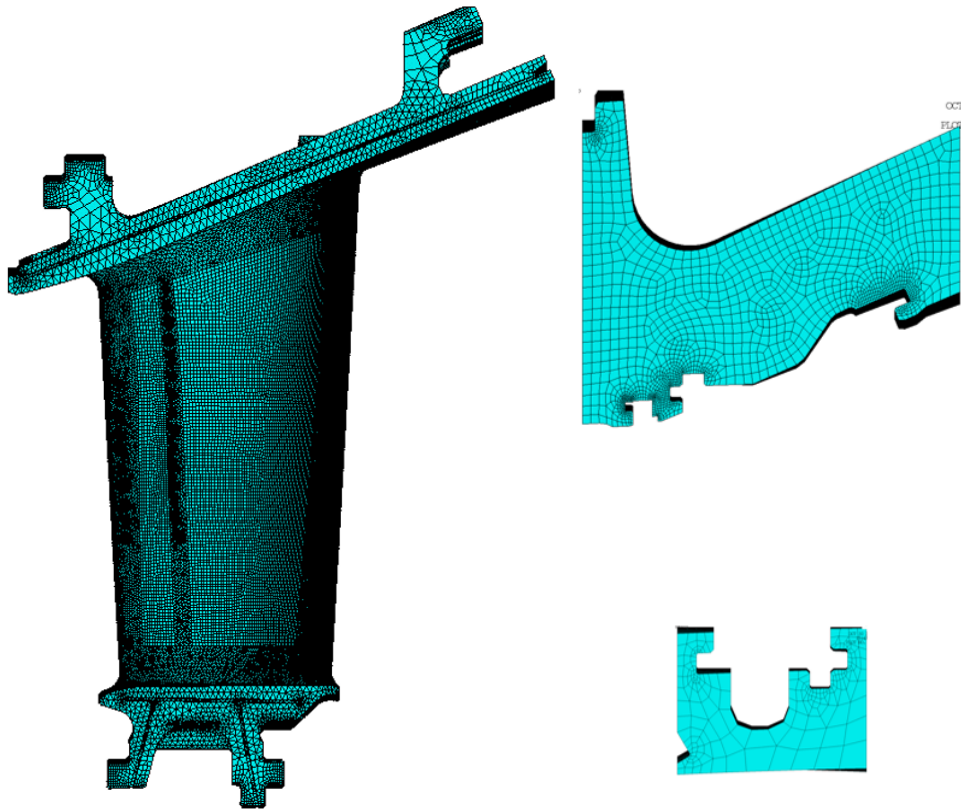


Figure 4.6: FEM model of each single component. On the left the TV2; at the top right the turbine vane carrier sector; at the bottom right the U-ring sector

Furthermore, a MI assessment has been done to the vane, studying the pressures, temperature gradients, displacements and stresses found in the component. In the Figure 4.7, the TV2 pressure status can be observed, where the two main airfoil zones can be noticed, normalized to the maximum value. Mostly in green, it can be appreciated the zone subjected to higher pressures, called *pressure side*. On the contrary, mainly in blue, it can be remarked the zone that bears lower pressures, called *suction side*.

Meanwhile, in the Figure 4.8, the vane temperature distribution is shown, normalized to the maximum value. It depends mainly on the gases heat transfer coefficient and the material thermal conductivity. It can be remarked that no temperature fall is attained, from the leading edge to the trailing edge, as it should be expected. The main reason of this effect is due to the cooling system (shower head) that actuates in the leading edge diminishing the temperature gradient around this zone.

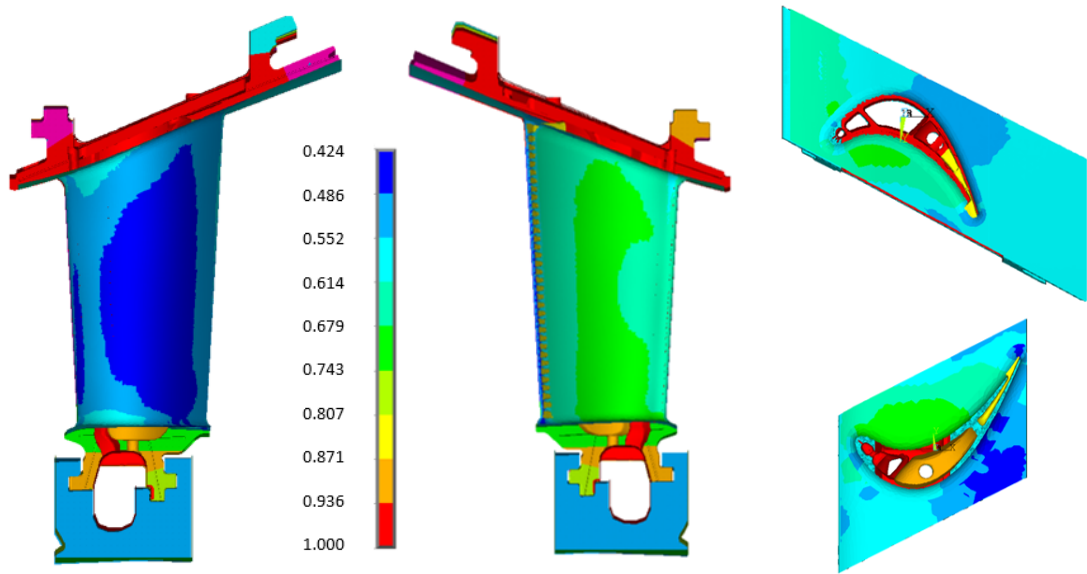


Figure 4.7: Pressure distribution on the TV2

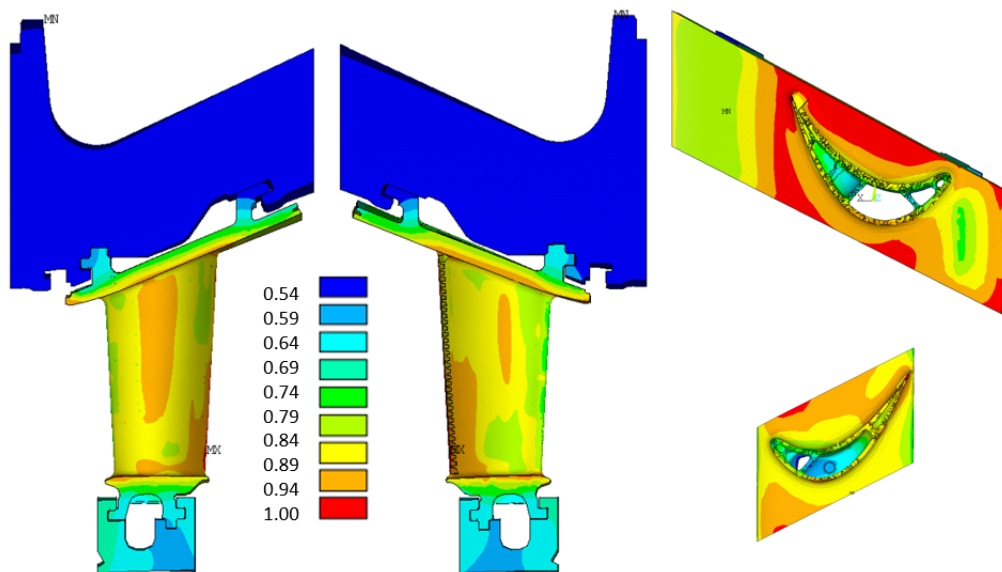


Figure 4.8: Thermal analysis on the TV2

Moreover, in the following picture, Fig. 4.9, the different vane displacements are presented, normalized to the maximum value. It can be remarked its consistency. For instance, within the radial displacement, a gradually growth can be noticed as it goes closer to the TVC.

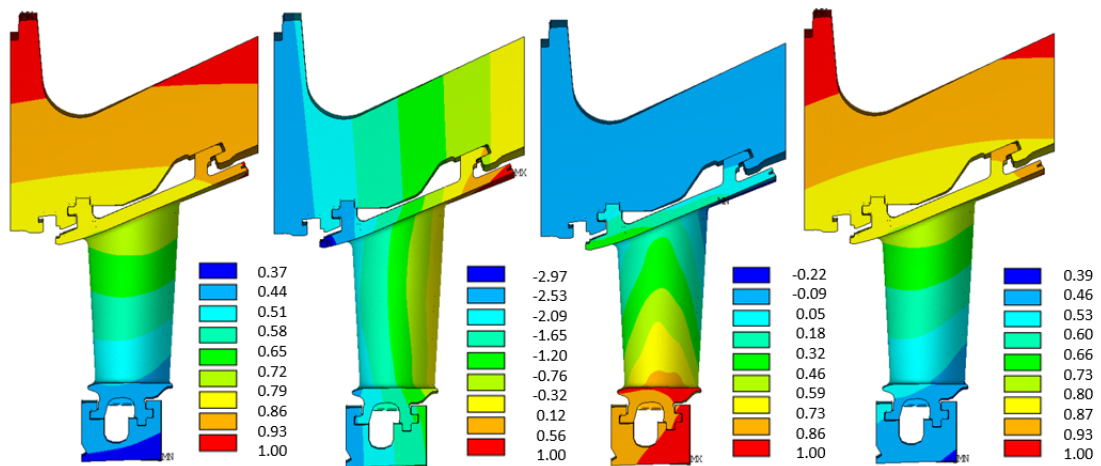


Figure 4.9: Displacements analysis on the TV2. From left to right; Radial displacement, axial displacement, circumferential displacement and total displacement

Furthermore, a stress evaluation in terms of *Von Mises equivalent* has been done, observing two critical points at the PETE (Platform External Trailing Edge) and PITE (Platform Internal Trailing Edge) where the stress overcomes the corresponding material's yielding stress. As a consequence, it can be highlighted these two locations as **critical parts** of the component where, due to a combination of mechanical and thermal loads, cracks may nucleate. For this reason, the two life limiting phenomena (fatigue and creep) that will be studied hereafter, will be focused on these life limiting spots.

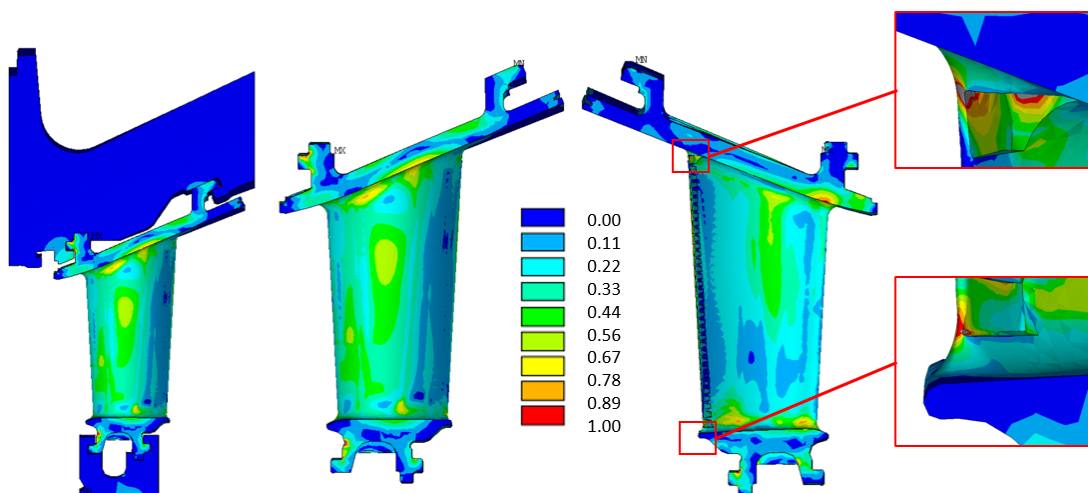


Figure 4.10: Von Mises Stress distribution, normalized to the maximum value

In a statoric vane, the two main effects that the component has to bear are the combination of mechanical and thermal cyclic stresses and strains. However, mechanical loads such as gas pressure and reaction forces, exert less considerable effect on this component, being the thermal gradients the major cause of stress on the critical parts.

For this reason, a creep analysis has been performed at the different intervals of maintenance. From this evaluation, it can be observed from the graph below (Fig. 4.11), that in the two critical areas already indicated (PETE and PITE), the creep strain limit, represented with the yellow line, is overtaken after only 1000 firing hours (working hours), which is a very short period of time. Hence, this analysis shows that the creep verification is not fulfilled. Moreover, it is observable, that the PETE location is even more dangerous than the PITE. Thus, from now on, it will be focused only on this critical location.

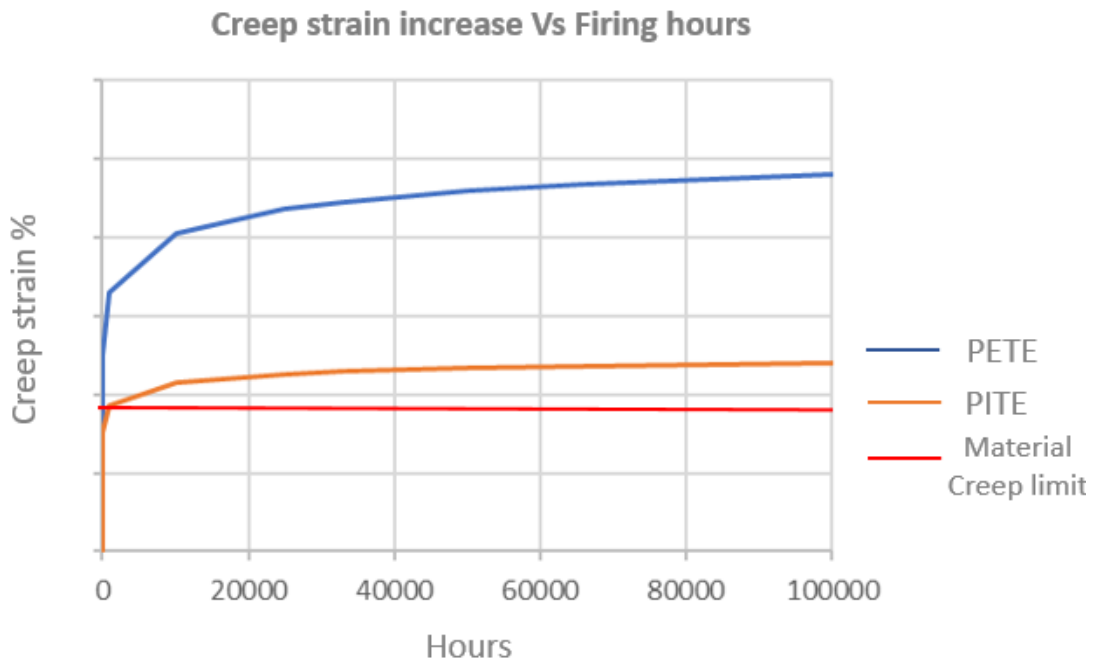


Figure 4.11: Creep strain vs Firing hours

In addition, in the figure below (Fig. 4.12), the creep analysis performed at 66 kFH (Firing Hours) is illustrated, normalized to the material creep limit value. It is remarked, at the PETE and the PITE, the creep strain limit overcome.

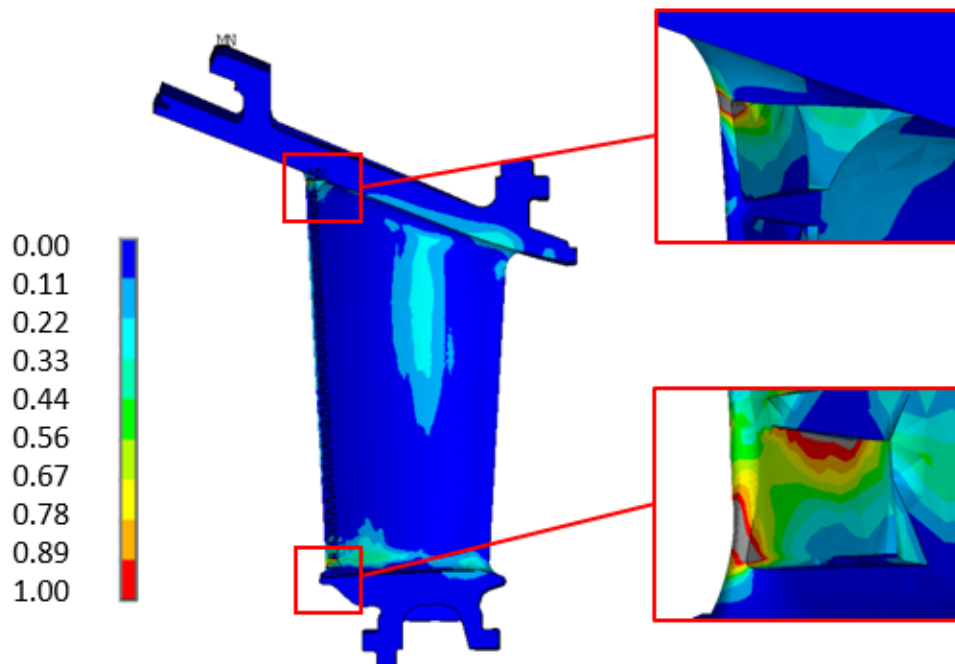


Figure 4.12: Creep Analysis at 66kFH where it is remarked the overcome of the strain limit at the PETE and PITE

To end this study, the LCF assessment has been carried out with two different approaches. The first one considering that no stress relaxation is taken into account, hence evaluating the number of cycles to crack initiation in the worst possible condition, $R=0$. Whereas the second one was realized considering the stress relaxation attained due to creep, which provides a higher number of cycles to crack initiation because this relaxation produce a shifting effect of the load cycle mean stress. However, it can be outlined that for both approaches, the whole component (in red as it can be appreciated in the Fig. 4.13) passes the required number of cycles, except in the PETE, where from the first approach, this number of cycles to crack initiation is very low. Although the second approach provides a higher number of cycles, it is clear that the truth will be at an intermediate value. Nevertheless, since the evaluation of the number of cycles once the crack has nucleated is the scope of this work, the measuring of the number of cycles to crack initiation will not be developed.

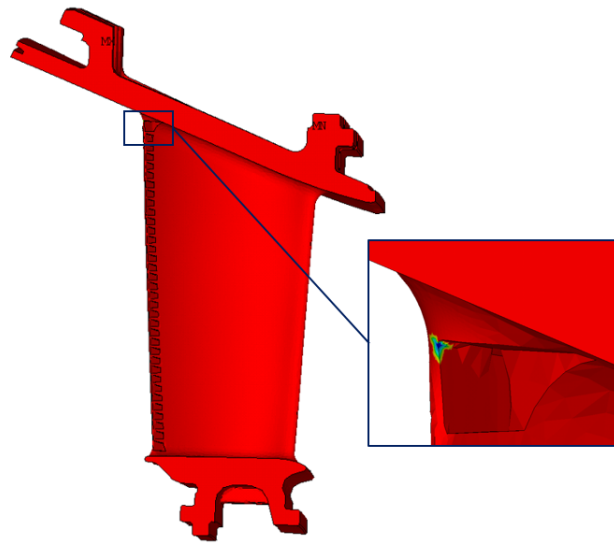


Figure 4.13: LCF Analysis with no stress relaxation

So, it can be concluded that the **PETE** is **the most critical part** of the component, where the **crack may nucleate**.

4.3 Submodel

From the previous conclusion, it is clear that the section to analyze preferentially is not the whole vane, but the zone around the PETE, where the crack may initiate. For this reason, in this subsection it will be explained the process done with *ANSYS Workbench* to the 3D component called *submodeling*.

One of the main problems of analyzing the whole model, apart time-consuming issues, is the coarse mesh that results in an inaccurate stress status on the component. Moreover, if the region to consider is a small and specific part of the given element, it will be required from a more refined mesh. In this way, based on St. Venant's principle: "...the difference between the effects of two different but statically equivalent loads becomes very small at sufficiently large distances from load", the submodeling technique is applied to the vane. This technique consists of the creation of a refined local model of just the area of interest, in this case around the PETE, as it can be observed in the illustration below (Fig. 4.14). It is important to underscore that the submodeling has been done to the **uncracked** component. [53]

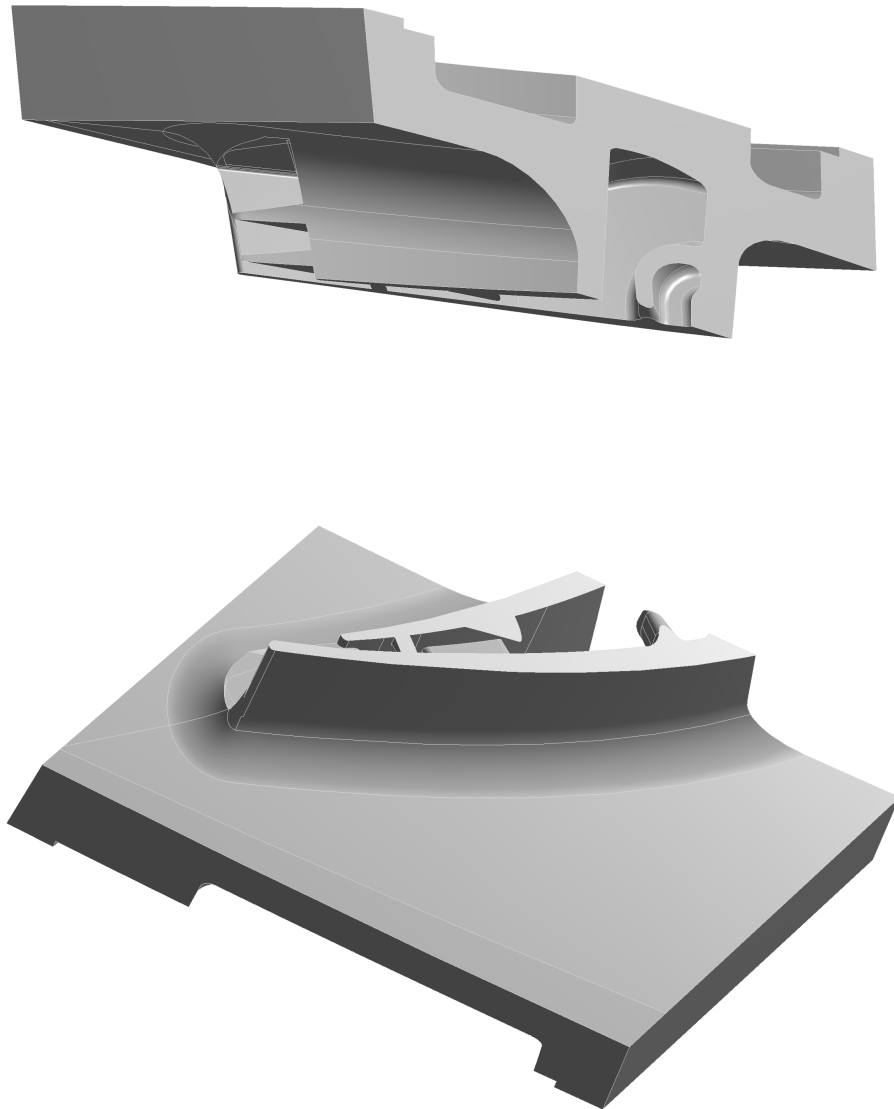


Figure 4.14: Submodel of the TV2 focused around the PETE area

What St. Venant demonstrated was that the stresses that are far away from the applied loads do not depend on the way these loads are introduced. Moreover, these loads can be replaced from the coarse model as an equivalent static deflection load, resulting in the same stress field. In this way, the displacement field and the temperature gradient from the coarse model, will be applied to the submodel as boundary conditions, getting the accurate highly-refined response at the interested

area.

As a result, the steps took for the submodeling creation were the following [53];

1. The whole model has been solved, obtaining the displacement field and temperature gradient.
2. A geometry model of the interested area has been made. The coarse model has been cut, as illustrated in Fig. 4.14, where the submodel faces that are "inside" the global model are called *cut boundary faces*.
3. The submodel has been attached to the engineering data and to the full model solutions, as shown in the figure below (Fig. 4.15).

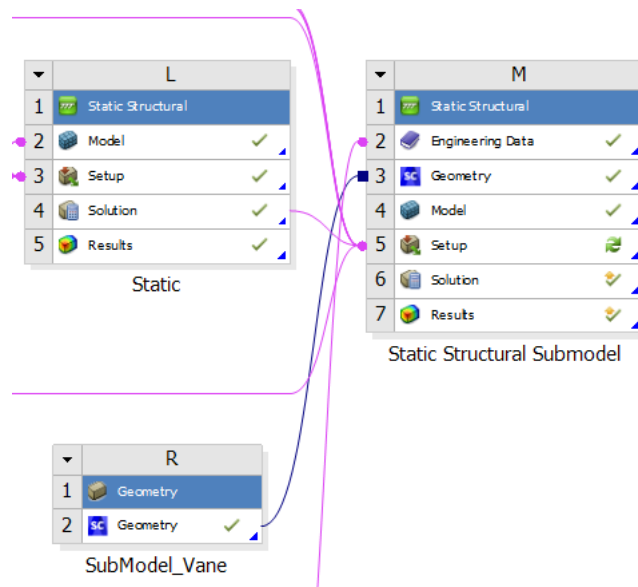


Figure 4.15: Submodel attached to the engineering data and solution of the full model in ANSYS Workbench

4. The displacement field has been applied into the cut boundary faces as boundary conditions, whereas the temperature gradient has been interpolated from the whole model, as illustrated below, all normalized to the maximum values.

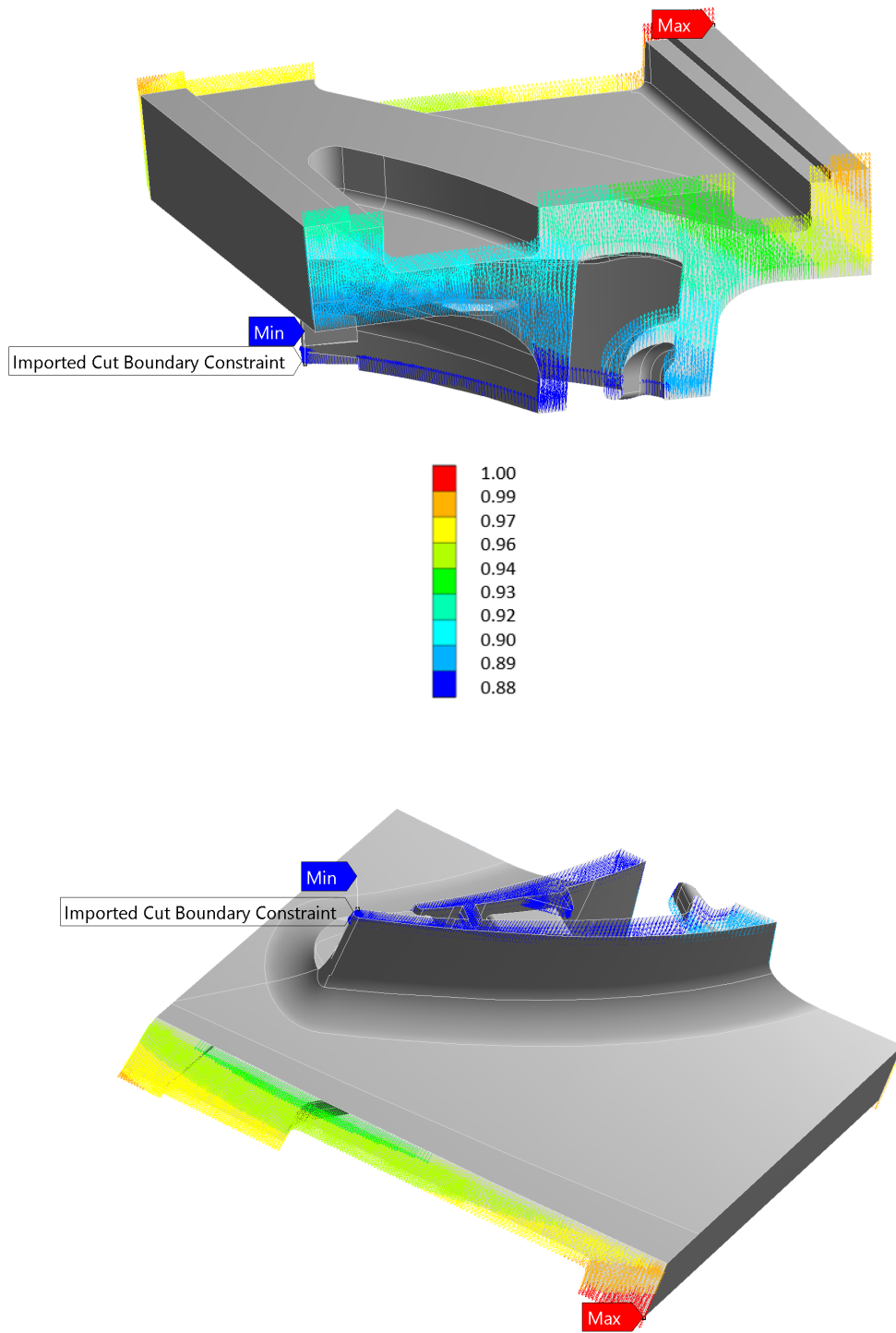


Figure 4.16: Displacement field of the whole model applied to the submodel as boundary condition

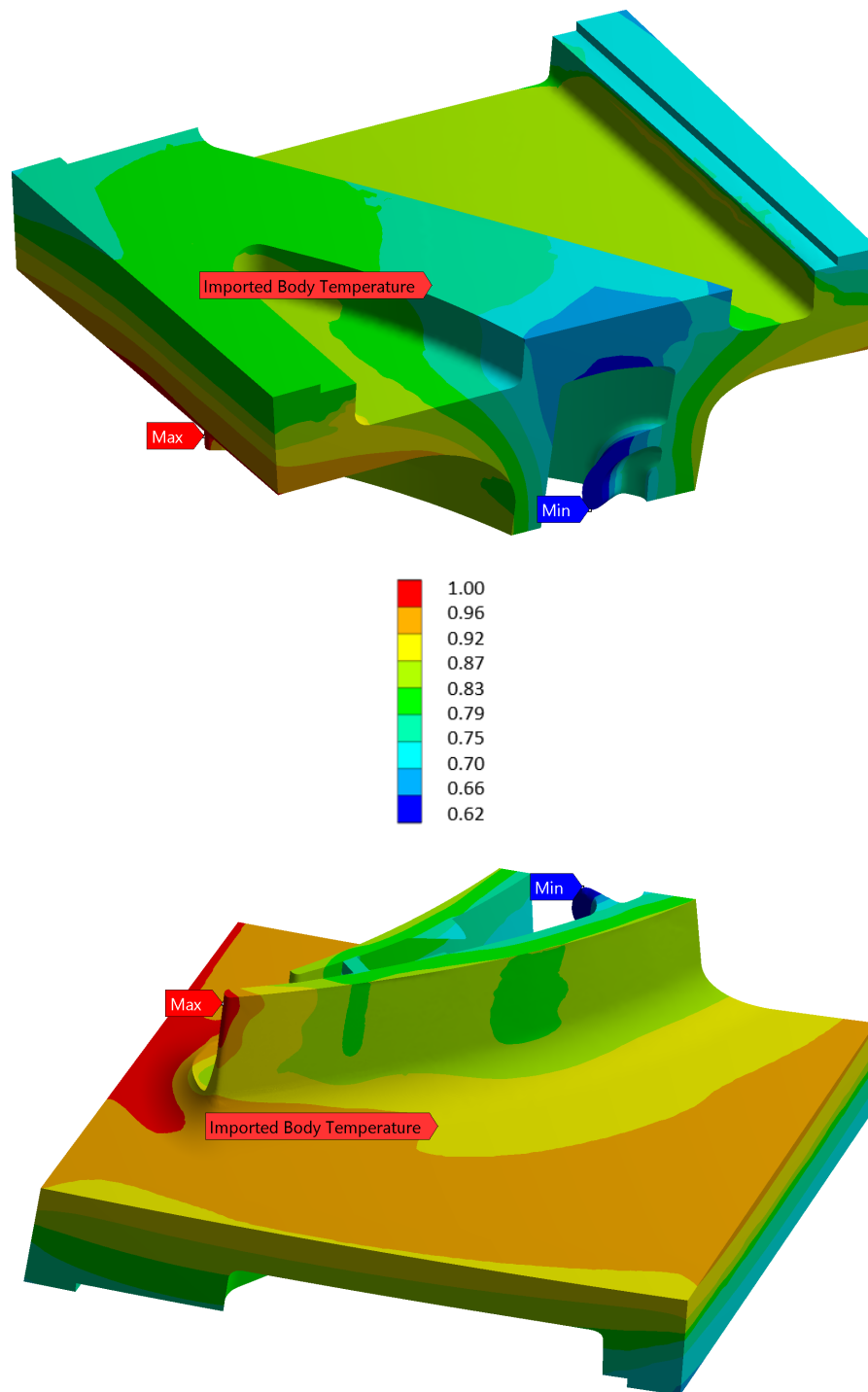


Figure 4.17: Temperature gradient of the whole model applied to the submodel as boundary condition

- The mechanical loads have been applied directly to the submodel. In this case, all the pressures that actuate in the airfoil have been imported, illustrated in the following figures, normalized to the maximum value.

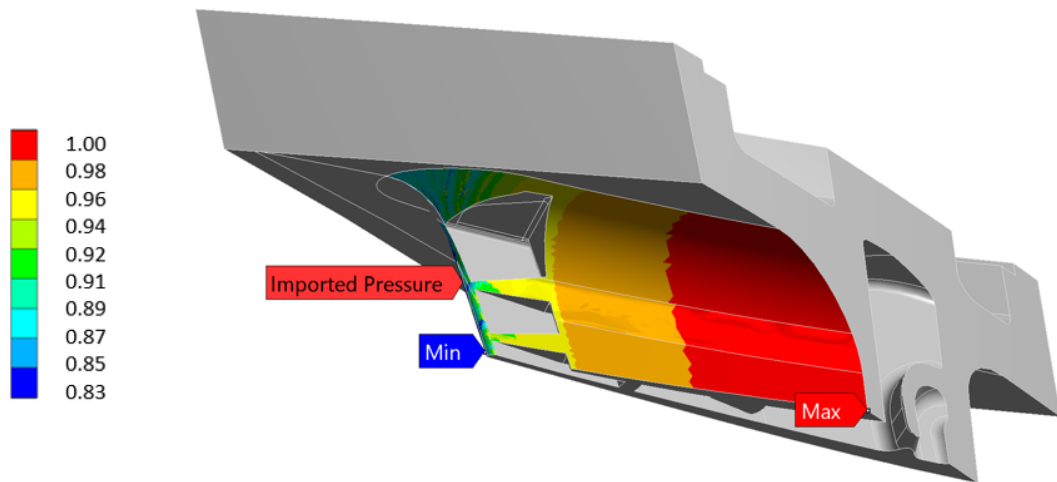


Figure 4.18: Imported pressure load on the pressure side of the airfoil

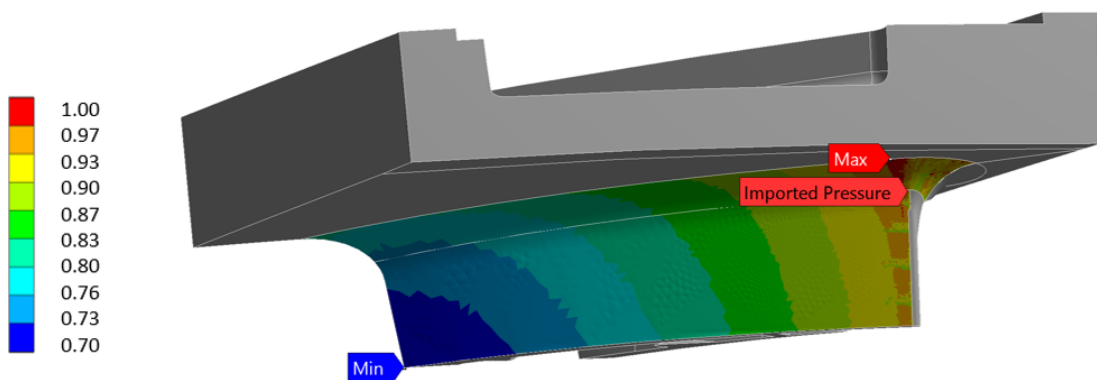


Figure 4.19: Imported pressure load on the suction side of the airfoil

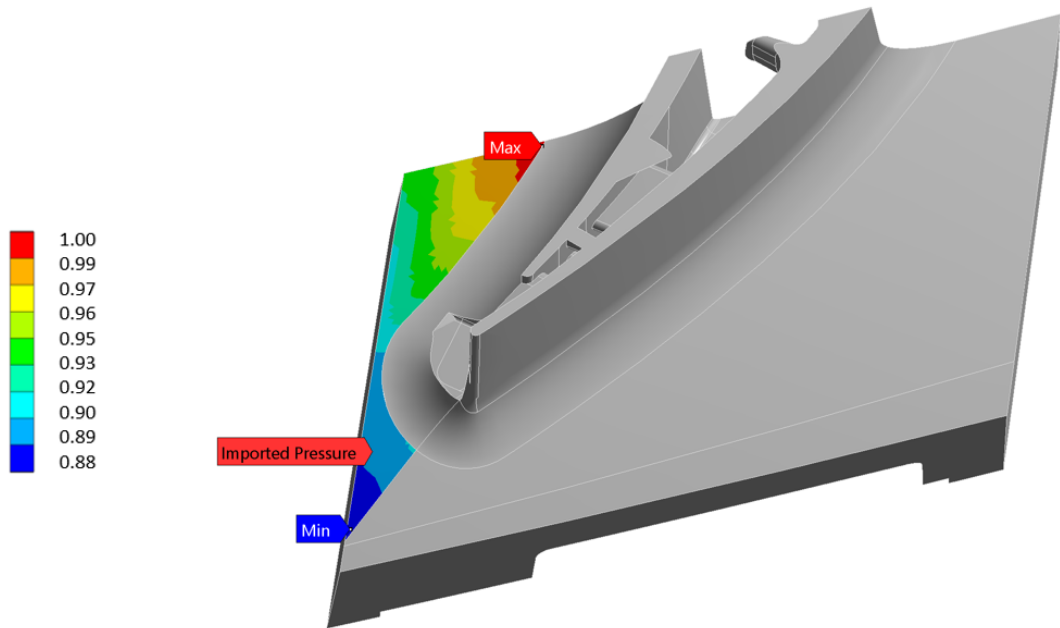


Figure 4.20: Imported pressure load on the pressure side of the exterior platform of the vane

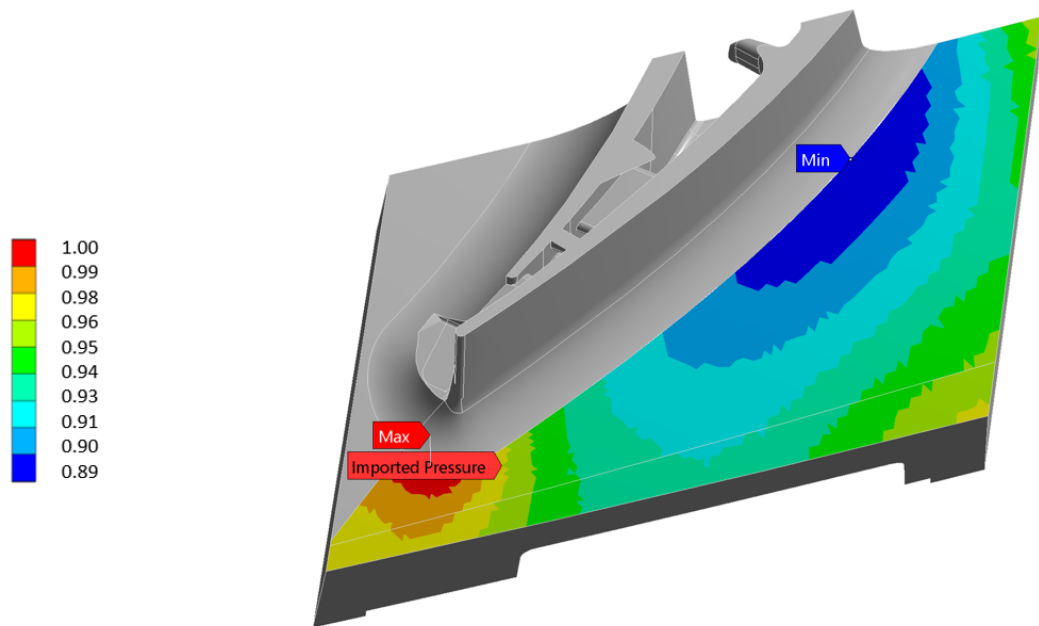


Figure 4.21: Imported pressure load on the suction side of the exterior platform of the vane

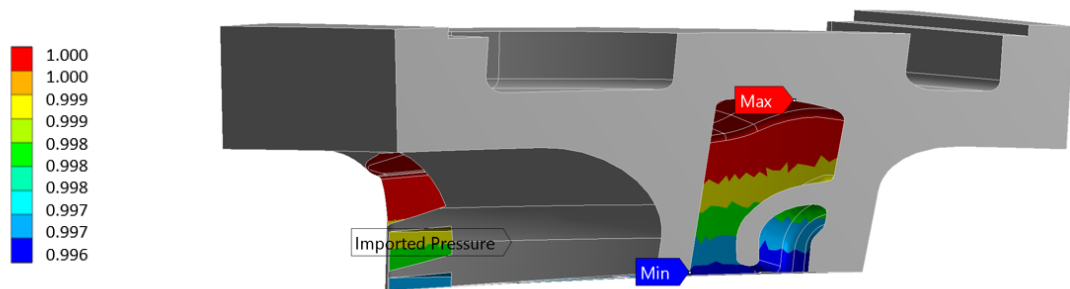


Figure 4.22: Imported pressure load on the internal cooling channels of the vane

6. The submodel has been solved.

Finally, it can be outlined that the same stress status, found in the whole model, has been reached in the submodel, guarantying therefore its correct functioning. Moreover, in the Fig. 4.23, this comparison can be appreciated, normalized to the maximum value. On the left part, the whole vane stress status is illustrated, cropped to the interested area. Meanwhile, on the right part, the submodel stress status with its boundary conditions is represented.

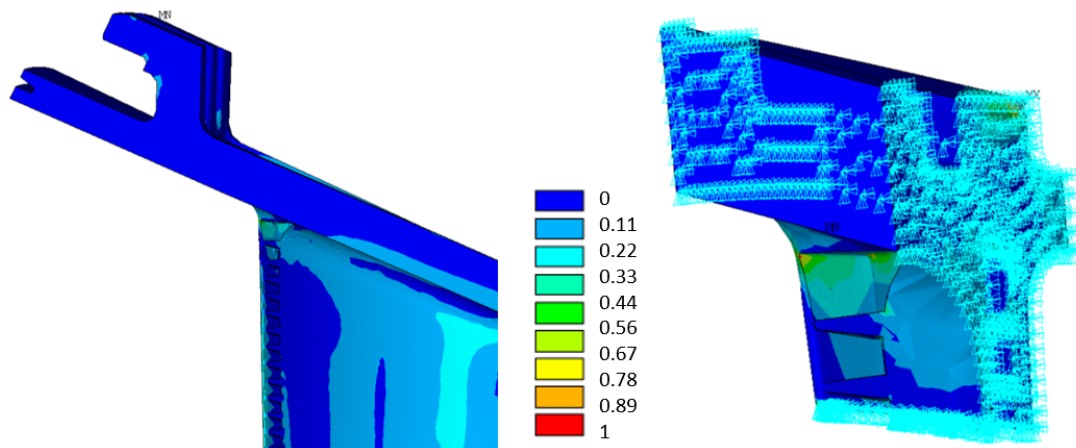


Figure 4.23: Comparison between whole model stress status and submodel stress status

4.4 Crack modeling

Among the several techniques employed to simulate fracture behaviour of complex structures, the Finite Element Method is largely adopted. For this reason, under this subsection, the way in which the crack has been modeled, under *ANSYS Workbench*, will be explained.

Once the submodel has been validated, the next step before starting with the crack modelisation, is the generation of the mesh. This step is of crucial importance since it will determine the accuracy of the results. For so, a suitable mesh may be implemented, in such a way that guarantees the approximation of all the singularities within this zone, obtaining a higher stress gradient. However, it is important to highlight, the need of a **quadratic tetrahedron** elements base mesh, in order to use the fracture tool. [54] Therefore, *SOLID187* has been implemented, which is a higher order 3-D, 10-node element (illustrated in Fig. 4.24). It has a quadratic displacement behavior and is well suited to modelling irregular meshes. [55]

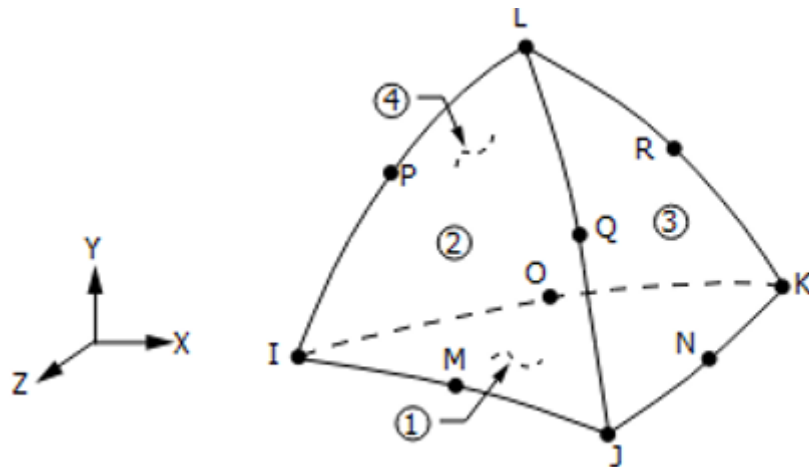


Figure 4.24: SOLID 187 Geometry [55]

Furthermore, with the objective of obtaining a refined zone around the PETE, a **sphere of influence** of 8 mm of radius and 0.5 mm of element size, has been implemented, as illustrated in Fig. 4.25. Meanwhile, the rest of the submodel has been meshed with quadratic tetrahedron elements of 1.5 mm of element size.

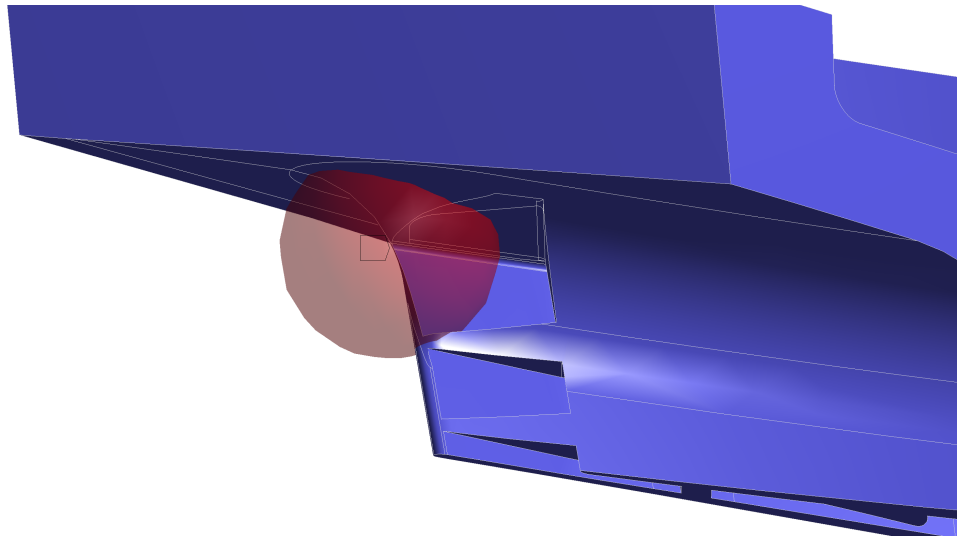


Figure 4.25: Mesh around the PETE with a sphere of influence of radius 8 mm and 0.5 mm of element size

The final mesh obtained can be appreciated in the following images. In the Fig. 4.26, it is shown the overall result, meanwhile, in the Fig. 4.27, it can be observed more precisely the sphere of influence result, obtaining a more refined mesh around the critical location.

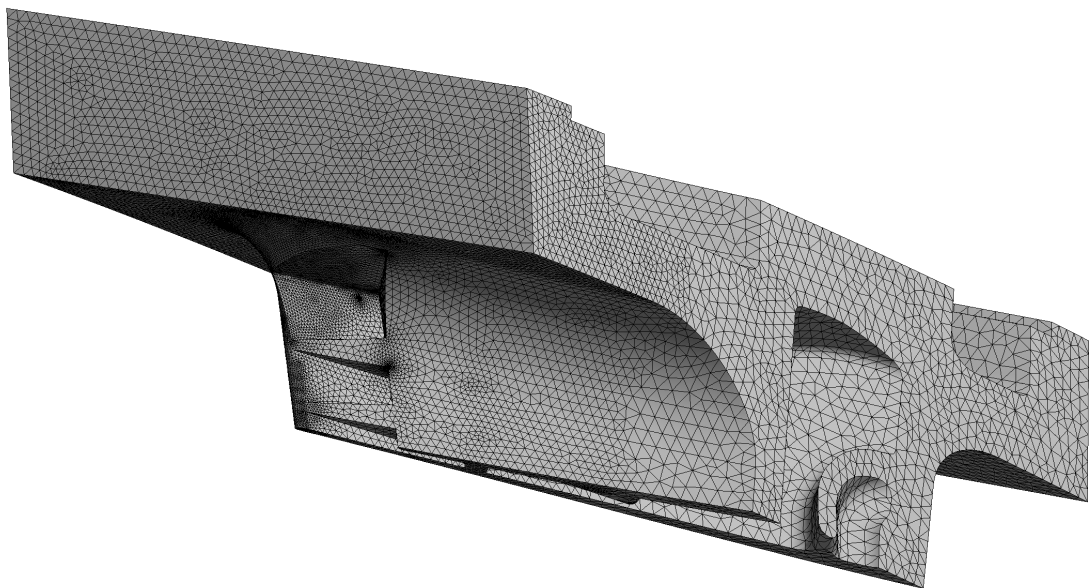


Figure 4.26: Final mesh on the whole submodel

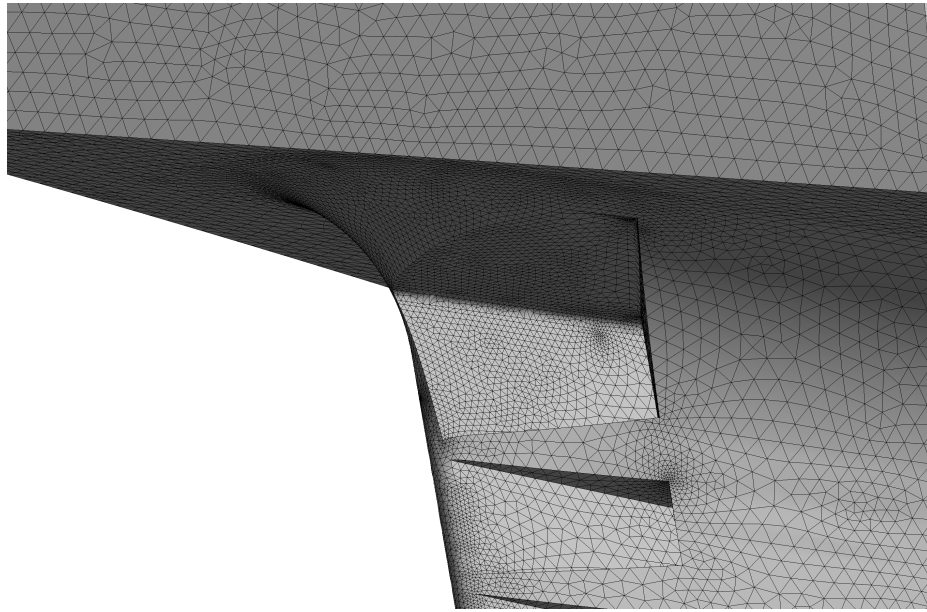


Figure 4.27: Mesh result around the PETE due to the sphere of influence

Once the mesh has been generated, fracture analysis can be subdivided in the following steps [56]:

1. Crack definition.
2. Fracture parameters computation.
3. Crack growth analysis and study.

To go ahead with this workflow, the following task is the crack definition. To proceed, the *Fracture* folder within *ANSYS Mechanical*, has been used. This tool presents several methods to define the crack, such as Semi-Elliptical Object, Pre-Meshed Crack or Arbitrary Crack. Under this work, it has preferred to adopt the last method, due to the analyzed component complexity. As a result, using the Arbitrary Crack method, the first step is the surface body creation that will represent the crack surface. In this study, a circle has been adopted as shape, putting it on the evaluated zone, as illustrated in the Figure 4.28.

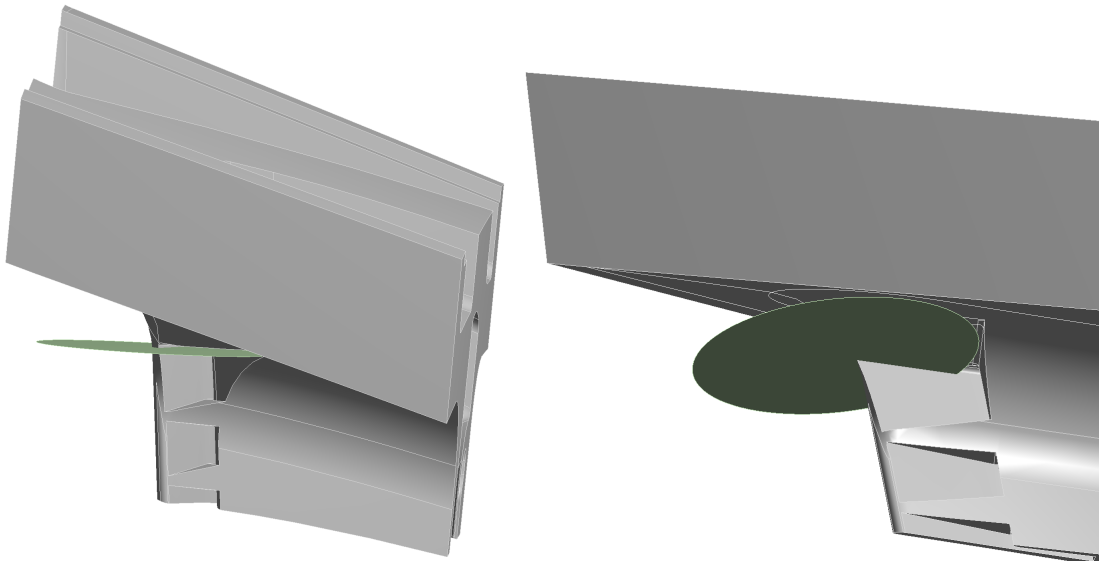


Figure 4.28: Crack modelisation with a circular surface body at the PETE

Once the surface has been created, a new coordinate system should be implemented with the origin in the crack tip, the Y -axis directed towards the normal of the crack's top face and the X -axis towards the crack extension direction, as shown in Figure 4.29. [57]

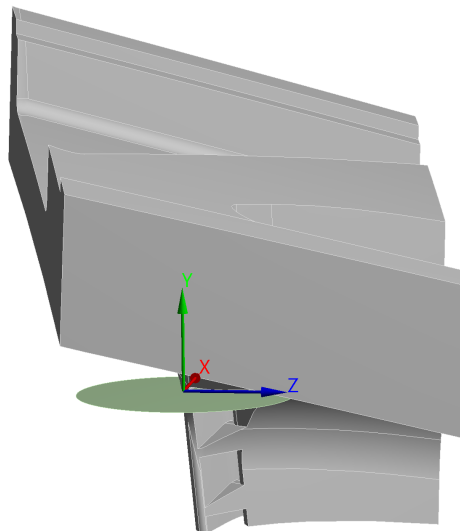


Figure 4.29: New Coordinate System at the crack apex

Then, within the Fracture folder, it should be specified the type of crack method (Arbitrary Crack) and its properties, as illustrated in the Figure 4.30. For instance, the coordinate system already created has to be indicated, the crack surface, the mesh method set to tetrahedrons, the mesh contours for the cracks shape, etc.

Moreover, the crack faces nodes can also be observed, *NS ArbCrack Front*, *NS ArbCrack TopFace* and *NS ArbCrack BottomFace*, where the first one is a named selection that contains the nodes at the crack front, used for fracture parameters results postprocessing. The other two are named selections located in the *XZ* plane, created automatically for the crack's top face and bottom face respectively, containing nodes for applying pressures to each face (in this case no pressure has been put on). [58]

Details of "Arbitrary Crack"	
Scope	
Source	Arbitrary Crack
Scoping Method	Geometry Selection
Geometry	1 Body
Definition	
Coordinate System	Crack_1
Crack Shape	Arbitrary
--Crack Surface	1 Body
Mesh Method	Tetrahedrons
<input type="checkbox"/> Growth Rate	Default (1,2)
<input type="checkbox"/> Front Element Size	0,10 mm
<input type="checkbox"/> Solution Contours	6
Suppressed	No
Buffer Zone Scale Factors	
<input type="checkbox"/> X Scale Factor	2,
<input type="checkbox"/> Y Scale Factor	2,
<input type="checkbox"/> Z Scale Factor	2,
Named Selections Creation	
Crack Front Nodes	NS_ArbCrack_Front
Crack Faces Nodes	On
--Top Face Nodes	NS_ArbCrack_TopFace
--Bottom Face Nodes	NS_ArbCrack_BottomFace

Figure 4.30: ANSYS Details of Arbitrary Crack method

Once all these parameters are set, the model is ready to generate the *fracture meshing* (clicking on **Generate all crack meshes**). It is a post mesh process, which occurs in a separate step after the base mesh is generated, overriding its settings within the crack limits. [59] As it has been said previously, for the base mesh inside the crack and the surrounding, the fracture meshing only supports quadratic tetrahedron elements. Also, it can be outlined that this fracture mesh permits the crack fronts analysis. As a consequence, once the model has correctly created all these steps, it will be ready for the SIF evaluation that will be presented in the following subsection.

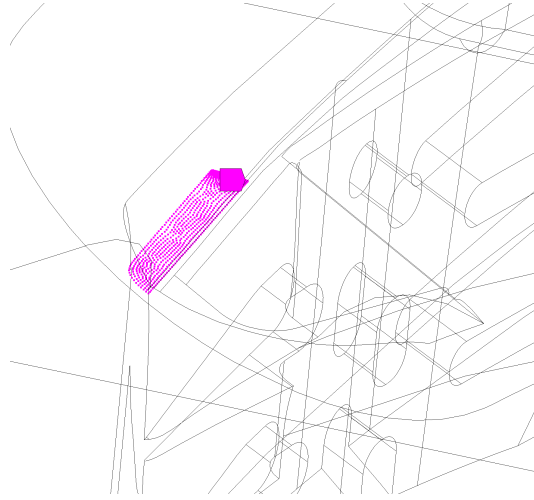


Figure 4.31: Named Selection on the top face of the arbitrary crack (NS ArbCrack TopFace)

4.5 Stress Intensity Factors evaluation

To go ahead with the workflow already defined in the previous subsection, the following step is the computation and evaluation of the **fracture parameters**. As it has explained in the **Chapter 3**, the stress and deformation status around the crack apex is not enough to assess the catastrophic failure of a structure. Therefore, fracture parameter computation and its comparison with the material fracture toughness must be examined.

Two possible methods are present when analyzing a crack in terms of LEFM. Its behaviour can be studied in terms of **energy** or **stresses**. The last one, in terms of stresses (SIFs), is the most used for evaluating industrial applications. As a result, it has decided under this work, to study and to evaluate the possible unstable crack propagation in terms of SIFs.

The analysis of these parameters has been performed thanks to the *Fracture Tool* that it is within the *ANSYS Mechanical* program. They are computed along the crack front using the interaction integral method, which is defined as [30]:

$$I_0 = -\frac{\int_V q_{i,j} [\sigma_{kl} \varepsilon_{kl}^{aux} u_{k,i} - \sigma_{kj} u_{k,i}^{aux}] dV}{\int_S \delta q_n dS} \quad (4.1)$$

where:

$\sigma_{ij}, \varepsilon_{ij}, u_i$ = stress, strain and displacement respectively
 $\sigma_{ij}^{aux}, \varepsilon_{ij}^{aux}, u_i^{aux}$ = stress, strain and displacement respectively of the auxiliary field

q_i = crack extension vector

Moreover, if the thermal and initial strains exist in the structure and the surface tractions act on crack faces, the interaction integral is expressed as [30]:

$$I = I_0 + \frac{\int_V [\sigma_{kl}^{aux} \varepsilon_{kl,i}^{th} - \sigma_{kl}^{aux} \varepsilon_{kl}^0] q_i dV}{\int_S \delta q_n dS} - \frac{\int_S [t_k u_{k,i}^{aux}] q_i dS}{\int_S \delta q_n dS} \quad (4.2)$$

where:

$\varepsilon_{ij}^{th}, \varepsilon_{ij}^0$ = thermal and initial strains respectively

t_i = traction on crack surfaces

As a result, the interaction integral method is associated with the stress-intensity factors as [30]:

$$I = \frac{2}{E^*} (K_1 K_1^{aux} + K_2 K_2^{aux}) + \frac{1}{\mu} K_3 K_3^{aux} \quad (4.3)$$

where:

K_i ($i = 1,2,3$) = Mode I, II and III stress-intensity factors

K_i^{aux} ($i = 1,2,3$) = auxiliary Mode I, II and III stress-intensity factors

$E^* = E$ for plane stress and $E^* = E/(1 - \nu^2)$ for plain strain

E = Young's modulus

ν = Poisson's ratio

μ = shear modulus

Additionally, to guarantee the accuracy of the stress-intensity factors calculations, the local crack apex coordinate system must fulfill the following specifications:

- Local x axis pointed toward the crack extension
- Local y axis pointed toward the normal crack surface
- Local z axis pointed toward the tangential direction of the crack front

It should be outlined that these specifications were already accomplished in the previous subsection, as it can be observed in the Figure 4.29. The local coordinate system consistency across all the nodes along the crack front, is important in order to obtain path-dependency, which results in a correct SIF behaviour. Additionally, it can be highlighted that the interaction integral method applies area integration for 2-D problems, and volume integration for 3-D problems. [30]

To continue with the study, prior to the SIFs evaluation at the critical vane location (PETE), a fracture parameter analysis, on a test plate, has been performed in order to verify the correct behaviour of the tool. As a consequence, it has modelled with *ANSYS SpaceClaim* the test plate shown in the Fig. 4.32a, at which it has inserted a crack of rectangular shape, following the procedure explained in the previous subsection. It has been loaded with a normal traction load of 1000

N at the top surface (illustrated in the Fig. 4.32b), and it has been inserted a fixed support at the other extreme (represented with the label B in the Fig. 4.32b). Moreover, regarding the mesh, it has set the base mesh to tetrahedrons, making a more fitted mesh around the crack, as it shows the Fig. 4.33. It also should be highlighted that these results are not dimensionless since it is just a verification of the correct functioning of the fracture tool with *ANSYS* pre-defined material.

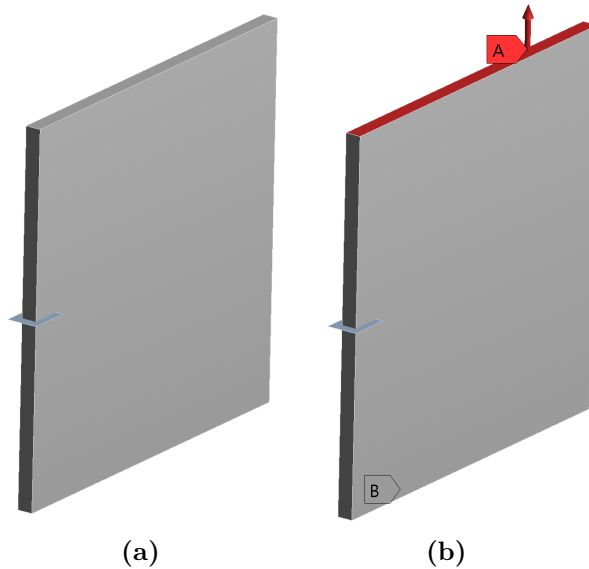


Figure 4.32: (a) Test plate with a rectangular crack shape in the middle of the specimen. (b) Test plate with the normal force applied on the top surface (A) and a fixed support at the opposite surface (B)

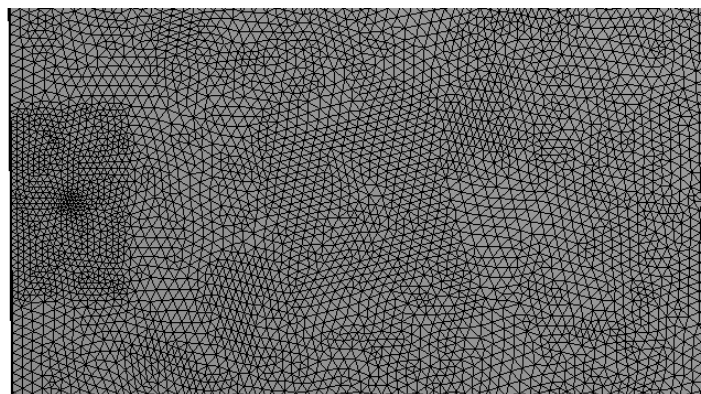


Figure 4.33: Mesh of the test plate

The main objective of this analysis is the establishment of KI as a function of the crack depth (a), in order to compare its variation given by *ANSYS*, with the theoretical one:

$$K_I = Y\sigma\sqrt{\pi a} \quad (4.4)$$

As a result, the procedure realized was the KI factor computation at the different crack lengths (1, 1.5, 3, 6 and 10). The increase of a was performed by increasing the rectangular length at each time. It should be highlighted that the code calculates the KI parameter on a number of circular paths (usually 6), around the front of the crack, where the "1" indicates the start of the crack front and "2" indicates the end of the crack front.

An example of this calculation is illustrated in the Fig. 4.34. Where, the X axis indicates the distance along the crack front, and the Y axis indicates the KI. It also should be noted that the first path is not displayed since the results are not reliable. Additionally, it is worth pointing out the distribution of KI along the crack front, as it can be appreciated, varies from the start of the crack front (1) to the end of it (2). This is due to the fact that the program computes the parameter KI for each node found in the crack front (the name selection *NS ArbCrack Front* already explained in the previous subsection), where the results at the extremes are not fully reliable. Indeed, it can be appreciated the almost constant values at the middle (where the results are fully reliable) as it is predicted, since the stress status around the crack front is expected to be constant due to both, constant applied load and resistant area.

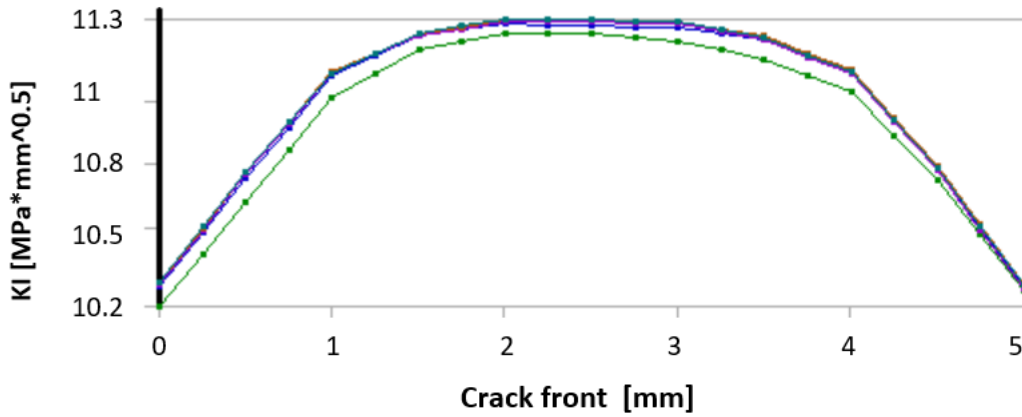


Figure 4.34: KI along the crack front with $a = 10\text{mm}$ calculated in the 5 paths at the plate

As a result, in order to evaluate the stress intensity factor, it has decided to take the KI mean value of the 5 paths (the first one is not considered), obtaining

then, the KI mean value found along the crack front. The outcomes obtained were tabulated (Tab.4.1) and represented graphically (Fig. 4.35), observing the expected behaviour of KI. This is to say, the SIF increase with the increase of a .

Mean value of KI [MPa·√mm]				
a = 1 mm	a = 1.5 mm	a = 3 mm	a = 6 mm	a = 10 mm
3.2	3.8	5.6	8.2	10.9

Table 4.1: Values of $\bar{K}I$ as a function of the crack length (a) of the plate

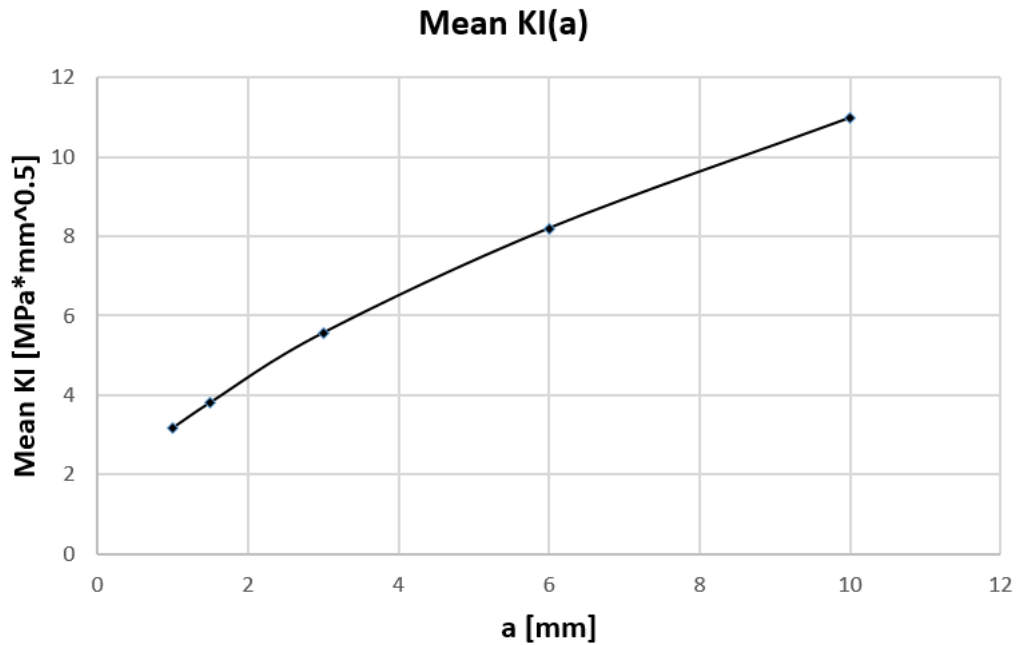


Figure 4.35: Evolution of $\bar{K}I$ with the length of the crack (a) of the plate

Additionally, in the following figure, it can be appreciated the opening of the crack with $a = 10$ mm, where it can be observed the distribution of the stresses due to the opening effect. Moreover, it is observed that the maximum stress is localized in the whole crack front as expected. Therefore, with all these considerations, it can be concluded from this pre-study, the correct functioning of the SIFs computation in *ANSYS*.

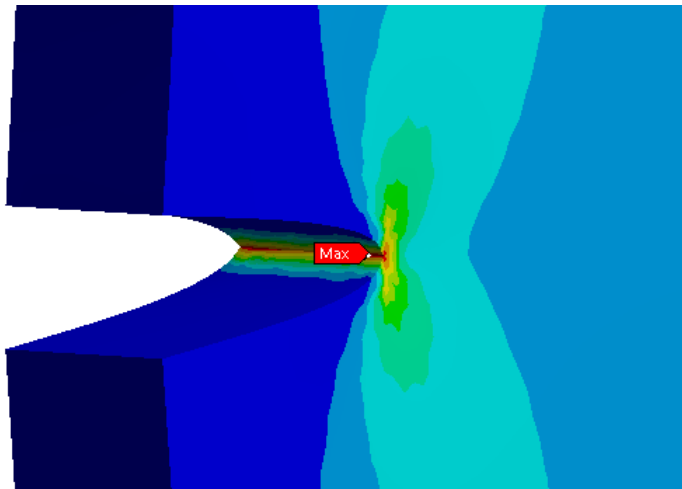


Figure 4.36: Stress status at the crack front of the test plate

Once evaluated the correct behaviour of the SIFs computation with the plate, it will go ahead analyzing the component under consideration. The procedure realized is the same done to the plate, namely the KI evaluation with the increase of a . In this case, since the surface employed as crack is circular, in order to increase the crack length, it has incremented the radius of the circle. The crack length values studied were 1, 2.5, 3, 5, 7.5 and 10 mm. The results are presented in the Fig. 4.37, where it can be observed for each crack length the obtained KI along the crack front, being the results normalized to the maximum value for privacy reasons.

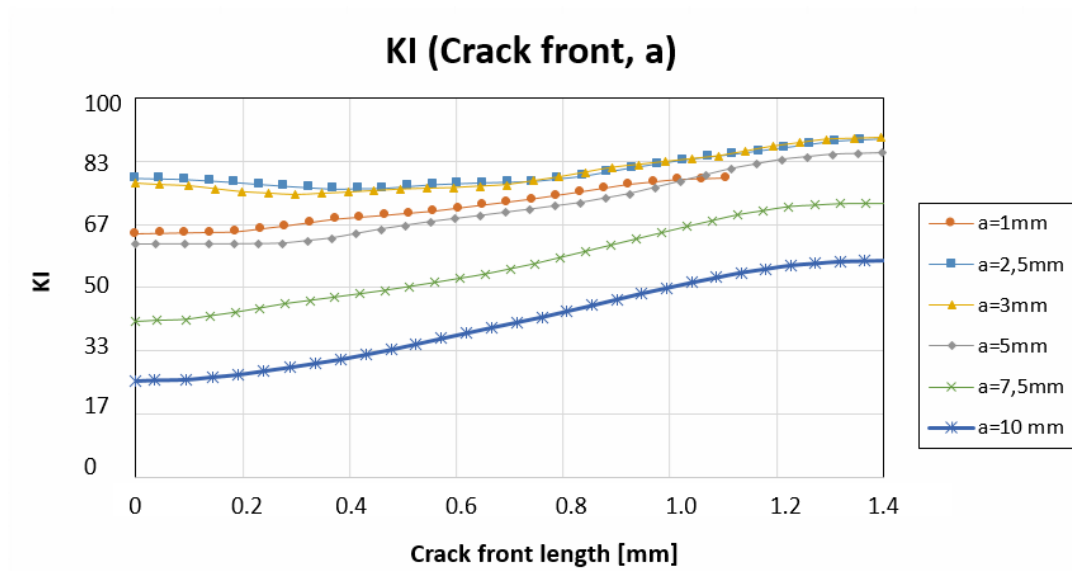


Figure 4.37: KI of each crack length along the crack front

It should be remarked that the KI obtained is the mean value of the five contour paths, for instances, in the Fig. 4.38, it is showed the values of KI obtained with $a = 10$ mm, within the five paths. From this graph, it can be remarked the consistency of the paths, being them quite similar, and additionally, it can also be outlined the increase of the KI as it approximates to the end of the crack front. This "end" (observed in the Fig. 4.39 and represented with a 2), coincides with the pressure side of the vane, and therefore, the place with higher stress status, as it was seen in the analysis done to the uncracked vane, where it was found that it was not constant and indeed was higher on this side. As a consequence, it makes sense the increase of the KI as it reaches the pressure side.

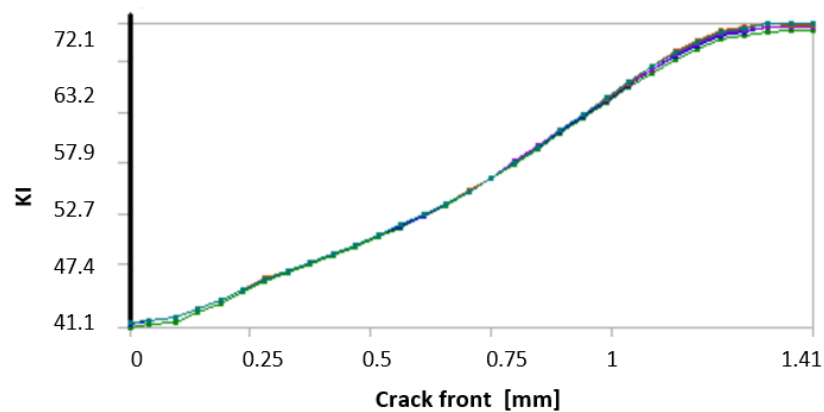


Figure 4.38: KI along the crack front with $a = 10$ mm calculated in the 5 paths

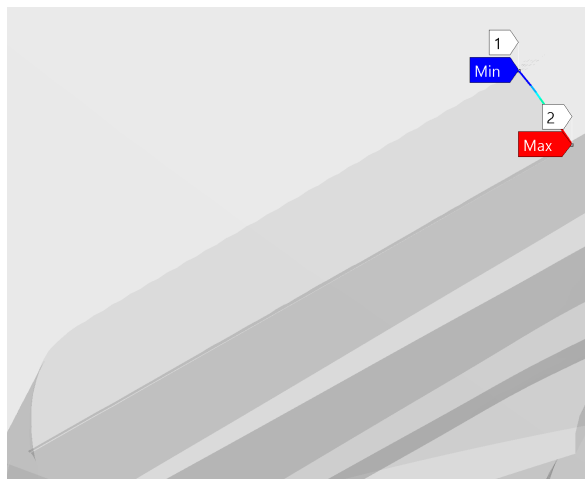


Figure 4.39: Crack front. The label 1 represents the start of it while the label 2 represent the end of the crack front

From Fig. 4.37, it can be observed as well, this tendency of the increase of KI as it reaches the pressure side. However, with the aim of obtaining a clearer graph, it has followed the same procedure as before (KI mean value along the crack front for each crack size), obtaining the results (normalized to the maximum value) seen in the Tab. 4.2.

Mean value of KI					
a = 1 mm	a = 2.5 mm	a = 3 mm	a = 5 mm	a = 7.5 mm	a = 10 mm
70.88	80.61	80.01	71.24	56.44	41.26

Table 4.2: Values of $\bar{K}I$ as a function of the crack length (a) at the PETE of the vane

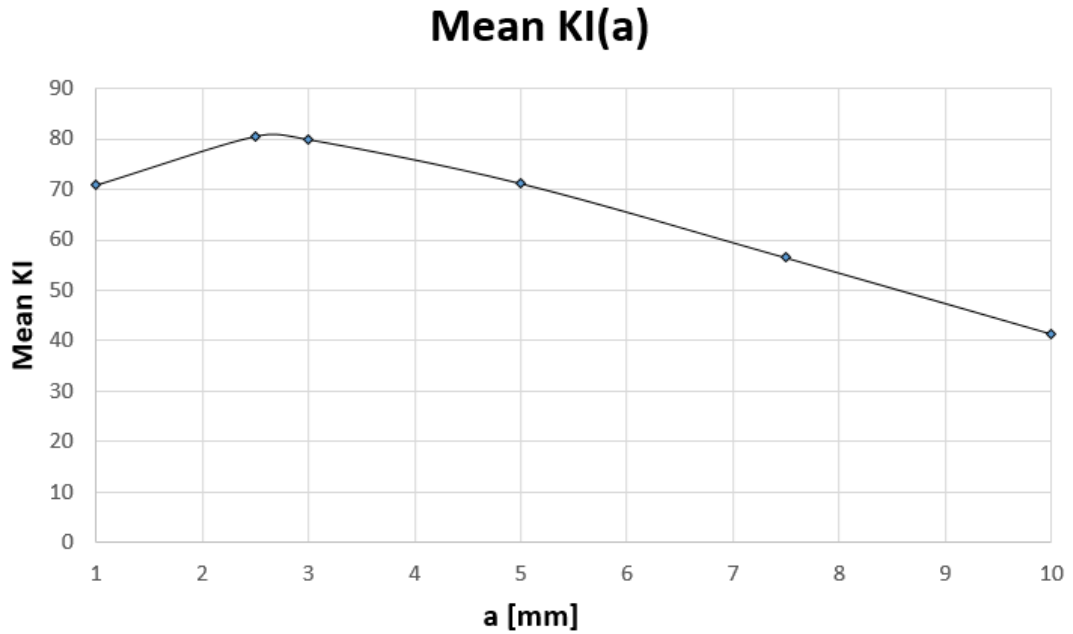


Figure 4.40: Evolution of $\bar{K}I$ with the length of the crack (a) at the PETE of the vane

In the Fig. 4.40, the trend of KI with the a can be observed more clearly. It can be appreciated an initial increment of the KI with the increase of the length until the arrival at a point where it starts to decline. In other words, differently from what it should have been expected from the theoretical value (the increase of the KI with the a), it has been found its reduction at a certain point. This can

be explained, not only due to the complex geometry of the component to analyze, but also to the extreme tough conditions that the element is subjected to, that makes this problem no longer applicable to the theoretical case. Additionally, what it has been discovered is that due to the stress status found in the vane, there is performed a redistribution of the stresses with the increase of the crack, that does not create an unstable increase of the stress around the crack that would lead to the unstable propagation.

From the figures below, all the previous statements are verified. In first place, it is observed how in the crack front it is always found the maximum stress as expected (due to the fact that the crack actuates as stress intensification). Secondly, it can be appreciated higher stresses at the pressure side than in the suction side, as it was discussed previously. Lastly, it can be noticed that there is no drastic increase of the stress status at the crack front, as it should be expected from a theoretical point of view, but instead it diminishes due to the redistribution of efforts that it is produced within the vane.

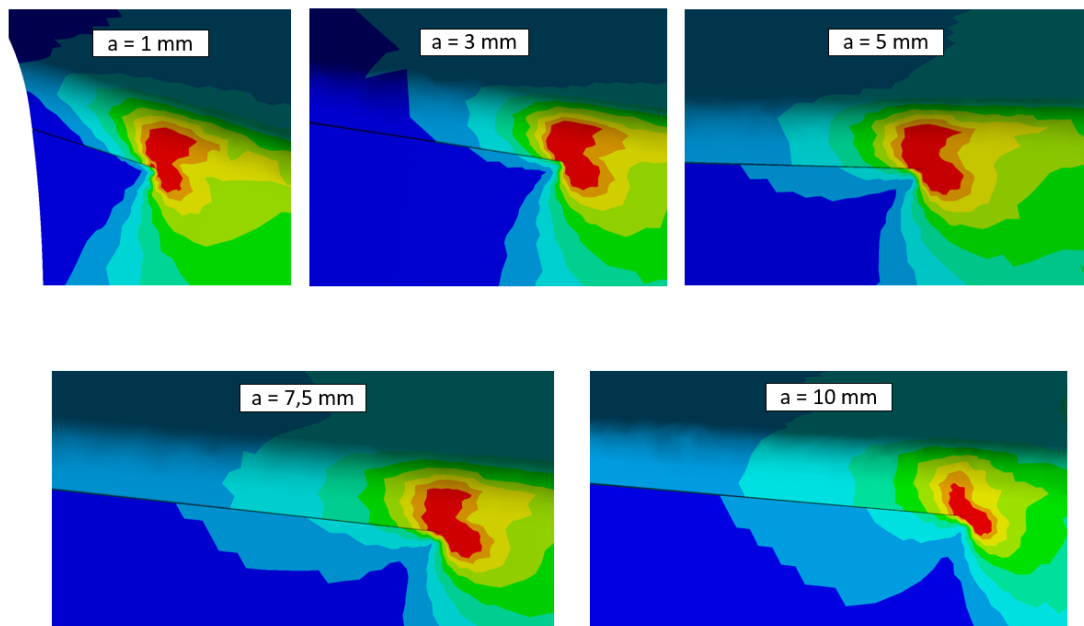


Figure 4.41: Distribution of the stress around the PETE on the pressure side at the different crack lengths

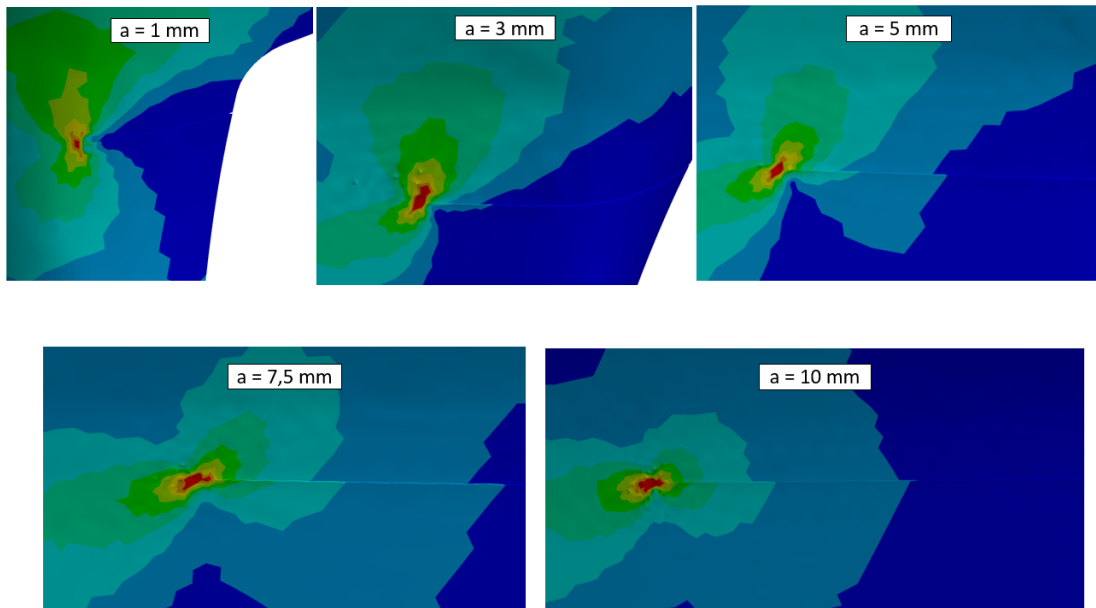


Figure 4.42: Distribution of the stress around the PETE on the suction side at the different crack lengths

Additionally, the two other SIFs (K_{II} and K_{III}) have also been studied. The results obtained are shown in the Fig. 4.43, where it is also represented the material Fracture Toughness. From this graph some conclusions can be made; firstly, it can be outlined that K_{II} and K_{III} are lower than the K_I results but of the same magnitude. Therefore, it can be said that K_I is the most representative SIF of the crack dynamics, acting as the "driving force" of its propagation, being the dominant one. Nevertheless, the other two should not be neglected in the crack growth assessment, that will be done in the following subsection. Additionally, from the comparison with the material fracture toughness, it is also important to remark, from this first analysis, that no unstable crack propagation is expected, since the fracture toughness is way above from the results obtained.

Finally, it should be remarked that due to the importance of the mesh utilized in order to obtain reliable results, a sensitivity analysis to the model has been done. In this sensitivity analysis, K_I obtained values for the different meshes have been studied, choosing the mesh that gave the more conservative results (showed in the previous subsection).

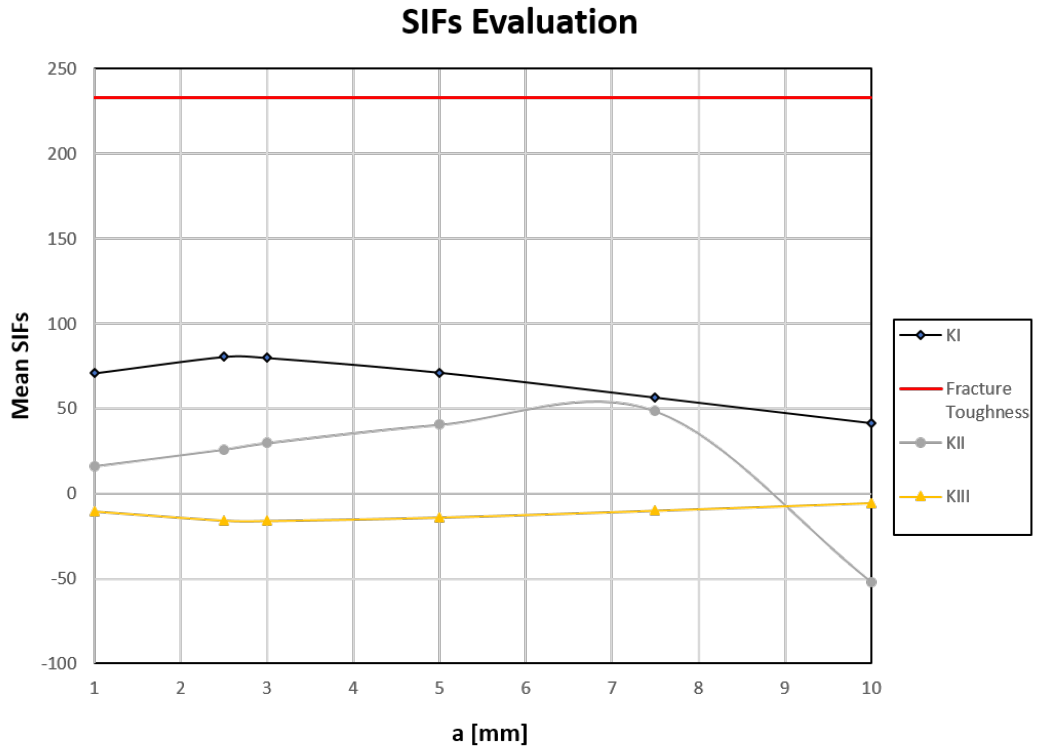


Figure 4.43: Evolution of the SIFs with the length of the crack (a) at the PETE of the vane compared with the Fracture Toughness of the material

4.6 Crack growth assessment

Once evaluated the SIFs, although no unstable propagation is expected with the obtained results, it is important to study the behavior of the crack when it is subjected to the phenomena of fatigue, creep and oxidation. As it has been explained in the Chapter 3, these effects lead to crack propagation.

To proceed, it has performed the analysis with an in-house tool developed in *Ansaldo Energia*, called *Propagangui*. It is a software programmed with MATLAB code which performs living evaluation of the components affected by cracks. Particularly, it carries out crack propagation calculation, failure assessment and probabilistic assessment of failure through Montecarlo analysis. However, under this work, in order to study the crack behaviour it will be developed only the two first points.

The calculations of the crack propagation are based on the LEFM theory

considering fatigue, creep and oxidation as the main processes for crack growth. Their contribution is modelled following the equations described in the Chapter 3, which are recalled below:

- **Fatigue Crack Growth** modeled through Paris' Law equation:

$$\frac{da}{dN} = C\Delta K^n \quad (4.5)$$

- **Creep Crack Growth** modeled through Arrhenius' dependent equation:

$$\frac{da}{dt} = A_0 K_{MAX}^m e^{\frac{-Q}{RT}} \quad (4.6)$$

- **Oxidation** modeled through a sub-parabolic Arrhenius' dependent equation which relates depletion zone thickness and time:

$$d\gamma'^n = A_{0,\gamma'} e^{\frac{Q_{\gamma'}}{RT}} t \quad (4.7)$$

The oxidation contribution is calculated assuming that gamma γ' depleted zone corresponds to a crack of the same length, therefore the **Oxidation Crack Growth** is modeled as:

$$\frac{da}{dN_{OXI}} = \frac{d \sum T_i \frac{\Delta a_{oxi}}{\Delta t} T_i}{dN} t_i \quad (4.8)$$

The model calculates separately the contribution of these phenomena for a given operation cycle, and assumes that these contributions shall be summed, which is the most common assumption in industrial applications. [52] Therefore, the overall propagation model will account for each increment related to fatigue, creep and oxidation crack propagation contribution as reported in the following equation:

$$da/dN_{tot} = da/dN_{OXI} + da/dN_{CREEP} + da/dN_{FATIGUE} \quad (4.9)$$

It should be outlined that it has defined a critical temperature of the material below which the crack growth is mainly due to fatigue loads, because of the absence of γ' -depletion zone and creep effect.

The software evaluates the failure of a component with a crack using the Failure Assessment Diagram (FAD). Its main objective is to study whether the component will fail when overcoming the FAD line or will remain in stable behaviour. It is important to remark that the x axis represents the variable Lr ($0 \leq Lr \leq Lr_{max}$), where its limit ensures the avoid of the plastic collapse. Meanwhile, the y axis represents the variable K_r , which is a function that does not depend on the load or

geometry but only on the material deformation behaviour and its limit will ensure that the condition of unstable propagation is not reached. Moreover, the FAD can be established in different ways depending on the available inputs and on the level of conservativity needed, where more inputs will lead to a less conservative diagram and vice-versa. The different FAD options are illustrated in the Fig. 4.44, where the requested inputs are reported in the Tab. 4.3.

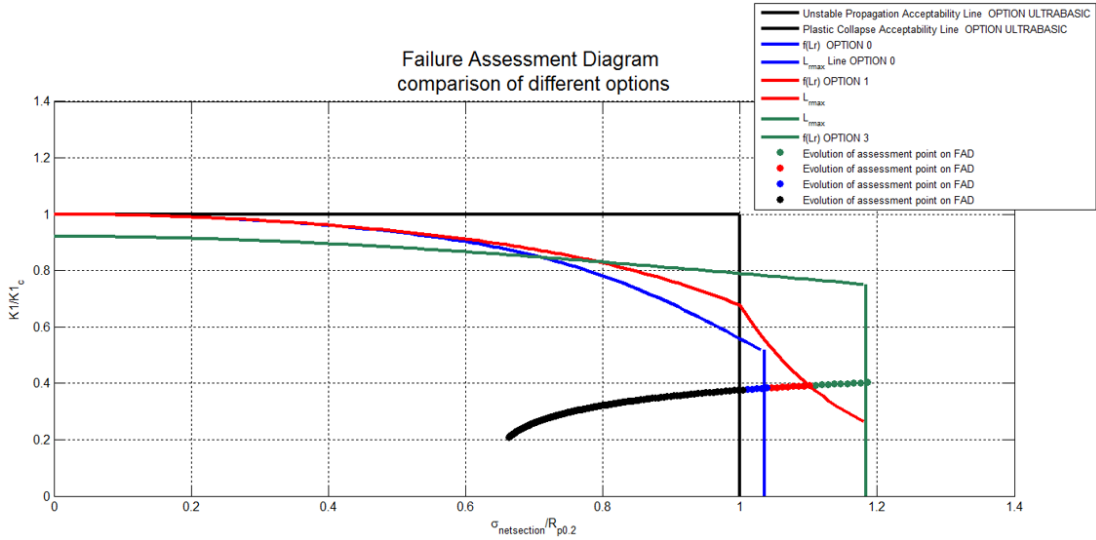


Figure 4.44: Comparison of the different Failure Assessment Diagram options

FAD Option	Inputs needed
Option 0 (SINTAP/FITNET)	Rp0.2
Option 1 (SINTAP/FITNET)	Rp0.2, E, Rm
Option 3 (SINTAP/FITNET)	Rp0.2, E, true-stress/true-strain curve
LEVEL 1A (BS7910)	-
LEVEL 2A (BS7910)	Rp0.2, Rm

Table 4.3: FAD Options with the requested inputs

The program will evaluate for each cycle, the corresponding assessment point, and therefore, the crack propagation behaviour, where an overcoming of the FAD line will imply the failure of the component. As it can be expected from the previous statement, this failure can be due to plastic collapse, if the assessment point reaches the right side of the FAD, or due to unstable propagation, if the assessment point exceeds the upper line of the FAD. Additionally, the reached

assessment point is expressed by the following coordinates:

$$\left. \begin{aligned} x &= L_r = \frac{\sigma_{ref}}{\sigma_y} \\ y &= K_r = \frac{K_{eq}}{K_{mat}} = \frac{K_I}{K_{Ic}} \end{aligned} \right\} \quad (4.10)$$

where σ_{ref} , also represented as $\sigma_{NetSection}$, is the Von Mises stress of the uncracked component found at the corresponding crack depth, considering only primary stress, and $\sigma_y = R_{P0.2}$, is the offset yield strength of the material. On the other hand, the K_{eq} can be equal to the K_I , or a function of K_I , K_{II} and K_{III} , depending on the multiaxiality state in the region of the flaw, while the K_{mat} is the material fracture toughness (K_{Ic}).

Afterwards, the software will make an estimation of the propagation analysis providing three graphs:

- **Crack evolution plot** which reports the crack growth among cycles.
- **Propagation plot** that illustrates the crack propagation rate among the stress intensity factor range.
- **FAD plot** in which it is represented the assessment point

Where the propagation calculation will stop if one of the following reasons takes place:

- The assessment point meets the FAD line where plastic collapse or unstable propagation can take place.
- The crack grows until the specified number of cycles without reaching the FAD line, therefore in simulated conditions the component can be considered safe.
- The calculation achieves the last crack length for which it has been obtained the SIF (in this case is 10 mm).

In order to proceed with the evaluation of the vane, it has been recollected from *ANSYS* the following inputs required to carry out the whole study:

- The set of SIFs already obtained in the previous subsection, where it can be underscored the use of multiaxiality correction, that is to say the use of K_I , K_{II} and K_{III} . This was mainly because the three of them were of the same magnitude and therefore the last two should not be neglected.
- The temperature along the crack path of the uncracked component in order to apply the oxidation and creep phenomena whether the temperature is above the critical one.

- The Von Mises Stress along the crack path of the uncracked component in order to establish the assessment point. It is important to outline that the stress related with the assessment point considers only the primary stress. In this sense, it has multiplied the obtained stress by the ratio between the primary and total stresses. To acquire this value, it has been performed three different analysis on *ANSYS*; with all the loads, with only mechanical loads and with only thermal loads. The obtained value at the PETE was about 0.76, which can be remarked its high value, since statoric vanes mainly are subjected to thermal loads. Nevertheless, in the Fig. 4.45, it can be appreciated this fact where it is observed that the main stress status is due to thermal. However in order to be conservative, it has decided to put the value obtained at the PETE although is not representative of the whole vane.
- The net area of the crack defined as $(total\ area - crack\ area) / total\ area$.

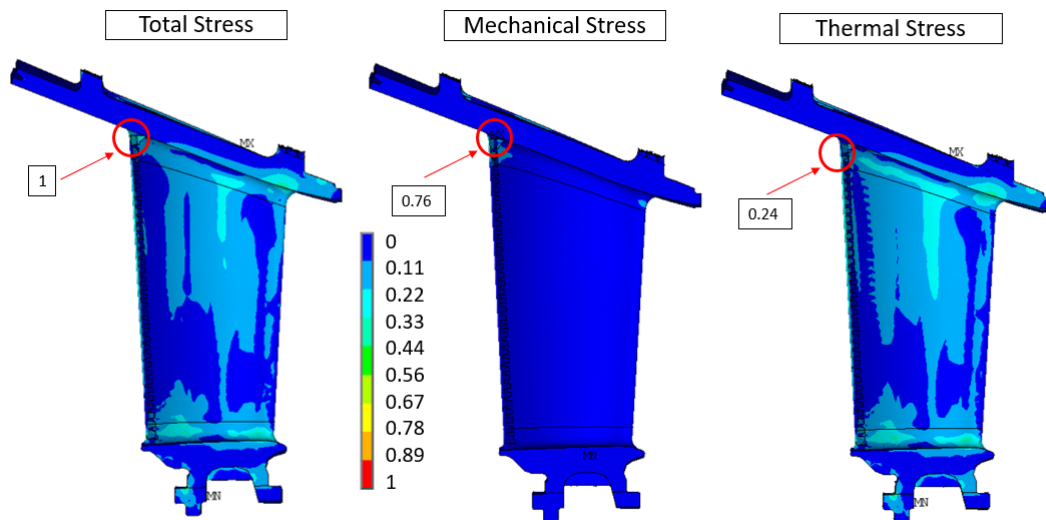


Figure 4.45: Stress status comparison between all loads, mechanical loads and thermal loads, normalized to the maximum value

Additionally, it should also be introduced the inputs related with the material (critical temperature, fracture toughness, yield strength, etc) and the parameters related with fracture mechanics (oxidation, creep and fatigue coefficients). Moreover, an initial crack size should be given (in this case was of 1 mm) and a cyclic target (3000 cycles) which, as it was mentioned before, it can be one of the causes of the end of the calculation.

With all these considerations, a first case has been studied with an operation cycle (start-up, base load and shut down) of 10 firing hours, as it can be observed in Fig. 4.46. From this analysis, a stable propagation has been obtained, as expected, finishing the program calculation because of the last crack size arrival, from which it has obtained the SIFs (10 mm).

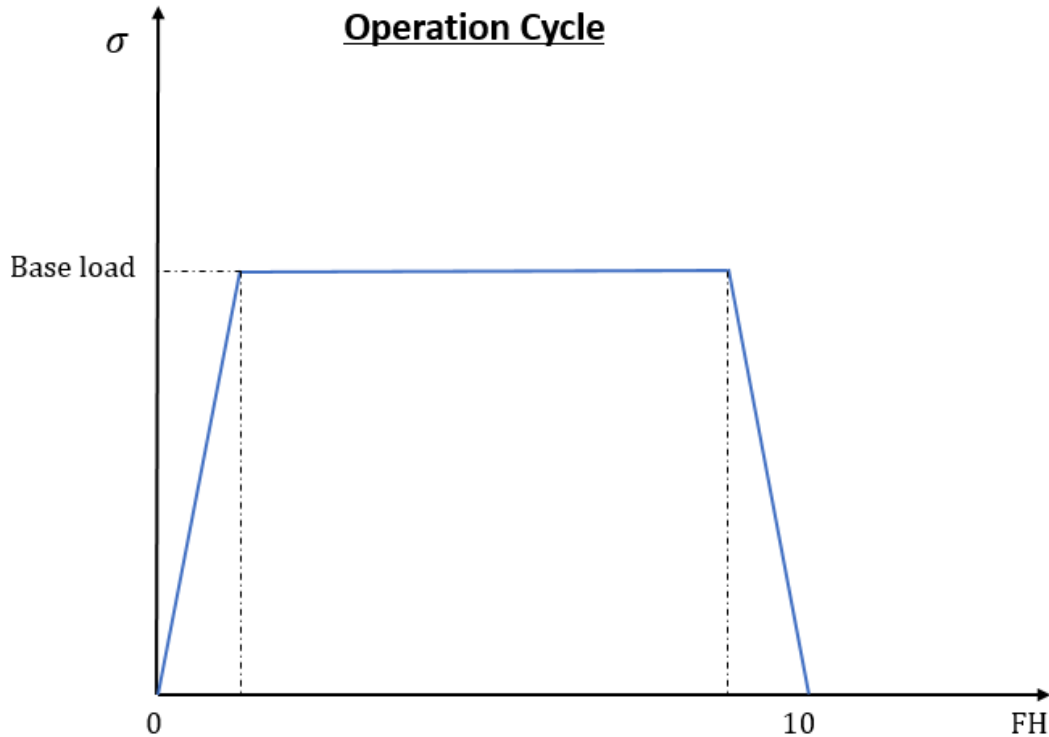


Figure 4.46: Operating cycle. Start-up, base load and shut down

Additionally, the following graphs were obtained, where in Fig. 4.47, it can be appreciated how the crack evolves with the number of cycles. It can be highlighted its consistency, that is to say the slow down of the crack growth rate as the crack length increases due to the reduction of the KI. In other words, as the crack evolves the stress concentration around the front of the crack is redistributed and diminishes, making its propagation slower.

On the other hand, Fig. 4.48 shows the crack propagation rate with respect to the SIFs, where it can be remarked the linearity of the fatigue and creep propagation with them, as expected from the equations 4.5 and 4.6 and the non dependency of the oxidation contribution.

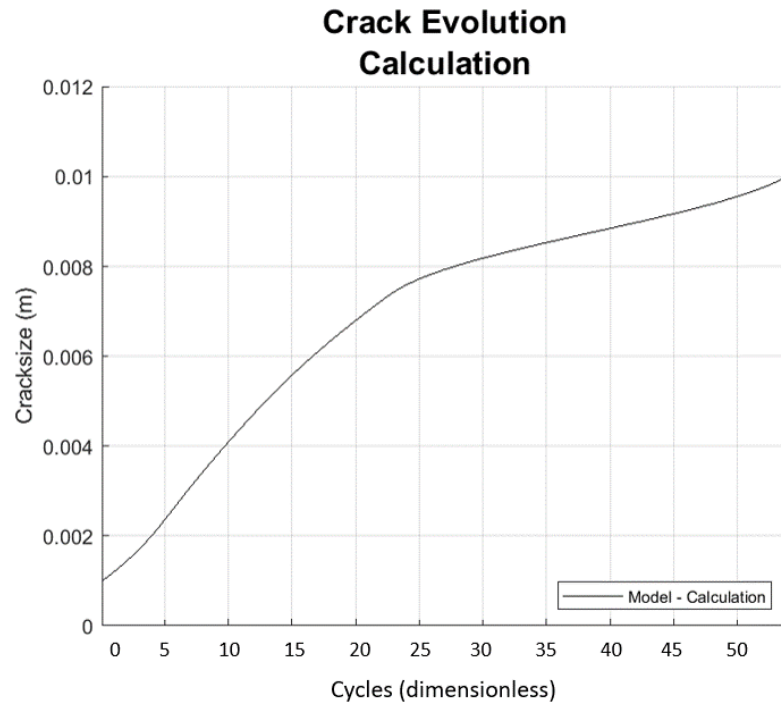


Figure 4.47: Crack Evolution at an operation cycle of 10 firing hours

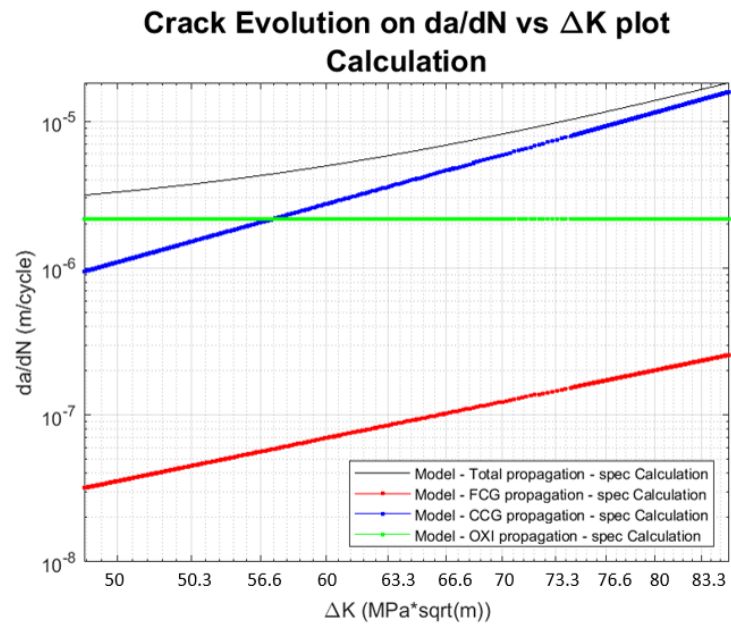


Figure 4.48: Crack Evolution Growth in terms of SIFs at an operation cycle of 10 firing hours

Finally, observing the FAD (Fig. 4.49), it can be appreciated the evolution of the assessment point among the cycles, where it can be highlighted that it is within the limits. Therefore neither plastic collapse, or unstable propagation is expected.

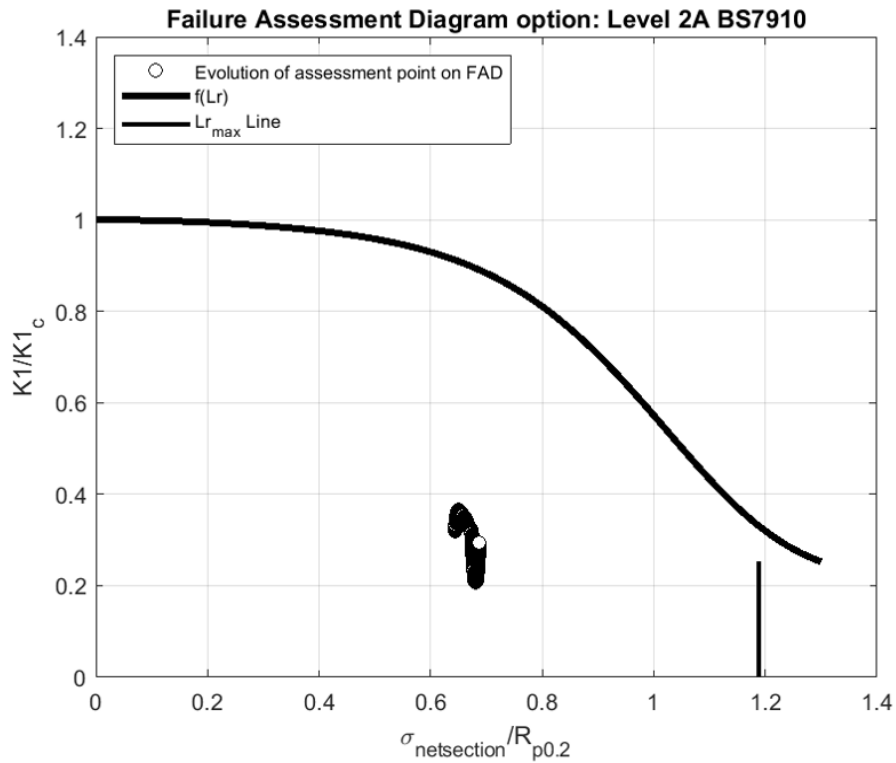


Figure 4.49: FAD of the crack

Once validated that the crack does not propagate in an unstable way, with the scope of determining the life of the component, different end of life lines have been developed. Previous to their explanation, it is important to recall that the life of a vane is expressed in terms of firing hours and number of start-ups (number of cycles). That is to say, in order to evaluate how long a vane can stand, the creep phenomenon, that will give the firing hours when reaching the established limit, and the fatigue phenomenon, that will give the number of cycles to crack initiation, have to be studied. In Fig. 4.50, a hypothetical end-of-life line is represented, below which the component will be in safe conditions.

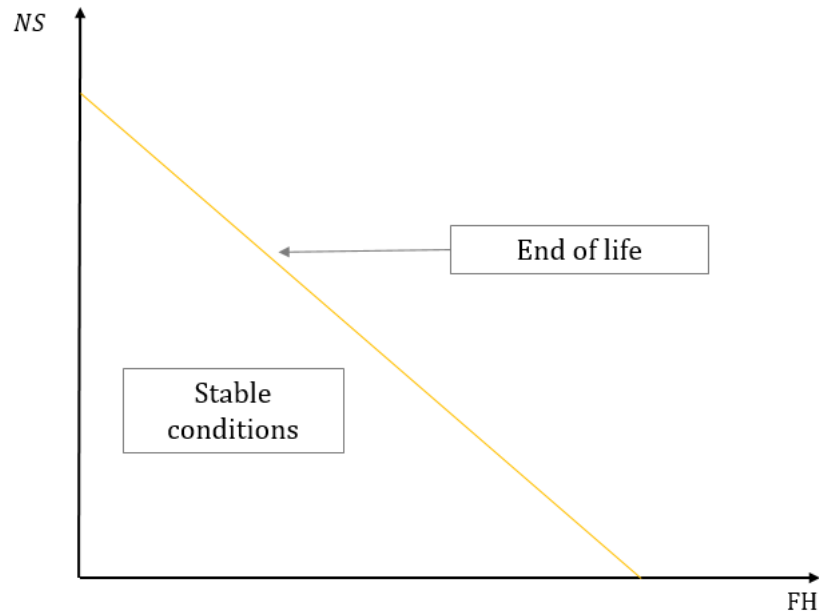


Figure 4.50: Hypothetical End-of-life line

However, in this study, due to the extremely low firing hours (obtained from the analysis done in the subsection 4.2) that did not guarantee the first interval of maintenance, and therefore, did not guarantee one life of the component, it has been needed the use of fracture mechanics in order to study the evolution of the crack, evaluating the new end-of-life lines.

It has decided to implement the end-of-life lines for different crack lengths (2 mm, 3 mm, 5 mm and 10 mm) at the component. That is to say, it will be implemented different lines that will give the area below which the component will not reach the specified crack size.

To proceed, several operating cycles with different firing hours for each cycle (4 h, 10 h, 20 h, 30 h, 40 h and 400 h), have been studied. Then, getting into the crack evaluation graph, represented in Fig. 4.51, the number of cycles until the arrival at each crack length (2 mm, 3 mm, 5 mm and 10 mm) have been obtained. Finally, making the relation between firing hours of each cycle and the total number of cycles, in order to obtain the total number of firing hours, it has built the graph represented in the Fig. 4.52, where it can be observed the different *End of life lines* for the different cracks size, in terms of the total firing hours and the total number of cycles.

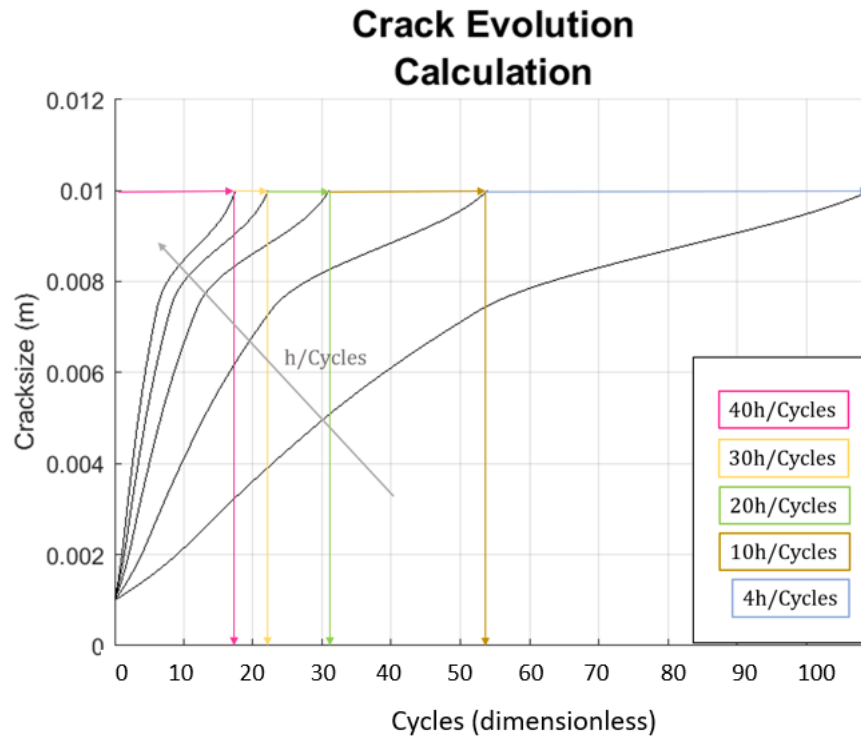


Figure 4.51: Crack Evolution with the different operating cycles

From the end-of-life lines graph two statements can be done. It can be obtained, depending on the crack size limit established and the duration of the operating cycle, the working condition in terms of cycles or firing hours, below which the vane can withstand without arriving at the specified crack size. This is to say, if for instance the critical crack size is supposed to be 10 mm, the vane will be in safe conditions when stays below the 10 mm line. The second statement is in relation with the crack propagation. As it can be observed, the propagation between 2 mm and 5 mm happens within low number of cycles (or firing hours), whereas the propagation between 5 mm and 10 mm will need more time. Again this is explained thanks to the obtained SIFs. Contrary to what it should be expected from a theoretical point of view, the increase of the propagation growth with the increase of the crack length, the drop of the KI will delay the arrival at 10 mm of crack size. In other words more cycles (or firing hours) will be needed until the arrival of the "critical" crack size.

From this last statement, this tendency can be extrapolated, concluding that each time the crack will grow slower, because it does not tend to propagate unstably and therefore, each time the crack will need more cycles until the arrival of a certain

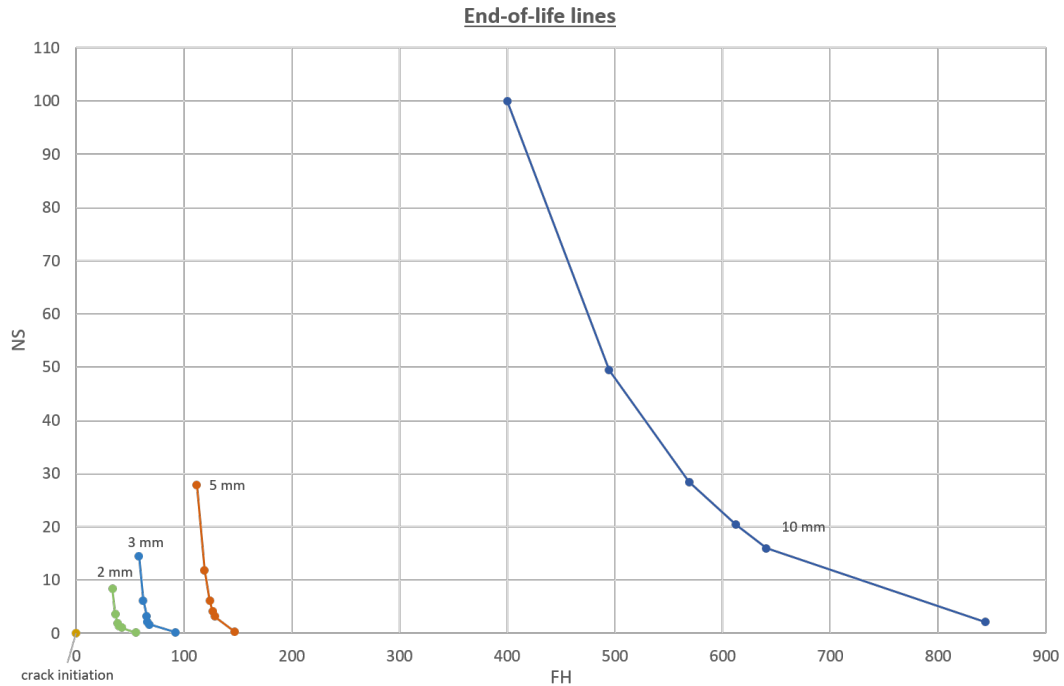


Figure 4.52: End of life lines of the different crack sizes

crack size. So, it can be concluded that the crack does not follow a tendency of propagating in an unstable way, but it follows an stable propagation in which as the crack evolves the crack growth rate diminishes.

Lastly, it should be remarked that the Fig. 4.51 is not only representative of the way the data has been collected to create the end of life lines, but also, it is interesting to examine it, since it shows the evolution of the crack with the number of cycles. Hence, the crack growth rate at the different operating cycles can be appreciated. It is remarkable how the number of cycles diminishes at the arrival of a crack size of 10 mm with the increase of the firing hours of each cycle. This is due to the fact that with higher hours per cycle, the total number of hours until the arrival of 10 mm (as illustrated) is much higher, and hence, the phenomena of creep, oxidation and creep count much more, arriving to this crack size earlier. For instance, with an operating cycle of 10 hours, it takes 50 cycles (dimensionless) until the arrival of 10 mm, therefore the vane is working for $10 \times 50 = 500$ firing hours. Meanwhile, for a cycle of 40 hours, the vane will need only 16 cycles until the arrival of 10 mm, because the total firing hours will be 640. So, under these last conditions, the vane will work 140 more hours, and hence more time that the phenomena are taking place. So, another conclusion from this statement is the fact that with higher hours per cycle the crack growth rate increases.

Chapter 5

Conclusions

A crack assessment on a second-stage GT vane, via LEFM approach, in particular by means of SIF evaluation, in addition with crack propagation analysis in terms of fatigue, creep and oxidation, has been presented under this thesis. The aim of this work is to study the evolution of a crack at the most critical zone of the GT vane, validating whether the crack propagation will follow a stable behaviour or rather it will propagate in an unstable way, causing possible component failure.

The applied procedure consists of, the MI Assessment to the whole TV2, validating the most stressed zones in which the crack may nucleate. From this first step, the **first conclusion** obtained was that the **Platform Exterior Trailing Edge (PETE)**, and the **Platform Internal Trailing Edge (PITE)** were the most stressed areas, where the corresponding material's yielding stress were overcome. Furthermore, the creep strain limit (experimental material limit) was overtaken within a short period of time, not fulfilling therefore its verification.

Hereafter, the **LCF analysis** showed that the required number of cycles were not accomplished at the PETE. Concluding, from this first analysis, that the **PETE was the most critical part** of the component, in which the **crack could nucleate**.

Then, it has proceeded with the SIF analysis via the *Fracture Tool* within *ANSYS Workbench*. However, prior to this study, the **correct functioning** of the *Fracture Tool* has been tested through a simple model: a plate with a crack inside, loaded with a normal tensile load. A comparison of this model with direct calculations by formula has been performed, appreciating **the increasing of the SIF KI with the rise of the crack length a** , concluding therefore **its validation**.

Next, the sub-modelling technique applied to the TV2 and the component meshing have been performed in addition with the crack implementation at the critical zone. Hereafter, the **SIF analysis**, namely the evaluation KI with the increase of a , has been done, highlighting the following comments:

- **The increase of KI** within the crack front, as it reaches the **end of the crack front**, correspondent to **the pressure side**, has been observed. This part of the component, as seen from the MI Assessment, is the one subjected to higher loads and stresses. Therefore, it can be expected that the stress intensification produced by the crack will be bigger at this side, as the results have shown.
- Regarding the **trend of KI with the a** , an **initial increment of the KI** with the increase of the length has been obtained. However, in contrast with the theoretical formula, it is followed by its decline when arriving at a certain crack length. This KI decrease is explained due to the **vane complex geometry** and the **severe working conditions** that the element has to withstand, which make that a **redistribution of the stresses** is performed as the crack length increases, diminishing the stress intensification at the critical zone. Therefore, no unstable increase of the stress around the crack is created.
- From the **KII and KIII analysis**, lower values with respect to KI, have been observed. Concluding that the most representative SIF of the crack propagation dynamics is KI, being the **dominant** one. Nevertheless, KII and KIII should not be neglected in the crack growth assessment, since they all have the same order of magnitude.
- Lastly, from the SIF comparison with the **material fracture toughness**, it has observed that this last one is way above from the obtained results.

Therefore, from the SIF study, it can be concluded that **no unstable propagation is expected**. Additionally, in order to validate the obtained fracture parameters, a stress status analysis of the sub-model at each crack length has been realized. From this exploration, the two first upper points have been checked. On one side, it has crosschecked that the pressure side is the one with higher stress intensification, obtaining a higher stress status around this zone than in the suction side. And, on the other side, it has verified that, from a certain crack length, the stress status around the PETE diminishes, redistributing the stresses and not producing therefore, an unstable stress intensification.

Furthermore, from the last analysis performed to the component, the **study of fatigue, creep and oxidation crack growth** thanks to a in-house software, called Propagangui, which carries out living evaluation of cracked components, some comments can be done:

- In first place, from the first study case (10 hours of operation cycle), a **stable propagation** has been obtained, stopping the program calculations because of the last crack size arrival. The crack evolution with the number of cycles has been attained, observing the **slow down of the crack growth rate** as

the crack length increases. This fact is mainly due to the KI reduction. As the crack evolves, the stress concentration at the crack front is redistributed, diminishing, originating a slower propagation.

- It has also been achieved the crack propagation rate with the SIF, observing fatigue and creep linear contribution and the oxidation non dependency contribution.
- Regarding the FAD, the evolution of the assessment point among the cycles is within the limits.

So, from the crack growth analysis in addition with the SIF valuation, it can be concluded that **neither plastic collapse nor unstable propagation** of the crack is expected.

Furthermore, with the scope of **estimating the component lifing**, different **end-of-life lines** for different crack lengths have been performed, obtaining the working conditions (in terms of cycles or firing hours) below which the vane can withstand without arriving at the specified crack size. From this study, concerning the crack propagation, it has been observed that as the crack evolves, the number of cycles needed until the next crack size arrival is higher. That is to say, **the crack each time needs more time to propagate**, hence it reduces its velocity. This tendency, can be extrapolated concluding that each time the **crack will grow slower**, because it does not tend to propagate unstably and therefore, each time the crack will need more cycles until the arrival of the following crack size. Finally, it also should be remarked the increase of the crack growth rate as the number of firing hours per cycle increases, obtaining therefore a faster propagation.

To sum up, with all these things considered, from this work it can be concluded that the crack propagation behavior does **not follow an unstable tendency**, but quite the opposite: it follows **a stable propagation** in which as the crack evolves, the stress redistribution attained makes the **crack growth rate diminishes**.

Bibliography

- [1] *ETD - Gas Turbine Training Course. Relazione corso a Londra 20 - 23 Maggio 2011*. AnsaldoEnergia (cit. on pp. 1, 13–17, 20–24).
- [2] *Mecánica de la fractura*. URL: <https://www.esss.co/es/blog/mecanica-de-la-fractura/> (cit. on p. 2).
- [3] *Fracture Mechanics*. URL: <https://mechanicalc.com/reference/fracture-mechanics> (cit. on p. 2).
- [4] Mladen Berković. «Numerical methods in fracture mechanics». In: *Structural integrity and life* 4.2p (2004), pp. 63–66 (cit. on p. 2).
- [5] Fabrizio Greco, Domenico Ammendolea, Paolo Lonetti, and Arturo Pascuzzo. «Crack propagation under thermo-mechanical loadings based on moving mesh strategy». In: *Theoretical and Applied Fracture Mechanics* (2021), p. 103033 (cit. on p. 2).
- [6] F. Vanti. «Development of an Automatic Procedure for Aeromechanical Optimization of Axial Turbomachines». PhD thesis. Università degli studi Firenze, 2019 (cit. on p. 5).
- [7] Frank Mevissen and Michele Meo. «A review of NDT/structural health monitoring techniques for hot gas components in gas turbines». In: *Sensors* 19.3 (2019), p. 711 (cit. on p. 6).
- [8] Wärtsilä Energy. *Gas Turbine for power generation: introduction*. URL: <https://www.wartsila.com/energy/learn-more/technical-comparisons/gas-turbine-for-power-generation-introduction> (cit. on p. 6).
- [9] Wikipedia. *Bryton Cycle*. URL: https://es.wikipedia.org/wiki/Archivo:Brayton_cycle.svg (cit. on p. 7).
- [10] Endesa Fundación. *Central térmica de ciclo combinado*. URL: <https://www.fundacionendesa.org/es/educacion/endesa-educa/recursos/centrales-electricas-convencionales/central-termica-convencional-ciclo-combinado#> (cit. on p. 8).

- [11] Wärtsilä Energy. *Combined cycle plant for power generation: Introduction*. URL: <https://www.wartsila.com/energy/learn-more/technical-comparisons/combined-cycle-plant-for-power-generation-introduction> (cit. on p. 8).
- [12] G. David. «Reduced Order Model of gas turbine bladed discs». MA thesis. Torino: Politecnico di Torino, 2020 (cit. on p. 8).
- [13] *Resistenza dei materiali di macchine TG - Superleghe*. Ansaldo Energia (cit. on pp. 9, 12, 14, 16, 19, 20).
- [14] *Design Practices- Mechanical Integrity Turbine*. Ansaldo Energia (cit. on pp. 9, 14, 25, 26, 32, 36).
- [15] Antonio Cilindro. *Performance Analysis and Economic Effects of Maintenance and Hot Gas Path Inspection of a Combined Cycle Power Plant*. Dec. 2015. DOI: 10.13140/RG.2.1.3088.5201 (cit. on p. 10).
- [16] Luai Al-Hadhrami, S.M. Shaahid, and Ali Al-Mubarak. «Jet Impingement Cooling in Gas Turbines for Improving Thermal Efficiency and Power Density». In: Nov. 2011. ISBN: 978-953-307-611-9. DOI: 10.5772/22020 (cit. on p. 10).
- [17] S. Can Gülen. *Gas Turbines for Electric Power Generation*. Cambridge CB2 8BS, United Kingdom: Cambridge University Press, 2019 (cit. on pp. 11, 13, 14, 21, 25, 27, 29–36).
- [18] Brent A Gregory and Oleg Moroz. «Gas turbine cooling flows and their influence in output». In: *Mechanical Engineering* 137.03 (2015), pp. 48–54 (cit. on p. 12).
- [19] Anastasia A Buravleva et al. «Spark Plasma Sintering of WC-Based 10wt% Co Hard Alloy: A Study of Sintering Kinetics and Solid-Phase Processes». In: *Materials* 15.3 (2022), p. 1091 (cit. on p. 16).
- [20] David Harris. *How Products are Made*. URL: <http://www.madehow.com/Volume-1/Jet-Engine.html> (cit. on p. 18).
- [21] DC Power. «Palladium alloy pinning wires for gas turbine blade investment casting». In: *Platinum Metals Review* 39.3 (1995), pp. 117–126 (cit. on p. 18).
- [22] Wikipedia. *Natural Frequency*. URL: https://en.wikipedia.org/wiki/Natural_frequency# (cit. on p. 28).
- [23] Suny Oer Services. *University Physics Volume 1. Simple Harmonic motion*. URL: <https://courses.lumenlearning.com/suny-osuniversityphysics/chapter/15-1-simple-harmonic-motion/> (cit. on p. 29).
- [24] Aeroengine Safety. Graz University of Technology. *Vibration Excitement and Vibration Stress in the HCF Range*. URL: <https://aeroenginesafety.tugraz.at/doku.php?id=12:126:1263:12631:12631> (cit. on p. 30).

- [25] Cyrus B. Meher-Hornji. «Blading vibration and failures in gas turbines. Part A: Blading dynamics and the operating environment». In: 10555 Rockley Road, Houston, Texas., June 1993, pp. 1–11 (cit. on p. 30).
- [26] *What is Fatigue Life – S-N Curve – Woehler Curve – Definition*. URL: <https://material-properties.org/what-is-fatigue-life-s-n-curve-woehler-curve-definition/> (cit. on pp. 33, 34).
- [27] Siemens Digital Industries Software. *Mean Stress Corrections and Stress Ratios*. URL: [mean-stress-corrections-and-stress-ratios](https://www.siemens.com/press/en/mean-stress-corrections-and-stress-ratios) (cit. on pp. 34, 35).
- [28] Bright Work Polish. *What Is The Difference Between Oxidation And Corrosion?* URL: <https://brightworkpolish.com/what-is-the-difference-between-oxidation-and-corrosion/> (cit. on p. 36).
- [29] Chun Hui Wang. *Introduction to fracture mechanics*. DSTO Aeronautical and Maritime Research Laboratory Melbourne, Australia, 1996 (cit. on pp. 37, 39).
- [30] *Fracture Analysis Guide*. Ansys. Canonsburg, PA, 2021 (cit. on pp. 37, 77, 78).
- [31] Md. Minhaj Alam, Zuheir Barsoum, Pär Jonse;n, Hans-Åke Häggblad, and Alexander Kaplan. «Fatigue behaviour study of laser hybrid welded eccentric fillet joints : Part I». In: *12th NOLAMP proceeding 2009 : Nordic Laser Materials Processing Conference ; 24th - 26th August 2009 in Copenhagen*. Godkänd; 2009; Bibliografisk uppgift: CD-ROM; 20090921 (minala). ATV-SEMAPP, 2009 (cit. on pp. 37–40, 44, 45).
- [32] Krystal Nanan. *How and Why a Material Fractures*. URL: <https://www.corrosionpedia.com/how-and-why-a-material-fractures/2/6569> (cit. on p. 38).
- [33] Guillermo Ávila Álvarez. *Estudio de la retracción y el agrietamiento de arcillas. Aplicación a la arcilla de Bogotá*. Universitat Politècnica de Catalunya, 2005 (cit. on p. 38).
- [34] *Linear Elastic Fracture Mechanics : Part One*. URL: <https://www.totalmateria.com/TR/page.aspx?ID=CheckArticle&site=kts&LN=ES&NM=295> (cit. on p. 39).
- [35] Wikimedia Commons. *Stress Concentration by a crack*. URL: https://commons.wikimedia.org/wiki/File:Stress_concentration_by_a_crack.png (cit. on p. 42).
- [36] Timothy D Burchell. *Carbon materials for advanced technologies*. Elsevier, 1999 (cit. on p. 43).

- [37] Dr. M. Medraj. *Modes of Crack Displacement*. URL: <https://pdfs.semanticscholar.org/fefa/d5551c4b90a5ab4b1143d2278eddf27b7aa2.pdf> (cit. on p. 42).
- [38] *Resistenza dei materiali di macchine TG - Resistenza Statica*. Ansaldo Energia (cit. on pp. 43, 45, 50).
- [39] *Role of Material Thickness*. URL: <https://www.nde-ed.org/Physics/Materials/Mechanical/FractureToughness.xhtml> (cit. on p. 45).
- [40] Dan Liu and Dirk John Pons. «Crack propagation mechanisms for creep fatigue: a consolidated explanation of fundamental behaviours from initiation to failure». In: *Metals* 8.8 (2018), p. 623 (cit. on pp. 46, 48, 52).
- [41] David Broek. *Elementary engineering fracture mechanics*. Springer Science & Business Media, 1982 (cit. on pp. 46, 47, 49).
- [42] John Frederick Knott. *Fundamentals of fracture mechanics*. Gruppo Italiano Frattura, 1973 (cit. on p. 47).
- [43] *Fatigue Crack Growth*. URL: <https://mechanicalc.com/reference/fatigue-crack-growth> (cit. on p. 48).
- [44] *Linear Elastic Fracture Mechanics (LEFM): Part Two*. URL: <https://www.totalmateria.com/TR/page.aspx?ID=CheckArticle&site=KTS&NM=299> (cit. on p. 48).
- [45] *Fatigue Crack Growth*. URL: <https://www.totalmateria.com/TR/page.aspx?ID=CheckArticle&LN=ES&site=KTS&NM=49> (cit. on p. 50).
- [46] SN Malik. «Elevated temperature creep crack growth: State-of-the-art review and recommendations». In: *Nuclear Engineering and Design* 72.3 (1982), pp. 359–371 (cit. on p. 51).
- [47] Santosh Balaji Narasimha Chary and Santosh Balaji. *Crack Growth Behavior Under Creep-Fatigue Conditions Using Compact and Double Edge Notch Tension-Compression Specimens*. University of Arkansas, 2013 (cit. on p. 51).
- [48] Sunil Goyal, K Mariappan, Vani Shankar, R Sandhya, K Laha, and AK Bhaduri. «Studies on creep-fatigue interaction behaviour of Alloy 617M». In: *Materials Science and Engineering: A* 730 (2018), pp. 16–23 (cit. on p. 52).
- [49] Jill K Wright, Laura J Carroll, T-L Sham, Nancy J Lybeck, and Richard N Wright. «Determination of the creep-fatigue interaction diagram for Alloy 617». In: *Pressure Vessels and Piping Conference*. Vol. 50411. American Society of Mechanical Engineers. 2016, V005T12A004 (cit. on p. 53).

- [50] Zhi Liu, Jian-Guo Gong, Peng Zhao, Xiao-Cheng Zhang, and Fu-Zhen Xuan. «Creep-fatigue interaction and damage behavior in 9-12% Cr steel under stress-controlled cycling at elevated temperature: Effects of holding time and loading rate». In: *International Journal of Fatigue* 156 (2022), p. 106684 (cit. on pp. 53, 54).
- [51] Dennis Fox. «Prediction of Oxidation Assisted Crack Growth Behavior within Hot Section Gas Turbine Components Graham Webb, Tom Strangman, Norm Frani, Chet Date, Lloyd Wilson and Rajiv Rana AlliedSignal Engines 111 S. 34th Street Phoenix, Arizona 85072-2181 USA». In: () (cit. on p. 54).
- [52] Karl Michael Kraemer, Falk Mueller, Matthias Oechsner, Andrea Riva, Dalila Dimaggio, Erica Vacchieri, and Eleonora Poggio. «Estimation of thermo-mechanical fatigue crack growth using an accumulative approach based on isothermal test data». In: *International Journal of Fatigue* 99 (2017), pp. 250–257 (cit. on pp. 54, 88).
- [53] Eric Miller. *Submodeling in ANSYS Mechanical: Easy, Efficient, and Accurate*. URL: https://www.padtinc.com/blog/submodeling_ansys_mechanical/ (cit. on pp. 64, 66).
- [54] *Nuove opzioni di meccanica della frattura in Workbench 14.5*. Ansaldo Energia (cit. on p. 72).
- [55] *SOLID187 Element Description*. Ansys Help (cit. on p. 72).
- [56] *Solving a Fracture Analysis*. Ansys Help (cit. on p. 74).
- [57] *Crack Overview*. Ansys Help (cit. on p. 75).
- [58] *Defining an Arbitrary Crack*. Ansys Help (cit. on p. 76).
- [59] *Fracture Meshing*. Ansys Help (cit. on p. 76).